SIMULATING THE DETECTION OF MUONS AND NEUTRINOS IN DEEP ANTARCTIC ICE

by

JOHN E. JACOBSEN

A dissertation submitted in partial fulfillment of the
requirements for the degree of

Doctor of Philosophy
(Physics)

at the
UNIVERSITY OF WISCONSIN — MADISON
1996

Abstract

RAVEN is a suite of Monte Carlo simulation programs written at the University of Wisconsin for AMANDA, the Antarctic Muon and Neutrino Detector Array. RAVEN (Radiating AMANDA Virtual Events, Numerically) is intended to be a comprehensive treatment of most signals and backgrounds present in AMANDA.

This document describes the physics built into RAVEN, especially the generation and propagation of high-energy (multi-GeV) muons and of light in ice with and without scattering impurities. It describes the design and implementation of the software, and contains an appendix which describes how to install and use the system. A comparison of RAVEN to limits that are calculable analytically (ice without scattering, and ice with diffusive propagation of light) is presented. A glossary is provided for terms which may be unfamiliar to readers outside the field.

Applications of RAVEN presented in the text include a simulation of showers produced by supernovae under various assumptions of ice properties. A estimated signal excess of 27 sigma is predicted for a supernova at the center of the galaxy, for the expanded 11-string array currently under construction at the South Pole.

The design of a muon neutrino filter is also presented, which enhances the neutrino event rate relative to cosmic ray muons in the data stream. In presenting the filter, the statistical properties of four-string AMANDA-B data taken in 1996 are compared with events simulated by RAVEN as a check on the Monte Carlo. Finally, an analysis of the 11-string AMANDA array is carried out, predicting atmospheric neutrino and cosmic ray muon rates for three different detector geometries, and a proposal is made for a ν_μ filter for the expanded array.

This document can be found in PostScript form at:
`http://alizarin.physics.wisc.edu/jacobsen`

Acknowledgements

For some reason I looked forward to writing this part more than any other.

First and foremost I must thank my friend and advisor Francis Halzen for many things. Few graduate students ever recieved as much generosity and respect from their advisors as I have. I owe Prof. Halzen a debt many times over for creating many opportunities for me in physics while simultaneously supporting my artistic endeavours. Also for being a role model, for great advice, and for some great meals!

Thanks also to my other AMANDA colleagues, especially Bob Morse, Igor Liubarsky, Serap Tilav, Vijaya Kandhadi, and Lori Gray. It has been great working, writing code, arguing physics and eating lunch with you.

The treatment of scattered light in this thesis was greatly informed by fruitful discussions with Albrecht Karle from DESY/Zeuthen, and Martin Moorehead and Doug Lowder at LBL. Thanks to Ralf Wischnewski, also at DESY, for setting me straight at the last minute about matters relating to the simulation of scattered light from supernova showers.

Thanks is also due to many others: To Ugo Camerini, my first physics employer and ally... *e bruto!*; to Jack Fry, John Finley, Almus Kenter, Pat Slane, John Jennings, and all the others on the Haleakala Gamma Ray Observatory project who taught me the ins and outs of research in physics while I was an undergrad, and also to Al Erwin and Theodoros Alexopoulos for the semester I spent on E735; to Sau Lan Wu and the ALEPH Wisconsin Group for the year I spent at CERN, where I learned many lessons about physics, politics, and living away from home.

My final big physics debt is to John Beacom, who supplied endless help on many problems ranging from the personal to the highly technical. If graduate students were paid as consultants, John could retire whenever he wished.

Thanks also to the following people:

- To Prof. C. H. Blanchard, for hooking me on physics with his great introductory lectures;
- To Bill Long for encouragement and advice on all sorts of matters;
- To art professors Jack Damer and Richard Long, who each supported my physics efforts while providing a sharp, critical eye to my work in

art;

- To past and current members of Omulu Capoeira do Istmo, for the friendship and beatings we have exchanged.
- To my other Madison buddies for years of friendship, and
- To Hilary, for waiting.

Finally, I give my thanks and my love to my parents, Jerry Jacobsen and Carla Peterson, to whom I dedicate this work.

Contents

List of Figures

List of Tables

Chapter 1

Introduction and History

1.1 Ice Fishing for Neutrinos

> Neutrinos are the most penetrating of the elementary particles. They all, and particularly those at low energies, pass through galactic space and–with no greater difficulty–material objects, planets, stars; because matter is far more transparent to them than glass is to sunlight. The experiments really should not have produced any result worth mentioning. But they did.
>
> –*His Master's Voice*, [1, p. 94]

1.1.1 The Neutrino

As physical objects go, the neutrino is as close as something can get to being nothing at all and still exist. It is chargeless, massless (or nearly so), and interacts only very weakly with other particles. In six decades the neutrino has gone from a somewhat ad-hoc explanation for the energy spectrum in nuclear beta decay to one of the basic building blocks of the Standard Model of particle physics. It is also a formidable astronomical tool for observing reactions deep in the core of the Sun and elsewhere far into the universe.

1.1.2 The Experiment

Because it interacts very weakly with matter except at the very highest energies, the neutrino is very difficult to detect. This fact necessitates three characteristics that have been a feature of neutrino detectors since Cowan and Reines' first direct observation of the $\bar{\nu}_e$ at the Savannah River nuclear reactor in 1953. These characteristics are: large detector volumes, a careful consideration of backgrounds, and long running times. AMANDA is no exception. With a currently instrumented geometrical volume exceeding 10 million tons of ice, AMANDA is one of the largest physics detectors ever built. AMANDA must contend with a down-going cosmic ray muon background one million times stronger than the more interesting flux of up-going muons produced by neutrinos which have traveled through the earth. To pick out the weak neutrino signals from such a background, sophisticated data analysis and track reconstruction schemes will be needed, as well as a running time measured in years.

The most cost-effective way to build a high-energy neutrino detector is to take advantage of large volumes of cheap, transparent material such as water or ice. The material serves as the target for the neutrinos to interact with to produce charged particles, the medium through which the radiation from the charged particles must propagate, and, in the case of ice, the structural support for the optical sensors which detect the light. The technique was proven in 1987 when, on the 23rd of February, the deep underground water-Čerenkov detectors IMB and Kamiokande measured the first flux of neutrinos from beyond the solar system: 19 events originating from the stellar collapse and subsequent supernova explosion of SN1987A.

For energies of a few GeV and above, far beyond those relevant for supernova detection, the creation of much larger detectors is underway, which aim to catch muons created by neutrinos going upwards through the earth. Two decades of research has been carried out using natural bodies of standing water, namely the DUMAND (Deep Underwater Muon and Neutrino Detector) experiment in the ocean near Hawaii; NESTOR, located off the shores of Greece in the Mediterranean; and the Lake Baikal detector in Siberia. The twist in AMANDA (Antarctic Muon and Neutrino Detector Array) is to use deep, Antarctic ice at the South Pole as the detector medium. Although the original idea was to detect radio pulses from large electromagnetic showers, it was quickly seen that the detection of visible Čerenkov light would be a simple, cost-effective way to build a large muon and neutrino detector. The challenge with ice is to use hot water to drill holes, a few kilometers in depth, quickly deploy the optical sensors, and have the equipment survive re-freeze. The idea has stood the test of three separate deployments, with the most ambitious deployment to date in preparation as this is being written.

Once a successful deployment has been carried out, the physics tasks begin. These include the survey and calibration of the detector, understanding the properties of the ice, and eventually the reconstruction of events, with the goal of picking out faint up-going neutrino-induced events from the much larger background of down-going muons from cosmic ray air showers.

The ultimate goals of such an experiment include the observation of supernovae within and outside our galaxy; the indirect detection of cold dark matter (WIMPS) via high-energy neutrino production in the Sun; the detection of neutrinos from active galactic nuclei with an eye to understanding the origin of the highest-energy cosmic rays; and, most exciting of all ... something nobody has thought of yet! The advanced physics possibilities of such an instrument have been discussed at length elsewhere[6,7]. This thesis will focus more on the nuts-and-bolts development of a set of programs used to simulate the AMANDA instrument and the physics therein; a comparison of simulation results to real AMANDA data, and predictions from the simulation as to the efficiency and rate for various signals and backgrounds.

1.2 AMANDA Deployments, Past, Present and Future

To date, the AMANDA collaboration has carried out three successful deployments of optical modules in deep, Antarctic ice. Each Austral summer season has brought forth new information about the technique of using ice as a particle detector. These deployments are as follows:

1991-1992: Deployment of test modules to 800 meters. The viability of ice as a medium for the detection of muons was proven[31] with the successful deployment of two test strings to 800 meter depth and the observation of hit coincidences due to muons. Low OM noise was observed (1-2 kHz), and the OMs had good survival rate during re-freeze.

1993-1994: Deployment of AMANDA-A. Four strings of 20 OMs each were deployed to a depth of 1km[29]. 73 modules survived refreeze (91% survival rate); laser calibration and data analysis indicated that ice was an order of magnitude clearer than expected, but also that isotropization of light was occurring, presumably due to microscopic bubbles, making muon track reconstruction difficult. However, the isotropization enabled energy reconstruction of pointlike energy deposits (showers)[2,19].

1995-1996: Deployment of AMANDA-B. Four strings with a total of 86 modules were deployed to a depth of 1900 meters. 79 modules survived refreeze. No evidence of bubbles was found. Laser and muon data analysis indicates the presence of some residual scattering, requiring careful Monte Carlo simulation techniques and sophisticated track reconstruction algorithms. (Chapter 4 discusses some simulation results for AMANDA-B).

1996-1997 (In progress): Deployment of 7 new strings. Preparation is in progress for the addition of 7 new strings to the 4-string AMANDA-B detector, bringing the total number of working modules up to ~300.

(Chapter 5 presents predictions for the expanded array).

A schematic of the AMANDA-A and AMANDA-B arrays can be seen in Figure 1.1.

1.3 Introduction to RAVEN

...Then this ebony bird beguiling my sad fancy into smiling,
By the grave and stern decorum of the countenance it wore.
"Though thy crest be shorn and shaven, thou," I said, "art sure no craven,
Ghastly grim and ancient raven wandering from the Nightly shore–
Tell me what thy lordly name is on the Night's Plutonian shore!"
Quoth the Raven, "Nevermore."[8]

`RAVEN` is a Monte Carlo (statistically-based) simulation of the AMANDA experiment and of similar experiments in the future.

The bulk of the work done by `RAVEN` consists in the generation of muons and the Čerenkov photons they emit while traveling at relativistic speeds through the ice. A full understanding of the properties of the photon detectors (photomultiplier tubes, or PMTs) and the trigger scheme used to record events is also required. Since a fast, relatively compact simulation is desired, huge particle physics codes such as `GEANT` are eschewed in favor of developing a simulation within the collaboration.[1]

`RAVEN` consists of several `FORTRAN` programs to be run in a step-wise manner, with the output of one program used as an input to the next. The programs are ideally suited to workstation-size platforms (Digital Equipment Corporation Alphas running Digital Unix were used at the University of Wisconsin). The first few chapters of this document outline the physics and mathematics used in the simulation. Input commands to various programs appear in Appendix A, "Using `RAVEN`." The last chapters give examples of calculations done using the software: the design of a neutrino filter (Chapter 4), the application of the filter to the study of an expanded AMANDA array (Chapter 5), and the study of supernova detection via the observation of $\bar{\nu}_e + p \rightarrow n + e^+$ events (Chapter 6).

---

[1] It is also desirable to have independent codes within various working groups, as a cross check.

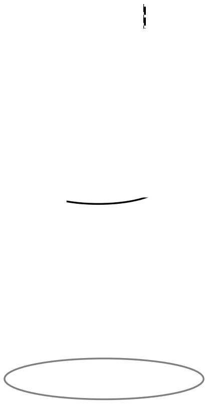

1.3.1 `RAVEN`: History and Contributors

`RAVEN` started out small. In 1990 or so, Almus Kenter wrote a short program at the University of Wisconsin to treat vertical, downward-going muons incident on a single string of photomultipliers. The program was a launching-point for what became a large programming effort. The software has undergone more than 24 different versions and developed on two different operating systems (VMS and Digital Unix). The code is now about 30,000 lines long, has a six-year history, and has many contributing authors. Although the basic structure and bulk of the coding was done by this author, significant contributions were made by Serap Tilav and Igor Liubarsky. Other contributors include Tim Stelzer and Lori Gray. Certain approaches to simulation taken by collaborators at DESY[21] in Germany and the Lawrence Berkeley National Laboratory[22] were also influential in the evolution of `RAVEN`.

The `RAVEN` package has been used at the University of Wisconsin–Madison since its inception to simulate possible and existing AMANDA configurations. It has also been used at Bartol Research Institute in Delaware, Stockholm University in Sweden, and the University of California at Irvine.

`RAVEN` is part of a long-standing simulation effort at the University of Wisconsin. Other work has included a very fast (10-100× the speed of GEANT or EGS) electromagnetic shower simulation, treating energies up to a PeV[3]; and a complete treatment of ν_e interactions in ice, including both electromagnetic and hadronic components[4].

Chapter 2

The Physics of Neutrino Telescopes

> There was a letter, it was sent, it fell to Earth, at our feet, and had been falling in a neutrino rain while the lizards of the Mesozoic plowed the mud of the Carboniferous forests with their bellies, while the paleopithecus, called Promethean, gnawed a bone and saw in it the first club.
>
> –*His Master's Voice*, [1, p. 195]

2.1 Overview: Ice As a Particle Detector

In order to do astronomy with South Pole ice, one needs to understand what sort of particles reach the ice, and what they do when they get there.

At first glance, ice at a depth of 1-2 kilometers has to be one of the most boring places on Earth. This utterly dark, cold and homogeneous environment is disturbed only by a cosmic rain of energetic muons passing through and stopping within the ice. Most of these particles are produced high in the Earth's atmosphere. The muons are the decay products of pions created in air showers induced by high-energy cosmic rays. The character of these "muon bundles" (for each shower event in the atmosphere can produce one or more muons deep in the ice) is determined by the energy spectrum of the primary cosmic rays, the physics of particle creation and decay, and the various modes of muon energy loss within the ice.

One of these energy-loss mechanisms is utterly insignificant for determining the travel distance of these muons, but is crucial for their detection. The so-called Čerenkov effect consists of the radiation of light by charged particles (electrons, muons, etc.) moving faster than the speed of natural light propagation in a medium (but slower, of course, than the speed of light in a vacuum). Ice is an excellent medium to detect such light because of its extreme transparency in the blue part of the spectrum. In AMANDA, the faint light signals from the muons are detected by optical modules containing photomultiplier tubes capable of detecting single photons. The nominal threshold for this detection method is of the order of several GeV, the exact number being determined by the average spacing between optical modules and the multiplicity required for the trigger.

Although much more plentiful than muons, most of the neutrinos passing through the ice have no observable effect. Occasionally, however, a muon neutrino will "notice" an atom in the ice via a weak charged-current interaction, resulting in a quickly-decaying hadronic component and a penetrating muon which "remembers" the direction of the neutrino to a sufficient accuracy (a mismatch angle of about a degree for neutrinos of energy 1 TeV) to allow one to do astronomy. In principle, neutrinos traveling in any direction can arrive near the detector and produce a muon. Of course, a clear neutrino signal occurs if the muon is traveling upwards.[1] See Figure 2.1.

The rate for such events is determined by the flux of ν_μs streaming through the ice, and the weak interaction cross section. The numbers work out to about a million down-going muons from cosmic rays for every up-going atmospheric neutrino-induced muon (at an ice depth of 1 kilometer). The problem is therefore to detect the muons and pick out the signal of neutrinos from the enormous background.

In addition to the production of muons by neutrinos, other processes are of interest for those hoping to catch neutrinos using masses of polar ice. Electron antineutrinos created in massive supernova explosions can interact with atomic protons via $\bar{\nu}_e + p \rightarrow n + e^+$ to produce positrons which, again, radiate detectable Čerenkov light. The energies of such neutrinos are of the order of a few MeV, far below the nominal GeV threshold for muon detection; however, so many electron neutrinos escape the expanding supernova shell and arrive over a 10 second period that one can observe a statistically significant signal in all optical modules taken together. The calculation of the sensitivity of AMANDA to such events is straightforward and is presented in Chapter 6.

At intermediate energies (several GeVs and above), muon production by ν_μs is of interest as discussed above. In addition, other neutrino flavors $\{\nu_e, \nu_\tau\}$ can interact with the nucleons N in the ice target via

$$\nu_{\{e,\tau\}} + N \rightarrow X + \{e^-, \tau^-\}$$

via a charged-current interaction, or

$$\nu_{\{e,\mu,\tau\}} + N \rightarrow X + \nu_{\{e,\mu,\tau\}}$$

with a neutral-current interaction.

---

[1] The probability that penetrating, high-energy particles other than muons and neutrinos arrive at such a depth in the ice is negligible.

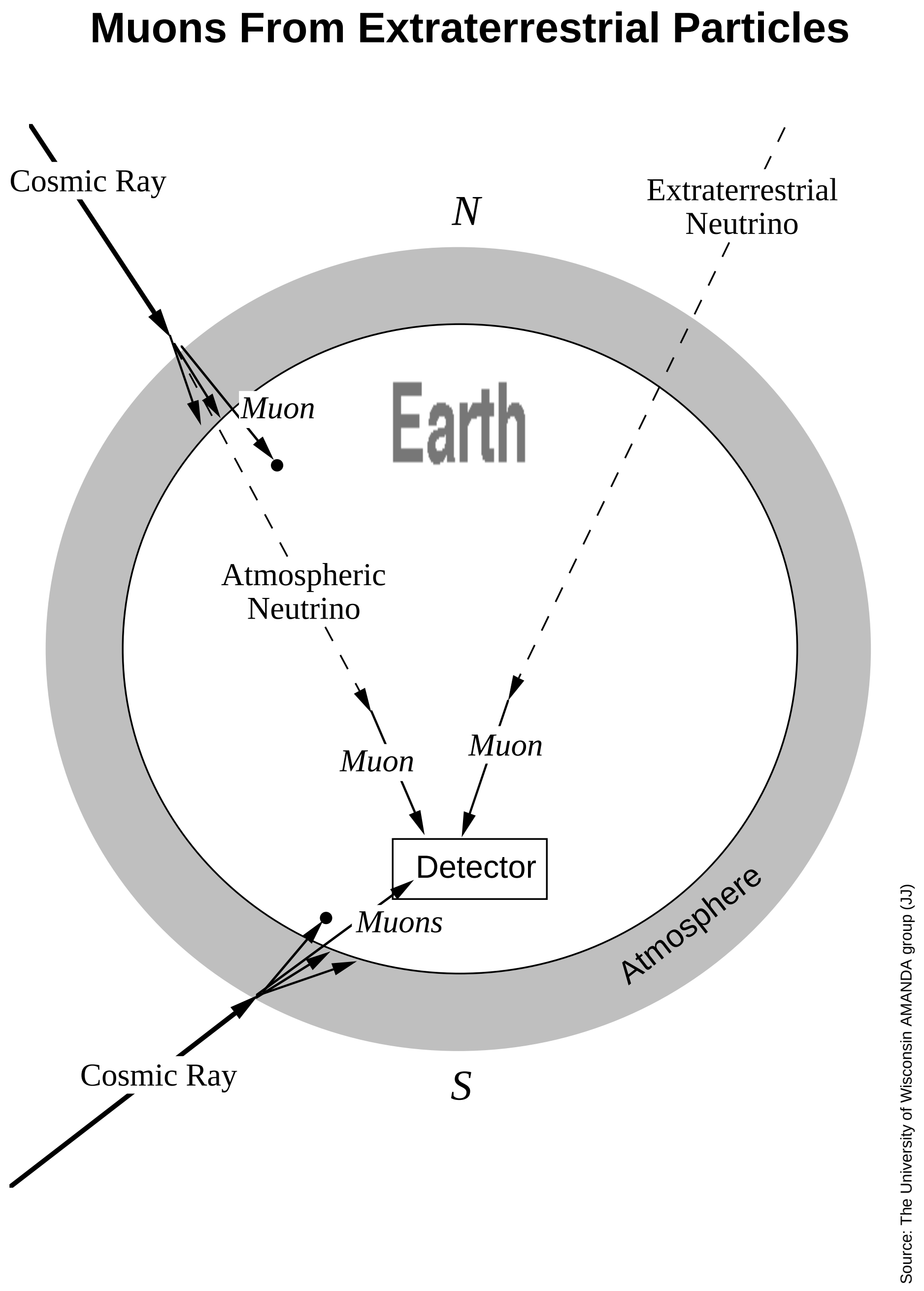

Source: The University of Wisconsin AMANDA group (JJ)

Figure 2.1: Penetrating muons are a primary quarry for the AMANDA experiment. Sources of high-energy muons in AMANDA include cosmic-ray muons, muons from atmospheric neutrinos, and (hopefully) muons produced by extraterrestrial neutrinos.

The same reactions apply if charged leptons and neutrinos are replaced by their antiparticles. In each case X represents a hadronic shower which has a relatively small spatial extent; electrons or tau leptons in the final state also give showers. The detection in this case is not done by resolving a single track, but by "calorimetry"– measuring the total light output from the showers which is an excellent gauge of the energy of the event.

At the opposite extreme in energy, electron antineutrinos of the highest energies can interact with atomic electrons via the s-channel production of a W boson,

$$\bar{\nu}_e + e^- \rightarrow W^- \rightarrow \begin{cases} \bar{\nu}_l \, l^- & (l \text{ lepton}) \\ \text{hadrons} & \end{cases}$$

The cross-section is negligible for the GeV neutrino energies most relevant for muon detection, but peaks at the 6.4 PeV (6.4×10^{15} eV) resonance energy for real W-production off of electrons at rest (the Glashow resonance). The cross section for the electron channel ($W^- \rightarrow \bar{\nu}_e e^-$) at the peak is[5]:

$$\sigma(E_{\mathrm{res}}) \;=\; \frac{1}{B(W\rightarrow \bar{\nu}_e e^-)} \frac{G_F^2 M_W^4}{3\pi\Gamma_W^2} \approx \frac{5.2\times10^{-32}\mathrm{cm}^2}{1/9} \approx 4.7\times10^{-31}\mathrm{cm}^2. \quad (2.1)$$

Here $\Gamma_W \approx 2.1$ GeV is the width of the W and resonance occurs for $E_\nu = E_{\mathrm{res}} = s/(2m_e) \approx 6.4$ PeV. (The factor $B(W\rightarrow \bar{\nu}_e e^-) = \frac{1}{9}$ comes from the three leptonic and six available hadronic channels.) Again, the final state particles produce showers which are detected.

It can be seen, then, that the task of simulating a neutrino detector depends on the treatment of fluxes of incident neutrinos and muons, on the interaction of the particles with ice, and especially on the propagation of Čerenkov light in a medium which, although exceedingly clear, quiet and uniform, scatters and absorbs the light to varying degrees depending on the depth of the ice and the color of the light.

The sections that follow are primarily concerned with the treatment of muons from cosmic ray air showers and muon neutrinos.

2.2 Calculating Event Rates in a Neutrino Telescope

One of the primary objectives of a simulation such as `RAVEN` is to determine the event rate in AMANDA due to various sources, given different detector configurations, triggers and event selection criteria. This requires an understanding of the incoming muon flux due to each source. The method of calculation depends upon whether the incoming flux is through-going (such as for cosmic-ray muons which are all created far from the detector), or volumetric (such as for neutrinos where muons are created at points uniformly distributed through the detector volume). See Figure 2.2.

For through-going events, the event rate is given by convolving the differential flux of muons with the efficiency ϵ of the detector:

$$R = \int \left(\frac{dN_\mu}{dA\ d\Omega\ dt\ dE} \right) \epsilon(\vec{x}, \Omega, E)\ dA d\Omega dE. \tag{2.2}$$

The Monte Carlo technique works by generating N_{gen} muon tracks passing through a plane of area A_{test} outside the detector volume. These muons are passed through the simulation, and events satisfying the trigger are kept as N_{trig}. The average efficiency is then $\langle\epsilon\rangle = N_{\text{trig}}/N_{\text{gen}}$. Assuming time-independent fluxes and efficiencies, N_{trig} and N_{gen} are given by:

$$N_{\text{trig}} = \int \frac{dN_\mu}{dA\ d\Omega\ dt\ dE}\ \epsilon(\vec{x}, \Omega, E) dA d\Omega dE$$

$$\begin{aligned} N_{\text{gen}} &= \int \frac{dN_\mu}{dA\ d\Omega\ dt\ dE}\ dA d\Omega dE \\ &= \left(\int \frac{dN_\mu}{dA\ d\Omega\ dt\ dE}\ d\Omega dE \right) \left(\int dA \right) = \Phi\ A_{\text{test}}, \end{aligned}$$

where Φ is the flux integrated over solid angle and the energy range $[E_0, \infty)$. The expression for N_{gen} factors in this way because it is usually independent of the spatial coordinates in the plane of A_{test}.

The calculation is independent of the lower energy bound E_0, provided the same value is used in both the flux calculation and the Monte Carlo generation, and provided $\epsilon(E \leq E_0) = 0$. It is also independent of A_{test}, provided the detector efficiency vanishes at the edges of the test area. When running the Monte Carlo, one typically has to check that suitable values of E_0 and A_{test} have been chosen.

Typically one quotes an effective area $A_{\text{eff}} = A_{\text{test}}\langle\epsilon\rangle$. The Monte Carlo rate is then:

$$R = A_{\text{eff}}\ \Phi. \tag{2.3}$$

For a source in which muons are generated uniformly throughout and around the detector, as in the case for $\nu \to \mu$ events, the calculation is the

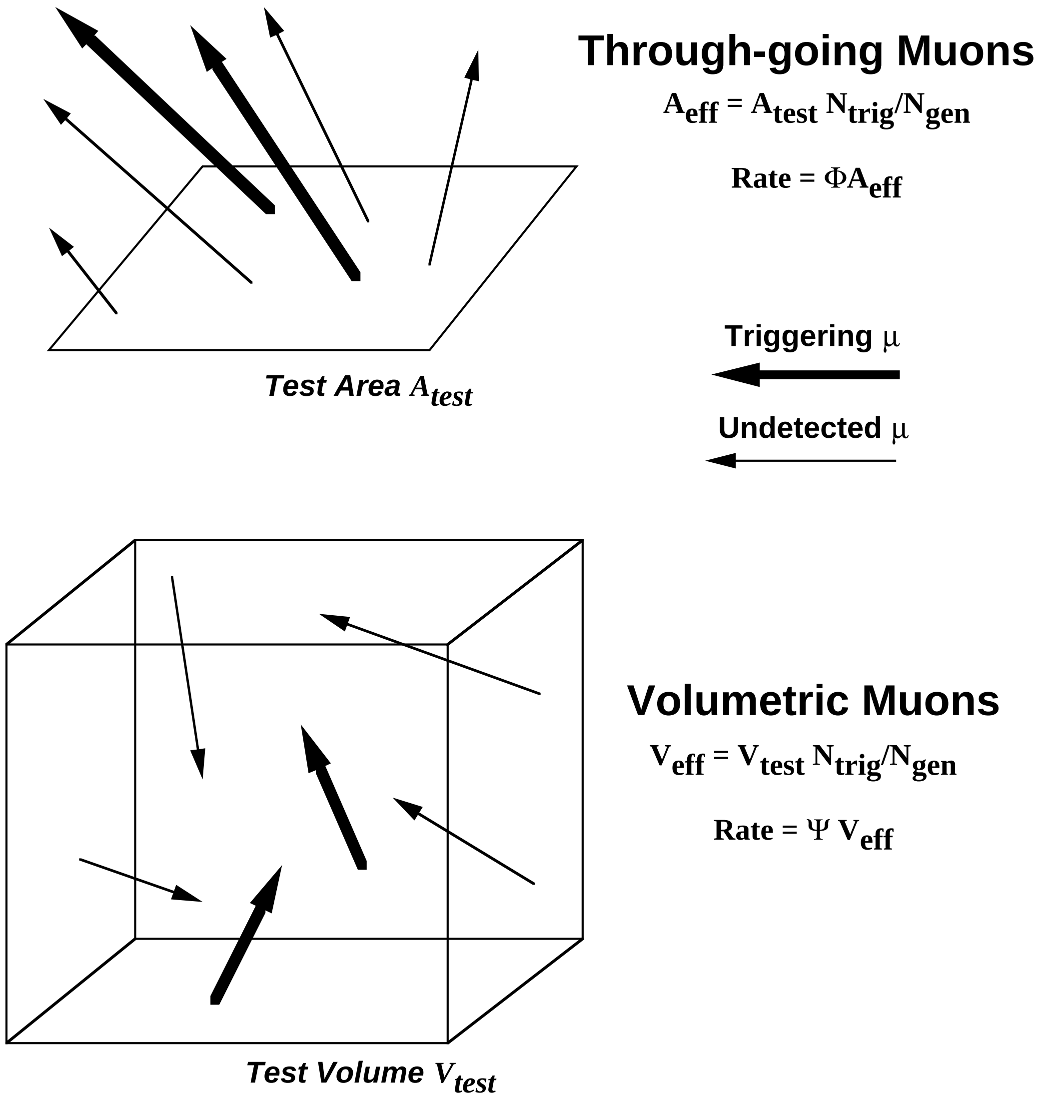

Figure 2.2: The two types of muon fluxes to be simulated: through-going (e.g., cosmic-ray muon) and volumetric (e.g., neutrino) fluxes. Here Φ is the number of muons/(cm^2 sec) passing through A_{test}, and Ψ is the number of muons/(cm^3 sec) created inside V_{test}.

same, with volume replacing area in each expression:

$$R = (V_{\text{test}}\langle\epsilon\rangle)\left(\int \frac{dN_{\nu\rightarrow\mu}}{dV\ d\Omega\ dt\ dE} d\Omega dE\right) = V_{\text{eff}}\ \Psi, \tag{2.4}$$

with $V_{\text{eff}} = V_{\text{test}} N_{\text{trig}}/N_{\text{gen}}$.

Calculating the event rate, therefore, is reduced to simulating many events and keeping track of the number of events triggering the detector. Obviously, for a comparison of signal and background rates (say, due to atmospheric neutrinos and down-going cosmic ray muons), one must compare the rates obtained by the above methods, using the *same* trigger and event selection criteria.

The distinction between through-going and volumetric fluxes is subtle and worth clarifying. The collection capability of neutrino telescopes is sometimes quoted as an effective area, which is misleading unless the energy region of interest makes the range of the neutrino-induced muon significantly larger than the scale of the detector. Typical atmospheric neutrino-induced muon energy thresholds for AMANDA are of the order of 10 GeV, with a steeply-falling energy spectrum, making the typical muon track length 100-200 meters, which is roughly the size of the detector. It is thus quite common for $\nu_\mu \rightarrow \mu$ conversions to happen inside the fiducial volume of the detector, an occurrence neglected by the approximation which treats the detector as an effective area relative to muons originating outside the array. To correctly calculate the rate, therefore, one must calculate the effective volume as above and multiply by the frequency Ψ with which neutrinos are converted to muons in the ice.

2.3 The Creation of High-Energy Muons

In order to calculate the effective area or effective volume to obtain an event rate, a sample of N_{gen} muons is created using `genevent`. These events must be generated according to the appropriate energy- and angle-dependent flux, and tracked from start to finish through the region near the detector. The resulting number of interest is N_{trig}, either from `genevent` or, if track reconstruction or sophisticated cuts are required, from `anaboth` or from running PAW on the resulting event NTUPLE.

Figure 2.3 is a rough guide to the simulation of an event. In general, the following things are done:

A: The Muon Track Starts: A muon is generated, its energy `mu.energy` and direction `mu.Dmu(3)` are found from input muon flux. The starting point `mu.ps(3)` is generated at random on the physics plane within the test area A_{test}.

B: End Point of Muon Track: The muon is propagated until it runs out of energy. Points of sudden energy loss due to radiation are found. The endpoint of the muon is `mu.pf(3)`.

C: Generation of Cerenkov Photons: The muon radiates light and photons are scattered and absorbed by the ice.

D: Generation of Hits in Optical Modules: Photons hit certain optical modules and generate photoelectrons. Although C and D are conceptually separate, they are combined in a single step, so that the OM response to a muon track or track segment is calculated in advance and stored in a table which is referenced for each OM-track combination.

Although not shown on the figure, the simulation requires two additional steps:

E: Trigger Simulation: Signals from each OM are passed through the electronics, trigger and data acquisition. Leading edge, trailing edge, time-over-threshold and ADC values are associated with each triggering OM. Multiplicity logic is simulated.

F: Data Selection: Cuts are placed on events to reduce background; if desired, track reconstruction takes place.

Figure 2.4 illustrates some of the variables used in muon propagation.

2.3.1 Cosmic Ray Muons from Extensive Air Showers

The dominant background in a below-surface neutrino telescope such as AMANDA consists of penetrating muons from extensive air showers (EAS) induced by high-energy primary cosmic rays striking Earth's atmosphere. The muons (both μ^+ and μ^-) are the decay products of pions and can penetrate to great depth if their energy is sufficiently large.[2] The `genevent` code in `RAVEN` treats these cosmic ray muons in three separate ways. The first, most straightforward method[3] is to use a parametrization of the single-muon flux. This is given in Ref. [9], and was used in order to get the flux right at large zenith

---

[2] The muons penetrate so deeply due to their relatively long lifetime, relativistic boost factor and large mass.

[3] Specified by the `param_crs` command in `genevent`

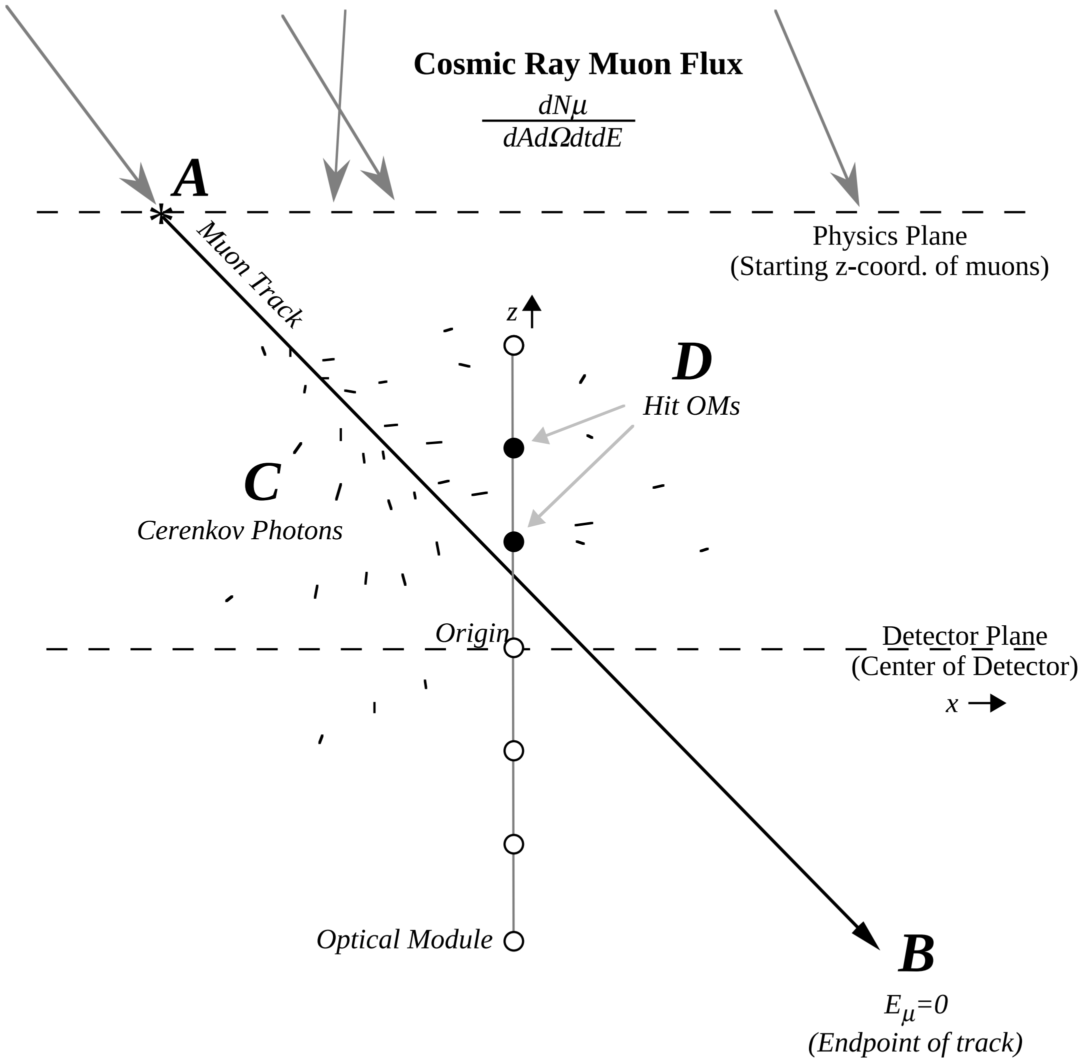

Figure 2.3: An example of the simulation of a down-going cosmic-ray muon event. The text contains a description of the stages marked **A** through **D**.

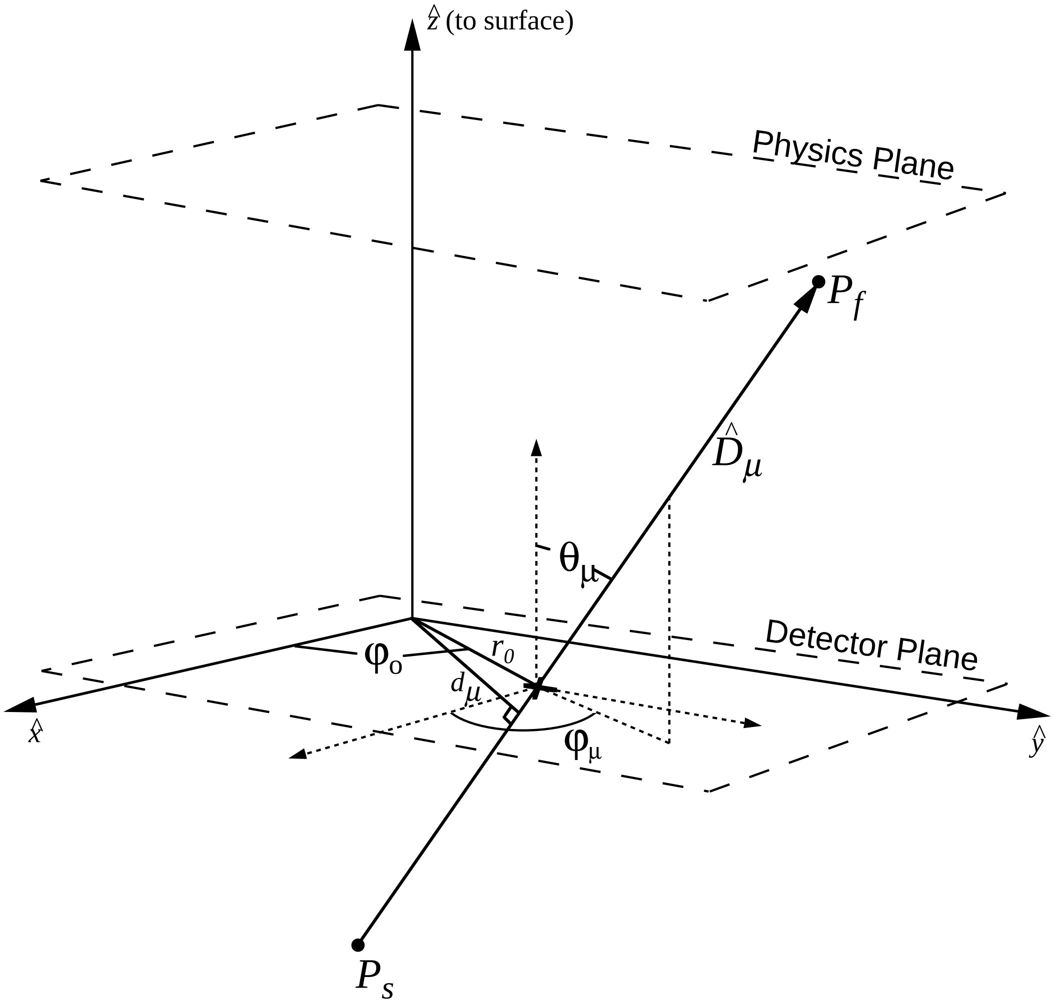

Figure 2.4: Coordinates used to describe muon propagation in `RAVEN`. An upgoing ν_μ-induced muon is shown; cosmic ray muons start at the physics plane.

angles. For this treatment, muon energies and zenith angles are chosen from the parametrizations, and muons are populated uniformly into the test area A_{test}. Muons are propagated from the top of the ice to the physics plane. Those that survive are considered for Čerenkov light production.

This method is somewhat computation-intensive; if the energy threshold for muon generation is fixed to E_{min}, the minimum energy required by a vertically-incident muon to reach the detector, then some muons at non-zero zenith angles will be lost due to muon energy loss. Typically only $\sim 10-20\%$ will survive to the physics plane. For long calculations in which the cosmic ray background rate after cuts is desired (as when exploring trigger criteria which will provide adequate signal/background to do neutrino physics), a faster method is to resample the energy and zenith angle distribution of muons that live until the physics plane. In this case,[4] one creates a file with a run created by the previous method, and then recycles through the list of energies and zenith angles, again populating the test area at random. The integrated flux from the initial run is kept, and the final rate is calculated using that flux as in Eq. 2.3.

The above methods give one muon per event; information about time correlations between muons is lost. In reality, more than one muon can be produced in a given EAS. The final, most complete treatment involves a complete EAS simulation, which hands off "libraries" of muons to `RAVEN`.[5] The software used to generate these muon libraries at Wisconsin is `airshow/SYBILL`[14]. Muons are again propagated to the physics plane and then considered for Čerenkov light generation.

2.3.2 Muons from Atmospheric Neutrinos

Atmospheric neutrinos are the result of the decay of pions in extensive air showers. Many of them travel through the earth and reach one's detector. There, they can interact with an atom in the ice and produce a muon, traveling in nearly the same direction. These up-going muon events are a both a "standard candle" signal for neutrino experiments, of interest for the study of neutrino mixing, and a background for more exotic potential neutrino sources such as active galactic nuclei.

The treatment[6] of atmospheric neutrino events in `genevent` proceeds somewhat differently than cosmic ray muons. As before, the muon energy E_{μ} and

---

[4] Invoked by the `fast_crs` and `ecosth_file` directives to `genevent`

[5] Invoked by the `multimus` and `multimu_file` commands to `genevent`

[6] Atmospheric neutrino events are invoked in `genevent` with the `atmospheric_nus` command

zenith angle θ_μ are generated. In this case the parametrization of Volkova[10] is used. However, the starting point of the muons $\vec{P}_s$ is generated, distributed uniformly through a test volume surrounding the detector.[7] The muon is then propagated to its end point $\vec{P}_f$, which may or may not be inside the test volume.

Example energy and angular distributions for cosmic ray muons and muons from atmospheric neutrinos can be seen in Figure 4.2.

2.3.3 Muons from Point Sources of Neutrinos

Since one hopes to see point sources of neutrinos with AMANDA, it is necessary to simulate the response of the detector to a uniform flux of neutrinos coming from a fixed zenith angle. In this case, events start at random positions within the test volume $V_{\rm test}$. `genevent` does this when issued the `agn_nus` command. An option is also available generate through-going events starting at points in a fixed test area. Example `genevent` input files can be seen in Sec. A.5.4.

2.4 Propagation of Muons Within the Detector

Muons in the Monte Carlo move in straight lines at the speed of light from their point of origin to the point at which they run out of energy. However, many of the muons selected never come near enough to an OM to detected. To this end, a "precut" was implemented which rejects the muon if the distance of closest approach to the origin d_μ is too large. The maximum allowed distance is calculated by finding the distance of the furthest OM in the array R^{max}, the maximum attenuation length $\Lambda_{\rm abs}^{max}$, and defining

$$d_\mu^{max} = R^{max} + \Lambda_{\rm abs}^{max} * \texttt{safefac} \tag{2.5}$$

`safefac` is 3.5 by default, but can be specified by the `precut_safety_factor` command in `genevent`.

If the muon fails the precut, it is given an arbitrary range (it travels to where it would intercept the $z = 0$ plane), and is ignored for the purposes

---

[7] The dimensions of the vertically-oriented cylindrical test volume are determined from the array geometry as follows: The top of the cylinder is the physics plane; the radius of the cylinder is given by the parameter `r0max` in `genevent`, typically of order 1 km. The bottom of the cylinder is `r0max` deeper from the bottom OM than the physics plane is from the top OM.

of light generation. If it passes, the actual range R of the muon must be calculated. The end point of the muon is then given by the initial starting point, the direction of the muon, and its range:

$$\vec{P}_f = \vec{P}_s + R\hat{D}_\mu. \tag{2.6}$$

2.4.1 Muon energy loss

The range of the muon is determined in two possible ways. The first and fastest way, suitable for rough work, is to integrate the parametrized average energy loss, from the muon energy E_μ at $\vec{P}_s$ until $E_\mu = 0$. The energy loss formula used for this treatment is

$$\frac{dE_\mu}{dX} = -\alpha - \frac{E_\mu}{\xi}, \tag{2.7}$$

where α is 2.0 MeV/(g cm^{-2}) and ξ is 2.5×10^5 g/cm^2. The first term is due to ionisation of atoms in the ice medium and is independent of the muon energy. The second, logarithmic term reflects an average over stochastic processes such as brehmsstrahlung. See Refs. [16,17].

A more complete treatment of muon propagation includes the fluctuating energy loss mechanisms averaged over in the logarithmic energy loss term. These include muon brehmsstrahlung, pair production and hadronic photoproduction. (The probability of losing the muon due to in-flight decay is negligible for the energy region of interest for AMANDA simulations). These mechanisms are simulated by a set of routines borrowed from T. Stanev and P. Lipari[13]. `genevent` uses these routines to find the range of the muon, as well as positions along the track where the muon loses a chunk of energy due to one of these processes (shower vertices).

The treatment of energy loss in `genevent` is specified by the `physics_code` directive. `physics_code` of 0 means that the average energy loss formula both to and into the region near the detector should be used. `physics_code` of 1 means that single muons from the parameterized cosmic ray flux use the stochastic routines, but the first method applies within the detector volume and for all other kinds of muons.[8] `physics_code` of 2 indicates that all range calculations are to be done using the stochastic routines, but that excess light generated by the shower vertices is to be ignored. Finally, `physics_code` of 3 causes light from showers to be added to the Čerenkov light of the bare muons.

---

[8] `physics_code` 1 exists purely for historical reasons, as does the somewhat non-informative name `physics_code`.

The complete specification of inputs to the `RAVEN` Monte Carlo programs is given in Appendix A.

Chapter 3

Simulating the Propagation and Detection of Light in Ice

> ... I had to keep going to the computer center, which was not the most pleasant thing, because the winds were hurricane-force then, and merely crossing a street—a hundred feet—was enough to get sand in your ears, mouth, nose, and down your collar.
>
> –*His Master's Voice*, [1, p. 150]

3.1 Introduction

Relativistic, charged particles traveling through ice can be detected by the Čerenkov light they emit. To understand this method of detection, one must take into account the spectrum and direction of the light emitted from the tracks; the scattering and absorption of light due impurities in the ice; and the collection capacity (effective area) of the optical modules used to detect the light. The following sections treat these matters in some detail, explaining the underlying physics and their implementation in `RAVEN`.

3.2 Čerenkov Radiation

The Čerenkov effect (discovered by Čerenkov in 1934) arises when a relativistic particle, traveling through a dense medium with index of refraction n, travels at a velocity $v > c/n$. The effect can be likened to the sonic boom of an airplane or a boat's wake. Although the complete treatment of the effect for a large range of photon wavelengths is quite detailed[3], the basic facts of Čerenkov radiation in the visible region of the spectrum (where the AMANDA optical modules are sensitive) are straightforward.

The number of photons produced per centimeter of track length is:

$$\frac{dN^{\gamma}}{dL} = 2\pi\alpha \sin^2\theta_c\left(\frac{1}{\lambda_{\mathrm{lo}}} - \frac{1}{\lambda_{\mathrm{hi}}}\right). \tag{3.1}$$

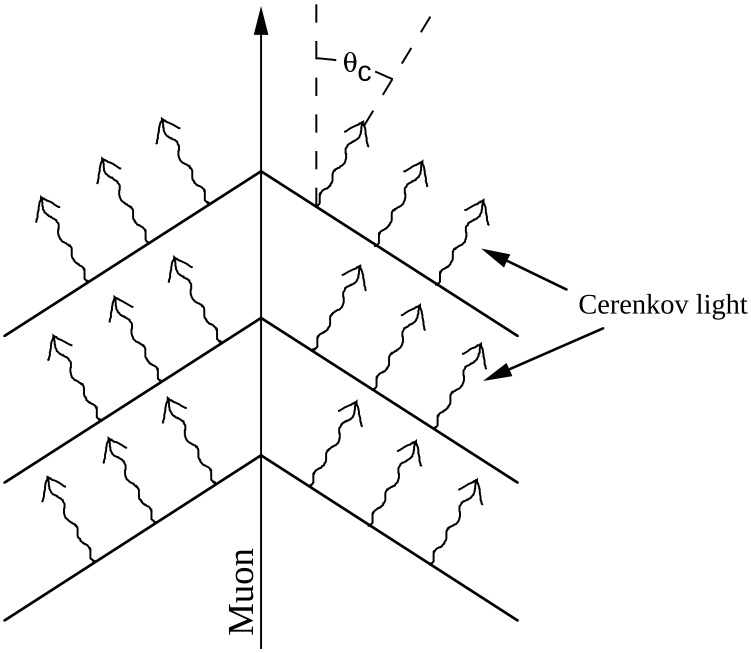

Figure 3.1: The radiation of Čerenkov light due to a charged particle (here, a muon) passing through a dense medium with a speed greater than c/n. The photons are radiated at an angle θ_c with respect to the direction of travel of the muon.

Here, α is the fine structure constant and θ_c is the Čerenkov angle; photons are emitted from the track at this angle with respect to the direction of propagation (see Figure 3.1). It obeys the equation

$$\theta_c = \cos^{-1}(\frac{1}{\beta n}) \approx 42^o \tag{3.2}$$

where β is the velocity of the muon ≈ 1 and $n = 1.33$ is the index of refraction of ice. λ_{lo} and λ_{hi} specify the bandpass of the problem; we use 300nm - 600nm. This yields $\frac{dN^{\gamma}}{dL} = 332.17$ photons/cm.

Čerenkov photons are produced with a flat frequency spectrum. Equivalently, their spectrum in wavelength is

$$\frac{dN_{\gamma}}{d\lambda} \propto \frac{1}{\lambda^2}. \tag{3.3}$$

This, coupled with the absorptive cutoff in ice at high wavelengths, specifies the high end of the bandpass of light. The low end is determined by the quantum efficiency of the photomultipliers (see Figure 3.7).

Absorption in ice is has the following exponential form: the survival probability ϵ_{abs} for a photon with wavelength λ is:

$$\epsilon_{\text{abs}} = \exp(-\frac{ct}{n\Lambda_{\text{abs}}(\lambda)}). \tag{3.4}$$

The absorption length $\Lambda_{\text{abs}}(\lambda)$ must be measured *in situ* by various direct and indirect techniques; in `RAVEN`, several different absorption length curves are available (Section A.5.3).

3.3 The Treatment of Čerenkov Radiation in Clear Ice

"Clear ice" here means ice without scattering impurities, but with absorption. `genevent` treats muons in clear ice by default. The other options include ice with bubbles, in which light propagation is essentially governed by isotropic diffusion (option `fast_bubbles`), and the intermediate regime which obtains at an ice depth of 2 km, presumably due to dust particles (option `do_distmc`). These treatments will be discussed in the next sections.

For clear ice, the problem is one of straightforward geometry. Light leaves the muon track at the Čerenkov angle θ_c and travels in straight lines. Each track is compared with each OM. A small subset of the photons generated by the track (the ones which would pass near the OM) is generated with the λ^{-2} spectrum, and each photon is absorbed by the ice according to Eq. 3.4 and examined to determine if it causes a photoelectron in the OM. This procedure is repeated for each OM–track combination for the duration of the run.

3.4 The Treatment of Čerenkov Light in a Scattering Medium

In order to treat light propagation and detection under the conditions which obtain at a ~2 km depth at the South Pole, some sophistication is required that is not necessary in pure ice or in 1 kilometer ice containing bubbles. A naive approach which would track all the photons generated by a long muon track and determine the response of $\mathcal{O}(100)$ OMs is computationally intractable. It is more feasible to generate a distribution of photons and use this to make a distribution of OM efficiencies for all points in space and OM orientations. The approach taken here is similar to [21,22]. The problem is broken down into three stages.

3.4.1 Generation of the Photon Field

In `photon_table`, Čerenkov light from a segment of muon track or isotropic light at a fixed frequency is generated. Photons are propagated and scattered. The propagation is rectilinear between scattering centers; the scattering is determined by the geometric mean free path between scatterers Λ_{geo} and the angular distribution for each scatter. The angular distribution is specified using one of two models:

GEO: Geometrical optics is used, scattering off a spherical inclusion of index of refraction 1 in the ice medium, which has an index of 1.33.

HG: Henyey-Greenstein scattering, the input parameter to which is the average cosine of the scattering angle, $\langle\cos\theta_{\mathrm{scatt}}\rangle$.

References [18,20] discuss the single-photon scattering models in greater detail. It should be noted that in this context Λ_{geo} and $\langle\cos\theta_{\mathrm{scatt}}\rangle$ are highly dependent on each other and therefore somewhat meaningless in isolation: one can increase Λ_{geo} and decrease $\langle\cos\theta_{\mathrm{scatt}}\rangle$ without producing a measurable difference in the time distributions produced by `RAVEN`.

Photons generated in `photon_table` cross a series of concentric spherical shells. At each crossing, photon positions, directions and times are stored in a binned, multidimensional table. Due to the azimuthal symmetry of the problem, two spatial coordinates are needed: ρ and ψ. ρ is the distance from the center of the track segment to the OM position, and ψ is the polar angle between the direction of propagation of the track and the OM position. ψ (and all other polar angles) are binned by their cosines in this treatment. The OM orientation is binned as $(\cos\theta_p, \phi_p)$. See Figure 3.2.

N_G photons are generated, and each time the photon passes through a shell of radius ρ, its position $(\rho, \cos\psi)$, direction $(\cos\theta, \phi)$ and time t are binned into a table $N(\rho, \cos\psi, \cos\theta, \phi, t)$. The table is written to a file on disk; to save disk space, only non-zero entries are written.

3.4.2 Generation of the Field of OM Responses

The next step is to convert the photon field into a field of responses (expected number of photoelectrons as a function of time) of optical modules due to the

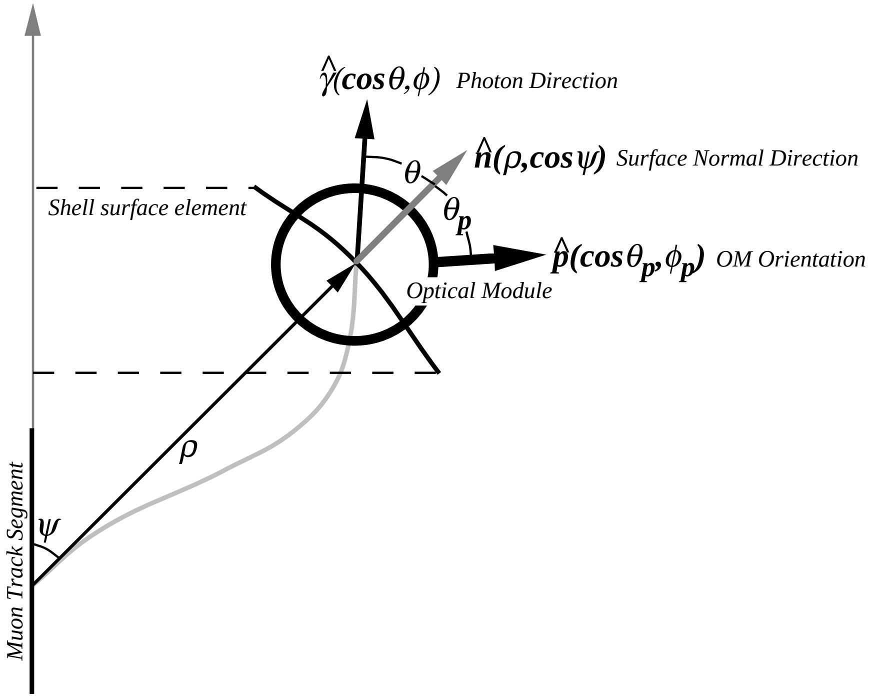

Figure 3.2: Coordinates used in the generation of phototube responses to scattered light (`photon_table` and `distmc`).

photon field. This is done in `RAVEN` with the program `distmc`. At this stage, the wavelength dependence of the Čerenkov photons is introduced, as well as the absorption of the photons in the ice medium and the collection efficiency of the OMs.

The table N describing the photon field is converted to a flux Φ (number of photons per area × time) as a function of time, photon position, and photon direction. Let N_P be the number of physical photons emitted from the track:

$$N_P = L_{\text{track}} \frac{dN_\gamma}{dL},$$

where $\frac{dN_\gamma}{dL}$ is given in Equation 3.1. For a fixed photon direction $\hat{\gamma}(\cos\theta, \phi)$, these photons pass through a projected area of size

$$A(\rho, \cos\psi)|\hat{\gamma} \cdot \hat{\mathbf{n}}| = 2\pi\Delta(\cos\psi)\rho^2|\hat{\gamma} \cdot \hat{\mathbf{n}}|.$$

A is the actual surface area of the ring-shaped section of the spherical shell, and $\hat{\mathbf{n}}$ is the unit vector normal to the shell surface. The dot product factor is necessary to treat off-axis photons correctly.

The flux is then

$$\frac{dN_\gamma}{d\Omega\ dA\ dt} = \Phi(\hat{\gamma}, \rho, \cos\psi, t) = \left(\frac{N_P}{N_G}\right) \frac{N(\rho, \cos\psi, \cos\theta, \phi, t)}{\Delta t\ \Delta(\cos\theta)\Delta\phi\ A(\rho, \cos\psi)|\hat{\gamma} \cdot \hat{\mathbf{n}}|}. \tag{3.5}$$

The increments $\Delta t, \Delta(\cos\theta), \Delta\phi$ are the bin sizes used to make the table N.

The number of photoelectrons N_{pe} generated in an OM is a convolution of the flux with the effective area A_{eff} of the OM (c.f. Section 3.6), the probability of photon survival against absorption, and the spectral distribution of photon wavelengths. If one fixes the OM orientation bin at $\hat{\mathbf{p}}(\cos\theta_p, \phi_p)$, the photon direction at $\hat{\gamma}$, the wavelength at λ, the time at t, and the position bin at $(\rho, \cos\psi)$, then the increment in N_{pe} is

$$d^4N_{\text{pe}} = d\phi\ d(\cos\theta)\ dt\ d\lambda\ \left.\frac{dP}{d\lambda}\right|_\lambda\ \Phi(\hat{\gamma}, \rho, \cos\psi, t)A_{\text{eff}}(\hat{\gamma} \cdot \hat{\mathbf{p}}, \lambda)\ \exp\left(\frac{-ct}{n\Lambda_{\text{abs}}(\lambda)}\right). \tag{3.6}$$

The wavelength spectrum $\frac{dP}{d\lambda}$ is normalized to 1 and follows Equation 3.3. One must integrate (sum) over photon directions and wavelengths to arrive at the final time-dependent distribution of N_{pe}:

$$\begin{aligned}\Delta N_{\text{pe}} &= \Delta t \sum_\lambda \sum_{\cos\theta} \sum_\phi \Delta\phi\ \Delta(\cos\theta)\ \Delta\lambda\ \left.\frac{dP}{d\lambda}\right|_\lambda \\ &\quad \times \Phi(\hat{\gamma}, \rho, \cos\psi, t)\ A_{\text{eff}}(\hat{\gamma} \cdot \hat{\mathbf{p}}, \lambda)\ \exp\left(\frac{-ct}{n\Lambda_{\text{abs}}(\lambda)}\right).\end{aligned} \tag{3.7}$$

$\Delta N_{\rm pe}(\rho, \cos\psi, \cos\theta_p, \phi_p, t)$ and its integral

$$N_{\rm pe}(\rho, \cos\psi, \cos\theta_p, \phi_p) = \sum_t \Delta N_{\rm pe}(..., t) \tag{3.8}$$

are the field of OM responses to the photon flux, and are written out by `distmc` for use by `genevent`. Again, only nonzero contributions to the table are saved.

Equations 3.5 and 3.7 incorporate all the physics of the detection of Čerenkov radiation by a photomultiplier tube! Absorption, scattering, the photon spectrum, the size, bandpass, and quantum efficiency of OMs, and the solid angle occupied by the OM are all there.

Although on a bin-by-bin basis $N(\rho, \cos\psi, \cos\theta, \phi, t)$ may be sparsely populated, there is substantially less statistical error per bin in $\Delta N_{\rm pe}$ due to the integration over the photon directions $\hat{\gamma}(\cos\theta, \phi)$.

It's a bit tricky to perform the integrations in Equation 3.7. There are three variables of integration and five free variables; the resulting 8-fold nested loop can be a large beast, computationally speaking. (For $N_\rho = 200$, $N_t = 300$, $N_{\cos\psi} = 15$, $N_{\cos\theta} = 8$, $N_\phi = 3$, $N_{\cos\theta_p} = 7$, $N_{\phi_p} = 3$ and $N_\lambda = 20$, one must evaluate the product of the flux, wavelength distribution, effective area and absorption survival probability nine billion times). The computation can be speeded up by intelligent arrangement of the order of the looping variables, and by creating initial tables of OM effective areas and of wavelength distributions × absorption survival probability before entering the loop. This eliminates the substantial overhead created by 10^9 subroutine calls; the inner-most loop involves a multiplication and sum only.

Another tricky point in the integration arises in the creation of the five-dimensional table of OM effective areas. If one picks only the center of the bin $(\cos\theta, \phi, \cos\theta_p, \phi_p, \lambda)$, and the number of bins in one or more coordinate is small (< 20), significant error arises due the use of the central value as an estimate of the average. `distmc` avoids this problem in the initial determination of the table of areas by sampling each bin 50 times, picking a slightly different angular value for each of $\cos\theta, \phi, \cos\theta_p, \phi_p$ within the size of the bin and averaging:

$$\langle A_{\rm eff} \rangle = \left(\frac{1}{50}\right) \sum_{i=1}^{50} A_{\rm eff}(\cos\theta^{(i)}, \phi^{(i)}, \cos\theta_p^{(i)}, \phi_p^{(i)}, \lambda). \tag{3.9}$$

With this treatment of the effective area table, one needs only 3-5 bins for the ϕ variables and 8-10 bins for the $\cos\theta$ variables.

The resulting program can be run in less than an hour on a DEC-Alpha (depending on the binning chosen). Also, the code only needs to be run once for a given choice of absorption and scattering model.

3.4.3 Comparison With The Analytic Solution Without Scattering

To understand the calculation of $N_{\rm pe}$ and to test one's code, it is instructive to consider the following example. Suppose we have the case where a point source of light generates N_P photons, where there is no scattering (or a very large mean free path between scattering centers) and there is only a single color of light (and therefore a single value of the absorption length). This is the case which would obtain if one pulsed one of the AMANDA calibrating lasers and looked at the number of p.e.s generated at different distances, in ice free of dust or other optical impurities.

The flux of photons at a radius ρ from the emitter is then

$$\Phi(\hat{\gamma}, \rho, \cos\psi, t) = \frac{N_P}{4\pi\rho^2}\delta(t - \rho n/c)\delta(\cos\theta - 1)\delta(\phi).$$

If the wavelength of light is $\tilde{\lambda}$, the absorption length is $\tilde{\Lambda} = \Lambda(\tilde{\lambda})$. Integrating over the three delta functions, Equation 3.8 is then, for this case,

$$N_{\rm pe} = N_P A_{\rm eff}(\theta_p, \tilde{\lambda})\frac{e^{-\rho/\tilde{\Lambda}}}{4\pi\rho^2}. \tag{3.10}$$

For an optical module oriented anti-parallel to the radial direction ($\hat{\rho}$), this is a simple analytic calculation. A comparison of Equation 3.10 to the numerical preparation of the table of values $\Delta N_{\rm pe}$ and $N_{\rm pe}$ can provide a consistency check for the simulation software. `RAVEN`'s `distmc` agrees with this theoretical calculation to about 1%, for the entire range of radii tested ($\rho \in [5{\rm m}, 200{\rm m}]$), when a sufficent number of bins in $\cos\theta$ and $\cos\theta_p$ are used (16 or more bins each).

Figure 3.3 shows a comparison of the analytical calculation with the results from `distmc` for no scattering and for one scattering model. The model chosen was the HG theory, with 7 m. geometric scattering length, $\langle\cos\theta_{\rm scatt}\rangle = 0.8.$, and an absorption function $\Lambda_{\rm abs}(\lambda)$ whose peak was 120 meters. At the light wavelength chosen, $\tilde{\lambda} = 337$ nm, the absorption length was 70 meters.

The resulting number $\langle N_{\rm pe}\rangle$ is shown for a small burst of light (332 photons). The result from `distmc` agrees with the theoretical calculation in the limit of no scattering. When scattering is present, there is more opportunity for absorption at larger distances, and $\langle N_{\rm pe}\rangle$ is suppressed.

Another case which can be analytically calculated and compared with the simulation is the other theoretical extreme: scattering length so short that the light propagation satisfies the diffusion equation. This is discussed in Section 3.5.

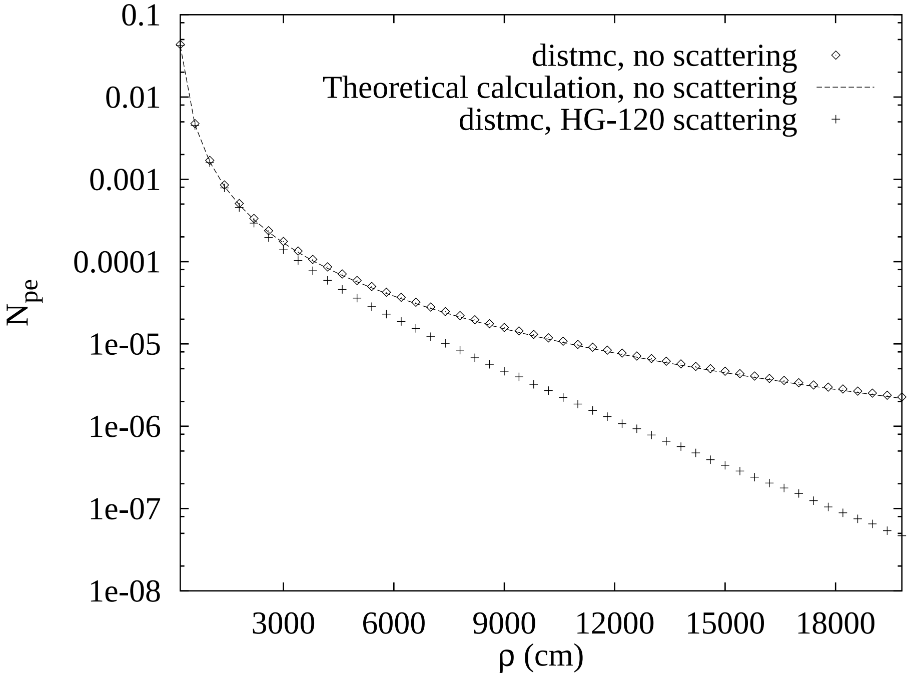

Figure 3.3: Expected number of PEs as a function of radial distance from a small laser pulse. The theoretical calculation with no scattering (line), `distmc` with no scattering (diamonds), and `distmc` with scattering (plus signs) are shown. The OM is looking back at the source.

3.4.4 The Response of the Detector to Muons

The final stage in the scattering treatment is that of event generation. `genevent` uses ΔN_{pe} and N_{pe} to pick numbers of photoelectrons and their times for each OM for each segment of each muon track. Algorithmically, the problem is this:

```
For every muon the event,
   For every OM in the detector array,
      For each muon track segment in the muon,
         Accumulate photoelectrons in the OM.
```

The coordinate transformation from the lab frame into the frame of the segment is straightforward and is done in routines supplied in `distmc.f`. After finding the cumulative response of each OM to the muon segments, the trigger of the entire array can be simulated.

A Trick to Speed Up the Muon Detection Simulation

The simulation of the detector response to muons would be quite a bit faster if one could store the OM response to the entire muon rather than just a small segment. The trouble is that a sizeable fraction of muons start and/or stop close to the array, so one would have to store separate N_{pe} and ΔN_{pe} tables for each muon track length, which is not feasible since the tables need to be kept in workstation RAM for speed's sake. However, one could treat those muons whose start and end points are far from any OMs in this manner. One would store two sets of tables; one for muon segments, and one for infinite tracks. This is currently under study.

3.4.5 The Treatment of Electromagnetic Showers from Muon Radiation

The mechanism for treating the light from muon track segments can be converted into a good approximation for light from electromagnetic showers which are caused by catastrophic muon radiation. In this approximation, one simply re-scales the number of photons in the track segment to correspond to the light output of the electromagnetic shower. In other words, the expected number of p.e.s due to a shower whose coordinates relative to an OM are $(\rho, \cos\psi, \cos\theta_p, \phi_p, t)$, is

$$\Delta N_{\mathrm{pe}}^{\mathrm{shwr}} = \Delta N_{\mathrm{pe}}(\rho, \cos\psi, \cos\theta_p, \phi_p, t)\left(\frac{N_{\mathrm{shwr}}}{N_P}\right). \tag{3.11}$$

$N_{\rm shwr}$ is the number of photons produced in the shower, and is proportional to the energy in the region $0.1 < E_{shwr} < 10^4$ GeV [17]:

$$N_{\rm shwr} = (9.6 \times 10^4) E_{\rm shwr} \text{photons/GeV}. \qquad (3.12)$$

Shower vertices are generated in `RAVEN` using subroutines supplied by Todor Stanev and Paolo Lipari[13]. They provide a list of vertex types (muon Brehmsstrahlung, pair production, or hadronic photoproduction); energies of the muon at each vertex (which, along with the fraction of energy carried off by the radiated photon or produced e^+e^- pair, gives the shower energy), and the distance from the start of the track to the shower position. Each muon thus has a list of shower vertices associated with it. The subroutines also compute the range of the muons.

The showers then manifest themselves in `genevent` when `physics_code` of 3 is specified in the input file. Each shower vertex within seeing distance ($\rho < \rho_{\rm MAX}$) of an OM is given the opportunity to produce a photoelectron in that OM. Shower information is written to the output (`.evt`) file as well, for further study.

This approximation treats the angular distribution of Čerenkov photons relative to the track direction as a delta function (before propagation of light through the ice). In addition, it considers all the light to be emitted from a uniformly-populated, infinitely-thin region of length $L_{\rm track}$ (typically 2 meters), rather than from a fully simulated shower (length of order 10 meters or less even to PeV scales of energy). The approximation is reasonable so long as scattering effects dominate, as is the case in ice at 2 km at the South Pole.

Figure 3.4 presents a summary of how muons are broken up into segments and showers to calculate the total number of photoelectrons and photoelectron times in an OM.

3.5 Calculation of Scattering Due to Bubbles

3.5.1 Analytical Treatment

It has been found[29] that South Pole ice at depths from 800 to 1000 meters is extremely transparent, yet scatters light to such an extent that, for the distance scales of interest (≥ 10 m), the light propagation satisfies the diffusion equation with absorption. The equation results from a treatment of photon propagation as a random walk, with the modification that the scattering angle distribution is anisotropic, and the photons can be absorbed. It gives the survival probability and time distribution independent of the photon or optical

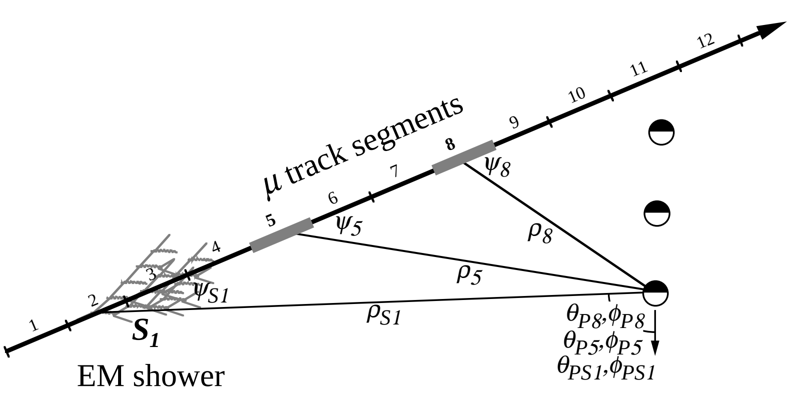

Figure 3.4: The treatment of scattered light from muon showers and track segments in `genevent`. The coordinates used to index the N_{pe} and ΔN_{pe} distributions for one EM shower and two track segments are shown. The process is repeated for each muon-OM pair in the event.

module direction. The scattering can be understood as arising from microscopic air bubbles frozen into the ice. For a photon originating at some point in space, the probability for the photon to be found a distance d away in a volume element dV is

$$u(d,t)\ dV = \frac{1}{(4\pi D^2)^{3/2}}\ \exp\left(\frac{-d^2}{4Dt}\right)\ \exp\left(\frac{c\ t}{n\Lambda_{\text{abs}}(\lambda)}\right)\ dV \tag{3.13}$$

where the quantity $D = c\Lambda_{\text{eff}}/(3n)$. Λ_{eff} is the effective scattering length, which depends on the geometric mean free path between scattering centers Λ_{geo} and the average of the cosine of the scattering angle:

$$\Lambda_{\text{eff}} = \frac{\Lambda_{\text{geo}}}{1 - \langle\cos\theta_{\text{scatt}}\rangle} \tag{3.14}$$

The diffusion regime is a result of the extreme number of scatterings undergone by each photon over distances of several meters. This well-understood limit can provide an excellent test of the `RAVEN` simulation programs, notably `distmc` and `photon_table`. For example, one can compare `RAVEN`'s values of N_{pe} as a function of ρ with those found by using the diffusion equation. This is done in `RAVEN` by averaging over $\cos\psi$, $\cos\theta_p$ and ϕ_p bins (since the flux does not depend on photon direction, and thus N_{pe} does not depend on the OM orientation).

The comparison can be simply done if one considers a fixed wavelength $\tilde{\lambda}$ (the case which obtains in the laser calibration). In this case, the problem is completely specified by the average OM effective area $\langle A_{\text{eff}}(\tilde{\lambda})\rangle$ (since all photon directions are considered to be equally likely), and the absorption and scattering lengths $\Lambda_{\text{abs}}(\tilde{\lambda})$ and $\Lambda_{\text{eff}}(\tilde{\lambda})$.

The probability function $u(d,t)$ can be interpreted as a photon density; for N_P photons emitted by the source, the time- and distance-dependent density of photons is $N_P u(d,t)$. The velocity c/n of the photons thus gives the photon flux as:

$$\Phi(d,t) = N_P\,\frac{c}{n}\,u(d,t), \tag{3.15}$$

which gives the resulting number of photoelectrons in an OM as:

$$N_{\text{pe}}(d) = \langle A_{\text{eff}}\rangle N_P\,\frac{c}{n}\int_0^\infty u(d,t)dt. \tag{3.16}$$

Carrying out the integral over time[18], one obtains

$$N_{\text{pe}}(d) = \frac{3N_P\langle A_{\text{eff}}\rangle}{4\pi d\Lambda_{\text{eff}}}\exp\left(-d\sqrt{\frac{3}{\Lambda_{\text{abs}}\Lambda_{\text{eff}}}}\right) \tag{3.17}$$

3.5.2 The Simulation, Using `RAVEN`

By running `photon_table` and `distmc` with the same geometric scattering length, $\langle\cos\theta_{\text{scatt}}\rangle$ and absorption length, and substituting the average OM effective area calculated in `distmc`, one obtains a consistency check on the stage of `RAVEN` which generates distributions of photoelectrons.

Figure 3.5 gives the number of p.e.s from a small point source of photons as a function of distance. Both the theoretical calculation and results from the simulation are shown. The simulation results are slightly larger in the tail, which will have a negligible effect on the effective volume of an OM. There is also a factor two enhancement in the nearest bin (0.5 meters), which is most likely caused by the breakdown of the diffusion equation at very short distances (where the photons have insufficient opportunity to scatter enough times for the diffusion approximation to be valid).

Although it above comparison is a useful consistency check for `photon_table` and `distmc`, `RAVEN` has a fast bubble treatment (specified by the `fast_bubbles` directive to `genevent`) which doesn't rely on output from `distmc`, but rather is an analytic solution obtained by integrating Equation 3.13 along a muon track.

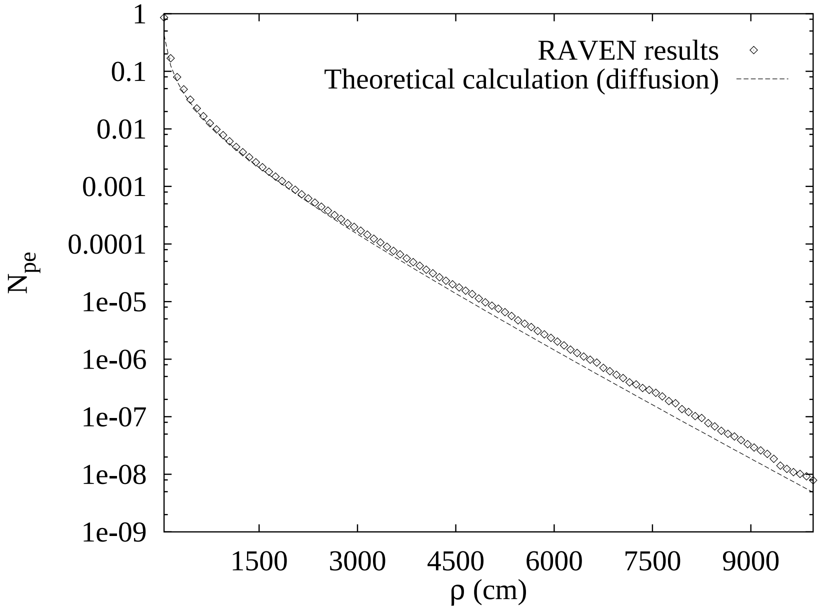

Figure 3.5: Analytic (solid line) calculation of number of photoelectrons as a function of ρ (cm), from a point source of 320 photons scattered according to the diffusion equation, and results from `RAVEN` for the same ice parameters ($\tilde{\Lambda} = 250$ meters, $\Lambda_{\rm geo} = 0.19$ meters, $\langle \cos\theta_{\rm scatt} \rangle = 0.726$).

3.6 The Detection of Čerenkov Light

3.6.1 How Photomultipliers Work

The photomultiplier tube (or phototube, or PMT) exploits the photoelectric effect, in which light is incident upon a thin metal film (deposited on the inside of a glass surface) and causes an electron (or "photoelectron") to be emitted. This electron travels across a voltage gap in a near-vacuum and hits the first of a sequence of dynodes. At each dynode the number of electrons is multiplied, due to the energy gain of the electrons falling through the voltage applied across each gap; the avalanch is collected by an anode which supplies the output signal.

The resulting multiplications can result in gains of up to 10^9 (Hamamatsu PMT), producing a measurable electric current at the base of the phototube. The intrinsic width of the resulting pulse is only of order 2 nsec, which provides excellent timing capabilities.

3.6.2 The Design of AMANDA Optical Modules

The AMANDA detectors in place rely on 8-inch hemispherical PMTs; AMANDA-A consists primarily of Thorn-EMI Model 9353 phototubes, and the AMANDA-B OMs contain mostly high-gain Hamamatsu PMTs.

The entire optical module in each case consists of a phototube; a glass pressure housing; an intermediate gel to supply a good optical connection between the PMT glass and the housing; an aluminum spacer ring between the two hemispheres of the pressure housing; a base which supplies the proper high-voltage to each dynode; and a set of cables with a feed-through connector to deliver high-voltage to the PMT and send the signal back to the surface. A picture of the OM can be seen in Figure 3.6.

3.6.3 Simulation of the Optical Modules

The capability of an OM to detect photons enters the simulation as an effective area $A_{\text{eff}}(\theta_{\text{imp}}, \lambda)$ (Equation 3.6). The effective area describes the capacity of the tube to collect light: it's size (facing the direction of travel of the photon flux), and various sources of inefficiency. The factors which enter into the expression for effective area in `RAVEN` are:

Photocathode geometry. The projected area of the photocathode, which is described as $A_{\text{geo}}(\theta_{\text{imp}}) = s(\theta_{\text{imp}})A_{\text{geo}}(0)$, where $s(\theta_{\text{imp}})$ is the fraction

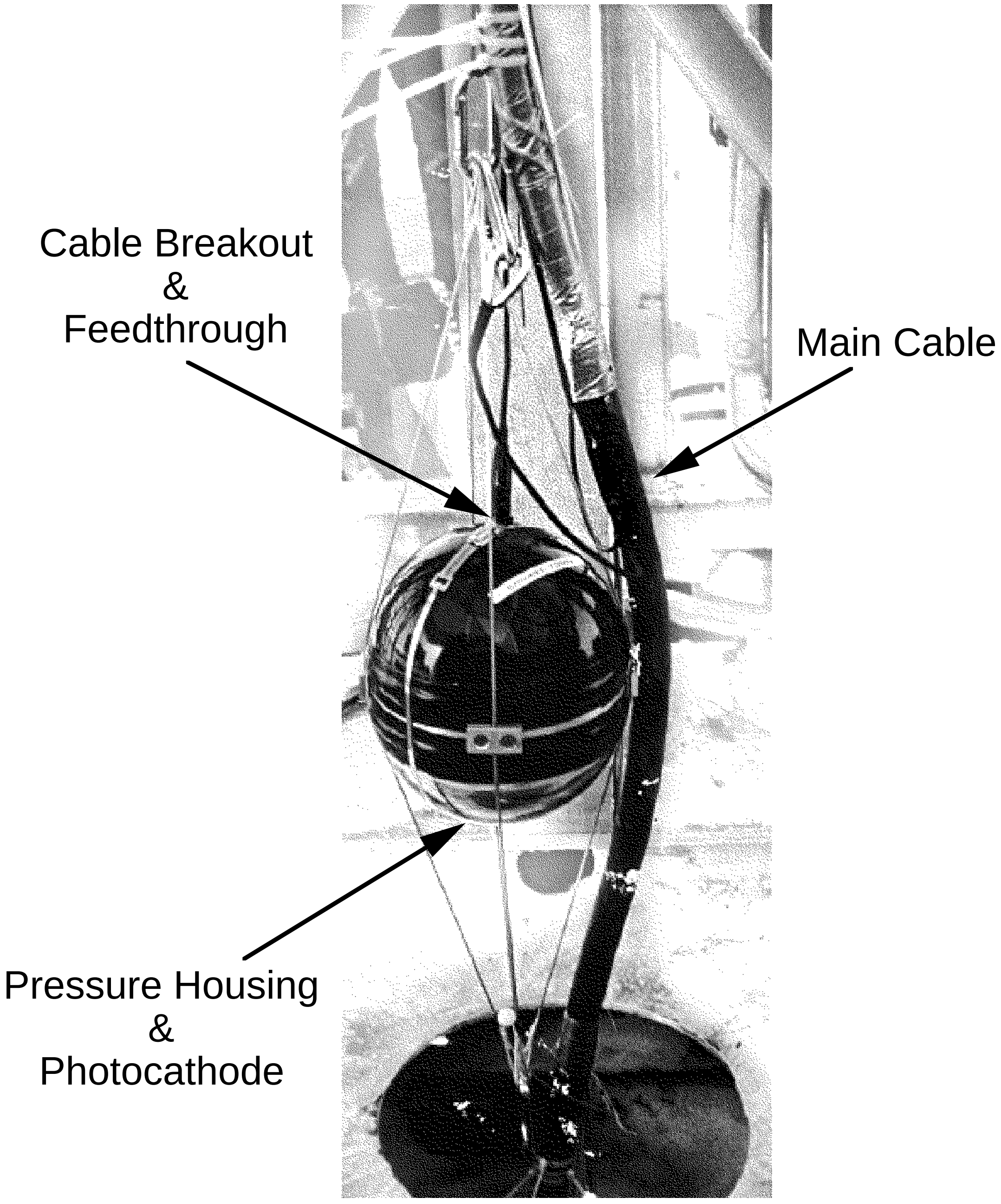

Figure 3.6: An AMANDA-B optical module ready to be lowered into the ice. The module is looking downward.

of projected area at an impact direction θ_{imp}, relative to normal incidence. The function s is measured in the laboratory[15]. The head-on geometrical area $A_{\mathrm{geo}}(0)$ is πR^2_{pmt}.

Photocathode quantum efficiency $QE(\lambda)$. The bialkali photocathode is not completely efficient in converting photons incident on the surface to emitted photoelectrons which make it to the first dynode. The peak efficiency is 30%, and reaches its maximum at 360 nm (see Figure 3.7). The curve is specified in `RAVEN` in the OM parameter (`.pmt`) file, described in Section A.5.2.

Transmission through the glass housing. The Billings glass spheres used in the construction of AMANDA-B have a cutoff in the far blue, rising to the 50% level at $\lambda = 365$ nm, then plateauing at 93%. The transmission efficiency curve $Tx(\lambda)$ is given in Figure 3.8. Like $QE(\lambda)$, this curve is also specified in the `.pmt` file.

Fresnel reflection at the ice/glass/gel interfaces. Some efficiency is lost due to Fresnel reflection at the different optical boundaries (ice-glass, glass-gel, gel-glass). However, the manufacturer quantum efficiency curves include the losses due to Fresnel reflection at an air-glass boundary, which exceed those for the optical modules in ice (since the index of refraction of glass is closer to that of ice than that of air). A correction is thus made which makes a slight wavelength-dependent increase $F(\theta_{\mathrm{imp}})$ to the overall efficiency. The correction is a small one, however (an increase of 7% at normal incidence, becoming larger for large angles θ_{imp}).

Efficiency at the first dynode. The first dynode has a 90% efficiency (ϵ_D) for converting a photoelectron to an avalanch in the dynode chain.

Obscuration due to external structures. Various hardware, including cables and caribiners, obscures a small fraction of the solid angle viewed by the OM. The efficiency ϵ_O used in `RAVEN` is 0.989.

The effective area of an OM is thus given as:

$$A_{\mathrm{eff}}(\theta_{\mathrm{imp}}, \lambda) = s(\theta_{\mathrm{imp}}) A_{\mathrm{eff}}(0) QE(\lambda) Tx(\lambda) F(\theta_{\mathrm{inp}}) \epsilon_D \epsilon_O \tag{3.18}$$

3.6.4 Generation of A_{eff} in `RAVEN`

For the treatment of scattered light in `RAVEN`, the effective area is calculated in `distmc`, in advance of the nested integrations which calculate the fields ΔN_{pe} and N_{pe}. The calculation of A_{eff} in advance greatly speeds up the integration

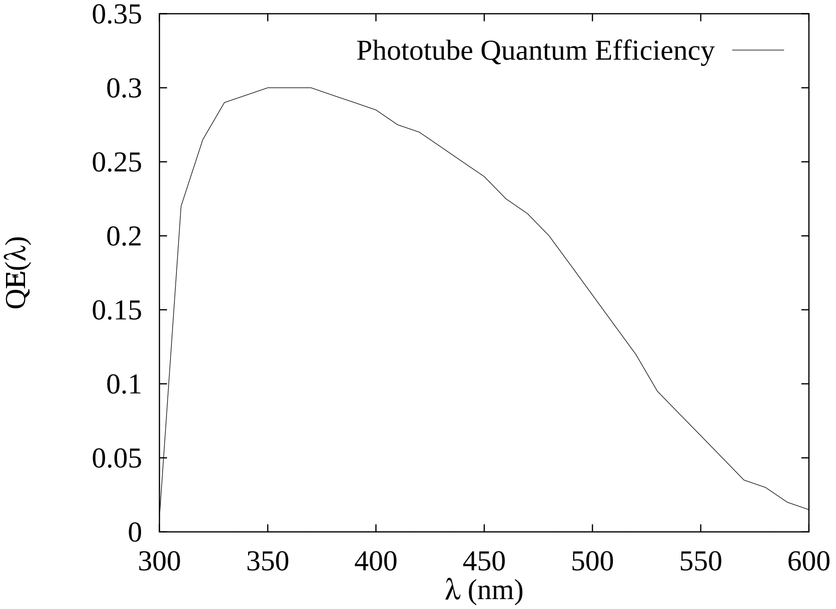

Figure 3.7: Quantum efficiency curve of a photomultiplier tube with a bi-alkali photocathode.

loops. The method used is to calculate A_{eff} for each bin of $\lambda, \cos\theta, \phi, \cos\theta_p$, and ϕ_p, and store the values in a five-dimensional look-up table.

3.6.5 A Final Comment About OM Efficiencies

The effective area of the AMANDA OMs is not measured with great precision (perhaps a few percent) and there are tube-to-tube fluctuations as well which are not accounted for in the simulation (although one could do so by having unique `.pmt` files for each OM). When one requires a large multiplicity N to simulate a trigger, the calculated trigger rate goes like $(A_{\text{eff}})^N$. So, for a 3% error in the phototube area, the resulting shift in the calculated 10-fold rate is a factor $1.3^{10} = 14$. Shifts of a few percent at the level of a single phototube can thus lead to an order of magnitude change in the overall rate. In the absence of extremely accurate data on the OMs, one is reduced to twiddling the module efficiency to match the rate and distribution of the number of hit OMs.

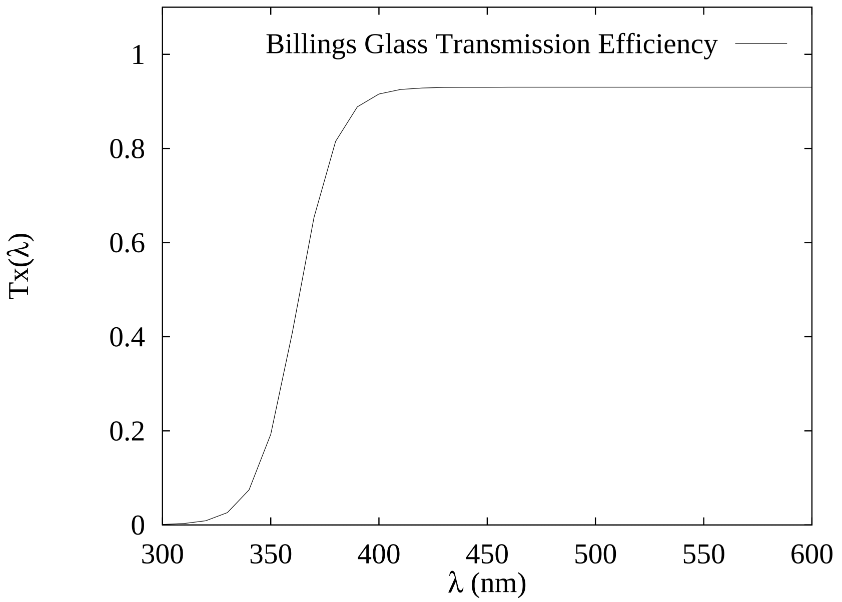

Figure 3.8: The transmission efficiency of the Billings glass housing used in AMANDA-B optical modules.

3.6.6 The Electronics and Data Acquisition System

Once photoelectron times have been generated for an OM, the output of the electronics must be simulated. A lightning-fast summary of the AMANDA-B electronics (muon trigger only) follows:

- Analog signals from the OMs travel from the OM base up the ∼2 km-long cable to the surface.
- Signals from each channel are amplified and then discriminated, sent to the TDCs and ADCs for that channel, and are also sent to the trigger logic. LeCroy peak-sensing (2250) ADC and multihit (2277) TDC modules are used, through a CAMAC interface.
- If enough OM channels "report" to cause a trigger, the trigger logic sends a stop signal to the TDCs and gates the ADCs. The leading edge (TDC) and trailing edge (TDC+TOT) values are determined by the start and end of each channel's logic pulse. Absolute time is supplied by the trigger logic pulse, which arrives at the TDC module after each channel's pulse arrives (common stop).

- A signal from the trigger also informs the computer that an event has occurred. A Macintosh$^{\text{TM}}$ computer reads out the channels in each CAMAC module for each OM, and the event information is written to disk.

More detailed descriptions of the AMANDA electronics and DAQ can be found in References [18] and [19].

For the purposes of simulation, the problem can be reduced to determining TDC, TOT and ADC values for pulses coming from each OM. `RAVEN` considers photoelectron times and simulates the output pulse of each PMT. This is done using a table from a real, digitized, one-photoelectron OM pulse and adding the functions if two or more p.e.s are needed. It then simulates amplification and the LeCroy 4413 discriminator in Burst Guard mode: it searches all crossovers of the threshold value (specified in the `.pmt` file), and forms leading-edge (LE) and trailing-edge (TE) values. The output of the discriminator is a logic pulse whose leading edge gives the TDC value, and whose time-over-threshold (TOT) value is given by TE − LE.

The ADC values are obtained by examining the pulse before discrimination and returning the peak value, within a 2 μsec gate after the first TDC time.

Reference [18] discusses the `RAVEN` simulation of the AMANDA-B electronics in somewhat greater detail.

Chapter 4

Application: Filtering AMANDA-B Events for Neutrinos

> The tome that contained the stellar code, delivered to me with great ceremony, was not especially interesting–at least not at first reading. The beginning went: "0001101010001111100110111111001010010100." The rest was more of the same.
>
> –*His Master's Voice*, [1, p. 82]

4.1 Introduction

This chapter presents a physics analysis of AMANDA-B events, the goal of which is to study a data selection procedure (filter) which enhances the atmospheric neutrino signal relative to the cosmic ray muon background. It provides an opportunity to compare results from the simulation with actual data as a check on the accuracy and completeness of `RAVEN`, as well as give hints about how to proceed with filtering algorithms for an expanded array, to be deployed during the Austral Summer 1996-1997. Chapter 5 shows the predictions for the expanded, 11 string array.

4.2 Introduction to the ν_μ Filter

The motivation for a neutrino filter comes from the inherently weak neutrino-induced muon flux relative to background, and the current bandwidth limitations which prevent us from retrieving data from every triggered event at the South Pole.[1]

For the current 25 Hz data rate in AMANDA-B, we can only retrieve $\sim$ 1000 events per day out of the expected 2.2 million. An experiment which picked

---

[1] Of course, every triggered event is available once the station opens and the actual data tapes are retrieved.

out $1\times10^3/2\times10^6$ muons out of a flux where cosmic rays dominated neutrinos by 10^6 would require 500 days to get one neutrino! Background rates in the 11 string array will likely be even higher (depending on the multiplicity threshold chosen). Filtering will therefore be need to have a reasonable chance of seeing neutrinos without having to wait until the winter season is over. It is also necessary in situations where a Northern Hemisphere source of very high-energy gamma rays produces a burst, and one wishes to immediately search for a corresponding neutrino burst.

The core of the filtering procedure discussed below is a line fit to optical module position vs. time. The idea is simple, but the technique provides a significant increase in signal strength relative to the background. The line fit can be calculated quickly and analytically, and so can be of use both as a filter in the data acquisition stream, and as a useful "first guess" as to the track direction and position, which can be passed on to more complete and time-consuming iterative fit procedures (which ultimately will provide better angular resolution).

4.3 AMANDA-B Data Extraction and Preprocessing

For this analysis, the following AMANDA-B muon data files were used:

`ab230_128-96-0.bin`   `ab230_128-96-1.bin`

The files contained 183562 raw triggers. We ran a program (`newamab`) based on R. Porrata's C program to unpack the raw data files. This writes events in the `.evt` format (see Section A.4). Only events with event register=2 were processed. Raw leading edges, ADCs and TOTs for the remaining 132713 8-fold events were written to the `.evt` files. The measured rate for these events was 25. Hz.

4.4 Monte Carlo Event Generation

The ice properties were simulated in `photon_table` and `distmc`. 10000 photons were generated using the HG model (see Section 3.4.1), into a photon field with the following binning:

Variable	Number of bins
ρ	200
$\cos\psi$	6
$\cos\theta$	6
ϕ	4
t	300

The mean free path between scattering centers was $\Lambda_{\mathrm{geo}} = 5$ meters, and $\langle\cos\theta_{\mathrm{scatt}}\rangle = 0.8$. In `distmc`, the binning for the OM orientations ($\cos\theta_p$,ϕ_p) was kept the same as that for the photon direction. The peak absorption length was 92 meters; the absorption curve can be seen in Figure 4.1

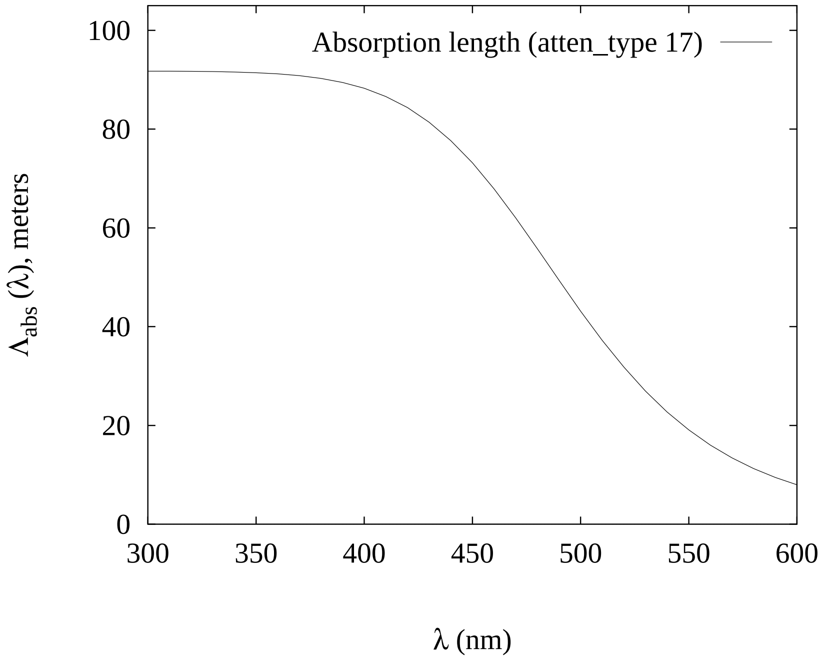

Figure 4.1: Absorption length curve used for event generation. The `atten_type` value used in `distmc` was 17.

The resulting N_{pe} field was written to disk and used in `genevent` for the generation of cosmic ray muon and atmospheric neutrino events.

4.4.1 Muon event generation

The cosmic ray muon event rate is ultimately governed by the flux of primary air showers in the atmosphere. These are calculated with a program `SYBILL/airshow` which simulates the air showers and determines the muons which penetrate to the surface of the ice. The simulation reflected the following:

The composition of the cosmic ray primaries. A variety of composition models are possible; only proton primaries were used for this simulation.

The atmospheric density profile and altitude of the surface of the ice. The appropriate values for the South Pole were used.

The energy spectrum of the primaries. The measured primary cosmic ray spectrum was used, reflecting the "knee" of the spectrum at 3×10^6 GeV. The proton primaries had energies ranging from 0.8 to 10^4 TeV.

The detector depth. Proton primaries were generated with zenith angles up to 72 degrees (giving a solid angle Ω_{gen} of 2.842 sr once the projection of the isotropic flux onto the flat test area is included) and the air showers they induced were propagated through the atmosphere. Events with muons of 400 GeV or more were kept and propagated through the ice to a depth of 1300 meters.

$N_{\mathrm{gen}} = 7.0143 \times 10^7$ proton primaries were simulated such that the axis of the shower core pointed into a circle whose radius R_s was 6833 meters. The measured proton primary flux is[27]:

$$\Phi_{\mathrm{prim}} = 8.8193 \times 10^{-2}\ \frac{\mathrm{protons}}{\mathrm{m}^2\ \mathrm{sec\ sr}}.$$

Since the number of events generated, the area and the solid angle are known, one can determine the time T_{gen} corresponding to this set of events:

$$T_{\mathrm{gen}} = \frac{\Phi_{\mathrm{prim}}}{\Omega_{\mathrm{gen}}\ N_{\mathrm{gen}}\ \pi R_s^2}.$$

This yields $T_{\mathrm{gen}} = 1.9092$ seconds.

Out of N_{gen} primaries, $N_s = 3334244$ events survived to yield muons of 400 GeV or more on the surface (400 GeV was chosen since the minimum energy required to reach 1300 meters is about 425 GeV). These events were "recycled" 10 times, varying the position on the surface, to improve statistics. The corresponding time duration T was thus 19.092 seconds. The recycled events were propagated to a physics plane of 1300 meters of depth (400 meters above the center of AMANDA-B), using the energy-loss routines described in Section 2.4.1 and Reference [13]. The events were kept if their shower core was within $R_d = 2832$ meters of the origin of the physics plane, and if any muons survived. The test area $A_{\mathrm{test}} = \pi R_d^2$ was 2.52×10^7.

2858596 events containing 3474311 muons remained, making the rate of events R_{test} passing through the test area equal to 1.50×10^5 Hz. The flux of muons at 1300 meters was thus 7.22×10^{-3} muons/(m^2 sec).

Muon bundles, comprising numbers of muons and their starting points, energies and directions, were passed in an input file to `genevent` (`multimus` option).

For muons from atmospheric neutrinos, the Volkova[10] atmospheric neutrino flux was invoked with the `atmospheric_nus` command. Energies and nadir angles were sampled from an existing distribution, and starting points of muons were generated uniformly throughout a test volume $V_{\text{test}} = 1.93255 \times 10^{10}$ m^3. The test volume extended to the sides and below the detector (554 m $< z <$-2180 m, radius 1500 meters). The rate of $\nu_\mu \to \mu$ conversions in ice (with muon energy $E_\mu > 10$ GeV) was taken to be 7.26×10^{-11} Hz/m^3[28], based on the convolution of the atmospheric neutrino flux, energy-dependent cross-section and nucleon density within the ice. This gives the $\nu_\mu \to \mu$ rate within V_{test} as 1.40 Hz.

Angle and energy distributions for both sources are shown in Figure 4.2.

4.4.2 Simulating the detection of muons

In `genevent` (as well as for analysis of real data), the optical module coordinates were taken from the AMANDA internal memo on the laser calibration of the detector, by Adam Bouchta [26]. The geometry included the relative offsets in the z-direction, but assumed the strings were parallel to one another. It also specified which tubes looked up, which looked down, and which were dead.

Dark noise hits were included at a rate of 560 Hz per channel (this is a conservative overestimate of the noise for the majority of channels).

Muons were propagated to their end points, using `physics_code` of 3, which caused additional light output from muon-induced electromagnetic showers to be included with the minimum-ionizing Čerenkov radiation (see Section 3.4.5).

Events with 8 or more OMs hit were written to `.evt` files. Sample events, viewed with the `scanner` program, can be found in Figures 4.3 and 4.4.

The rates for 8-fold events were:

Source	Rate R_8 (Hz)	R_8 (/day)
Data	25.	2.16×10^6
MC μs	28.3 Hz	2.44×10^6
MC νs	4.04×10^{-5}	3.49

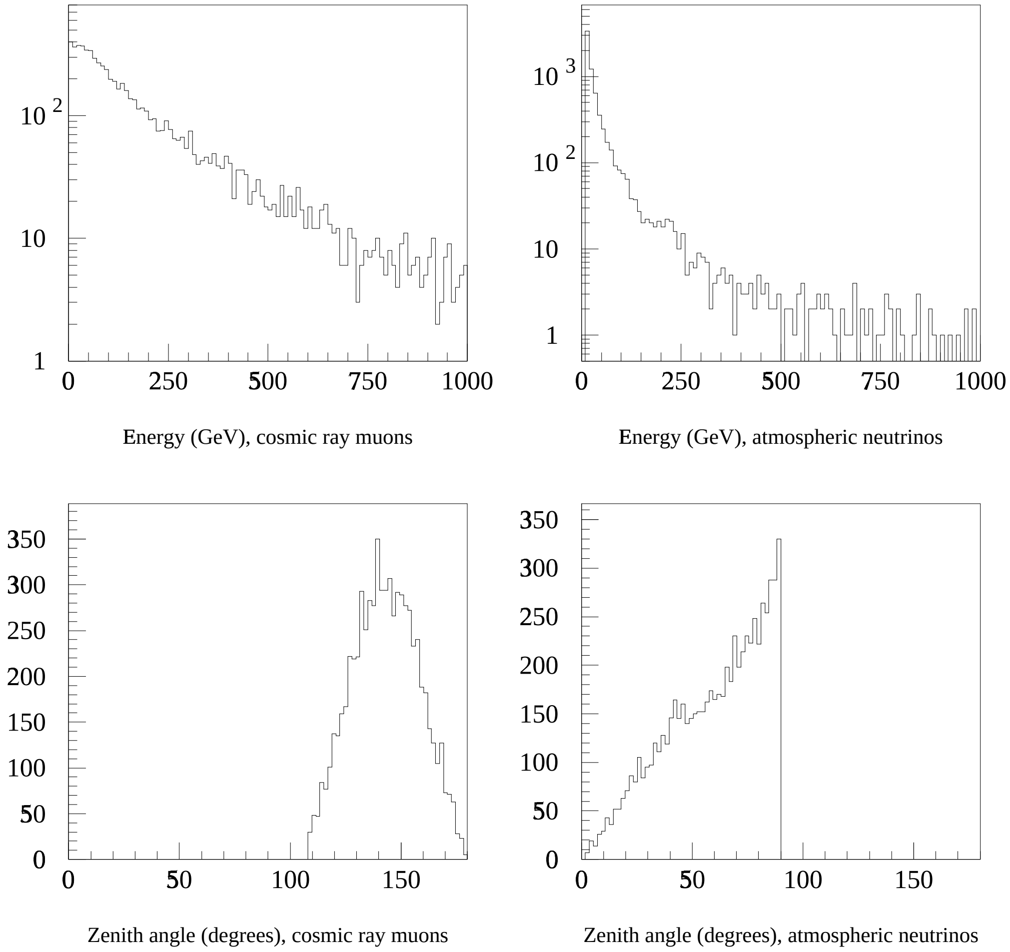

Figure 4.2: Energy and angular distributions for simulated cosmic ray muons (at the physics plane) and muons from atmospheric neutrinos, before detection.

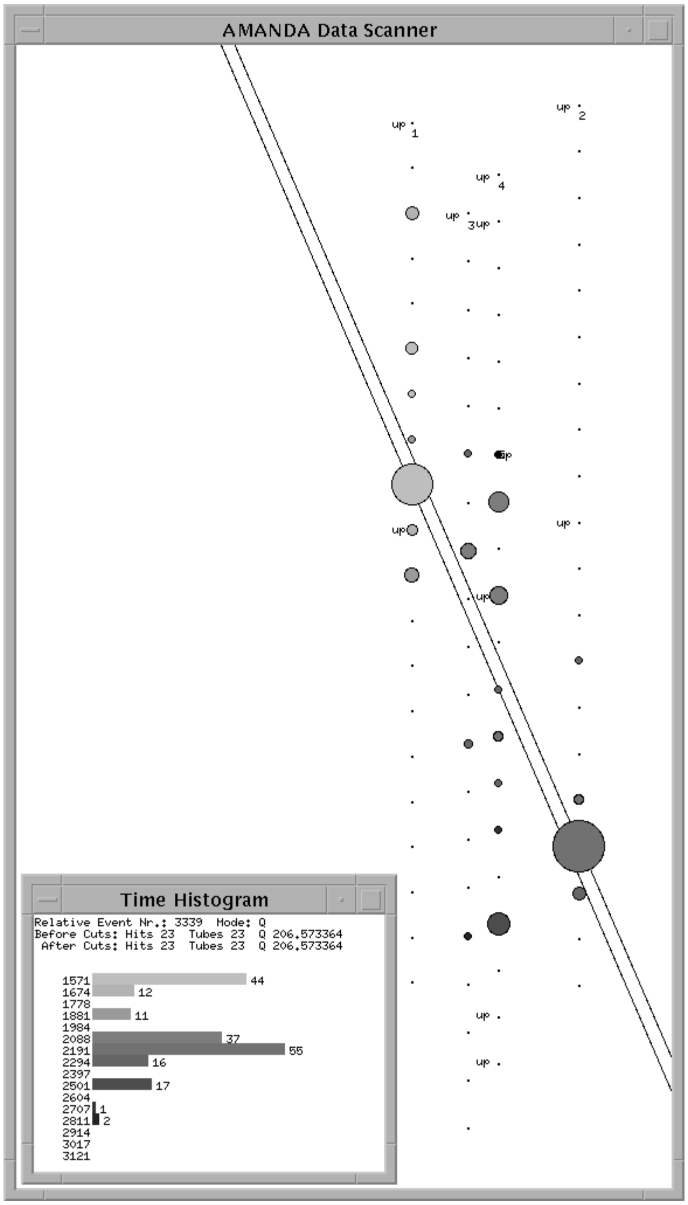

```
Relative Event Nr.: 3339  Mode: Q
Before Cuts: Hits 23  Tubes 23  Q 206.573364
 After Cuts: Hits 23  Tubes 23  Q 206.573364
```

Figure 4.3: Sample simulated cosmic ray muon bundle event in AMANDA-B containing two muons. The hit OMs are represented by open circles; dark circles are later than light ones, and the size of the circle corresponds to the pulse height (ADC) in that OM.

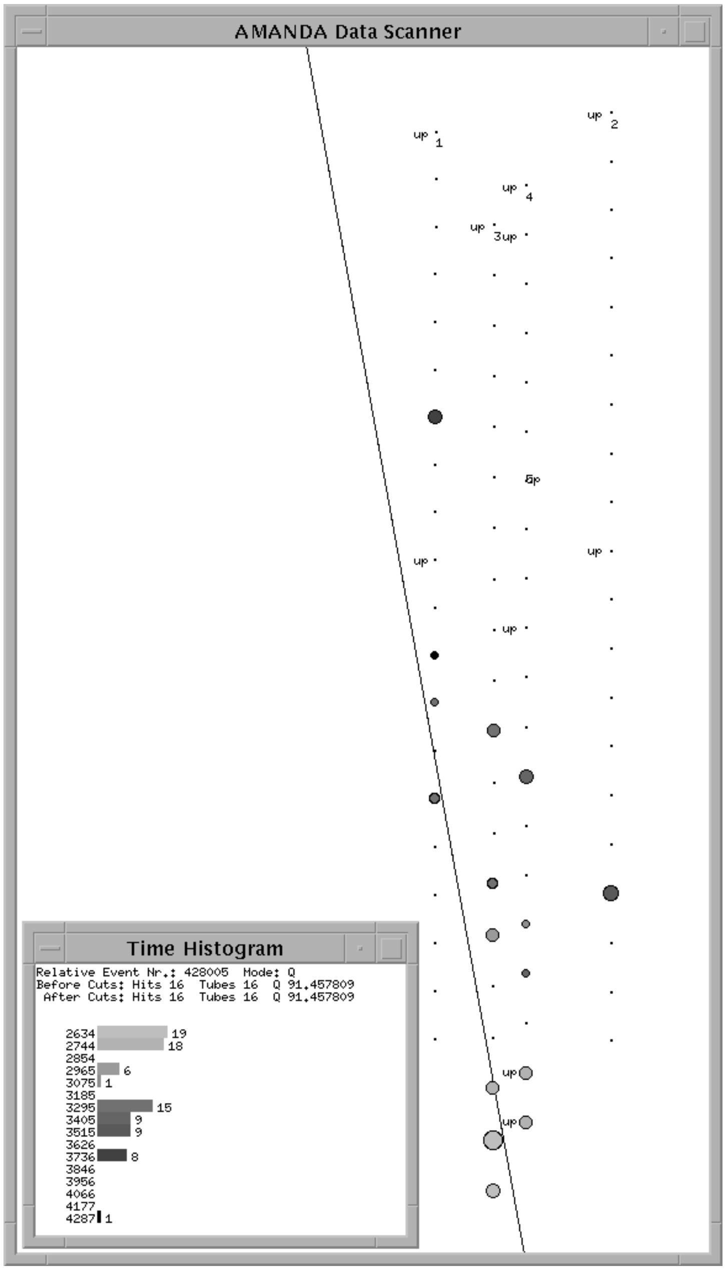

```
Relative Event Nr.: 428005  Mode: Q
Before Cuts: Hits 16  Tubes 16  Q 91.457809
 After Cuts: Hits 16  Tubes 16  Q 91.457809
```

Figure 4.4: Sample simulated atmospheric neutrino event in AMANDA-B.

Multiplicity (N_{hit}) distributions can be seen in Figure 4.5. The distribution for Monte Carlo multimuons is slightly steeper than for data; this is most likely due to an underestimate in the simulation of the effective area of the phototube, to which the N_{hit} distributions are particularly sensitive. See Section 3.6.5. This effect can be eliminated by adjusting the OM efficiencies which are input to the simulation.

The energy threshold of the array can be determined by an examination of the lower end of the energy distributions for triggering events (Figure 4.6). The 8-fold trigger threshold of AMANDA-B is seen as roughly 125 GeV for cosmic ray events, and 10 GeV for atmospheric neutrino-induced muons.

4.5 Event Selection and Processing

Data and Monte Carlo event files in the `.evt` format were passed to `anaboth`. After reading in the event information, `anaboth` performed timing offset and pulse height slewing corrections (data only, based on corrections measured during the laser calibration). Only the first leading edge time was used for each channel. The hit times are required to come from a 8000 nsec window, starting at 0 for MC and 17,500 nsec for data. OMs 1-80 only were used (OMs on twisted pair cables were eliminated). Also, hits coming 1 μsec earlier than any subsequent hits were tossed out. Figure 4.7 shows the cleaned, corrected TDC distributions.

After eliminating unwanted hits, we demanded finally that the event have a series of eight or more hits, with each hit less than two μsec from the previous hit ("overlapping 8-fold" condition).

4.6 The Line Fit

For each event, the N surviving hits characterized by TDC times t_i and OM coordinates $\mathbf{x}_i$ were fit to an equation of the form

$$\mathbf{x}_i^p = \mathbf{x}_0 + \mathbf{v}t_i. \tag{4.1}$$

This was done by minimizing the total χ^2:

$$\chi^2 = \sum_{i=1}^{N} (\mathbf{x}_i^p - \mathbf{x}_i)^2 = \sum_i \chi_i^2. \tag{4.2}$$

Since the deviations of the $\mathbf{x}_i$ are not distributed normally, χ^2 does not follow the canonical χ^2 distribution; χ^2 should just be looked at as some fitting function to be minimized.

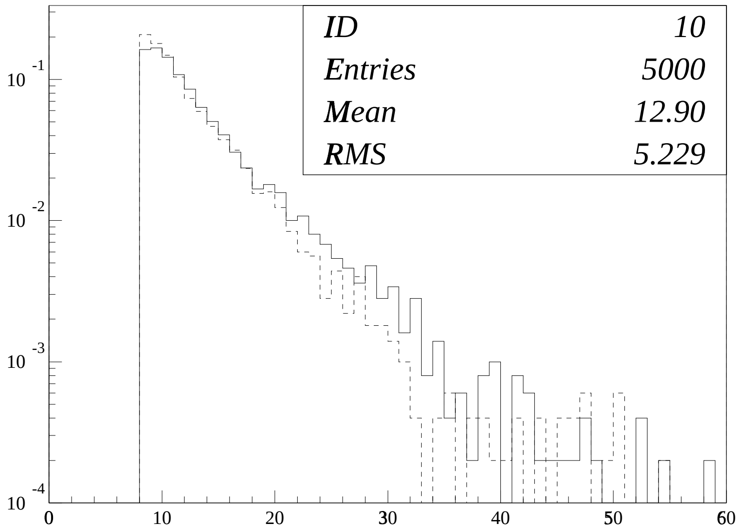

Hit multiplicity, multi-muons, data (solid) and MC (dashed)

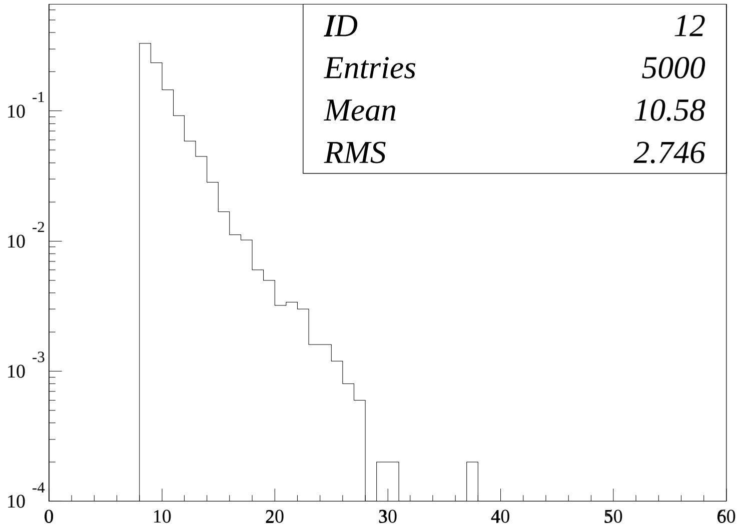

Hit multiplicity, Monte Carlo atmospheric neutrinos

Figure 4.5: Hit multiplicities after cleaning and time corrections, for data, MC multiple muon events, and atmospheric neutrino events.

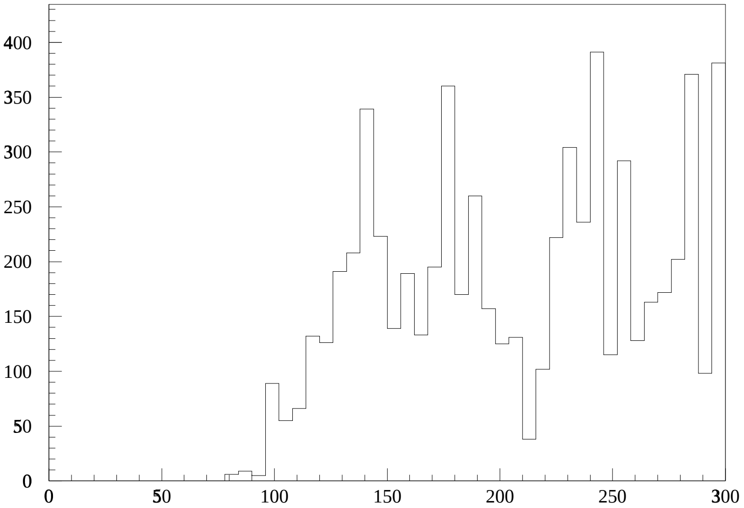

Total muon energy (GeV) in event, MC multimus

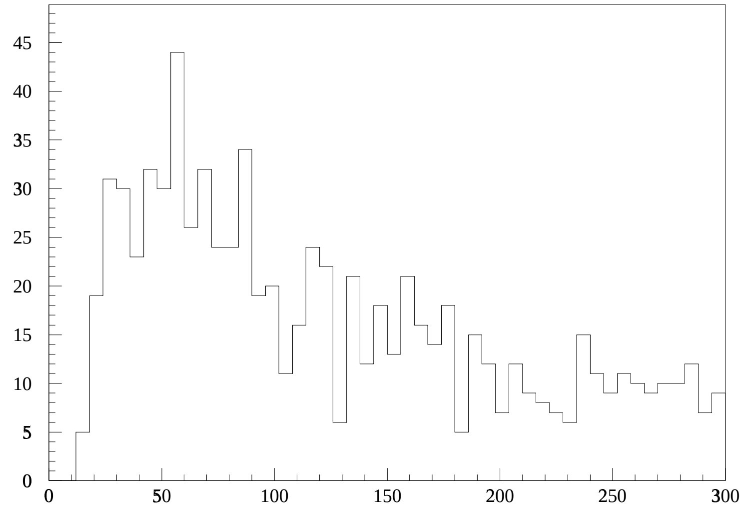

Muon energy (GeV), Monte Carlo atmospheric neutrinos

Figure 4.6: Total muon energies for triggering cosmic-ray muon events (top) and single muon energies for muons from atmospheric neutrinos (bottom). The energy threshold of the array for cosmic ray muons is seen as roughly 125 GeV for cosmic ray events, and 10 GeV for atmospheric neutrino-induced muons. Only the lower end of the distribution is shown.

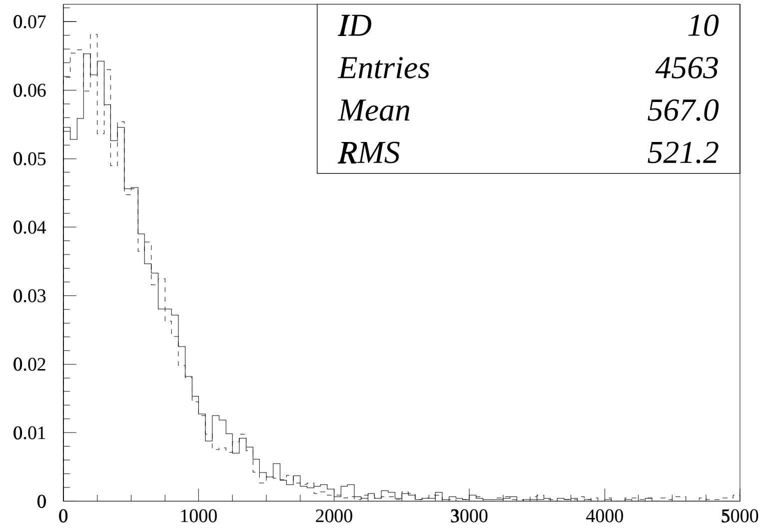

Corrected, cleaned TDCs, data (solid) and MC (dashed)

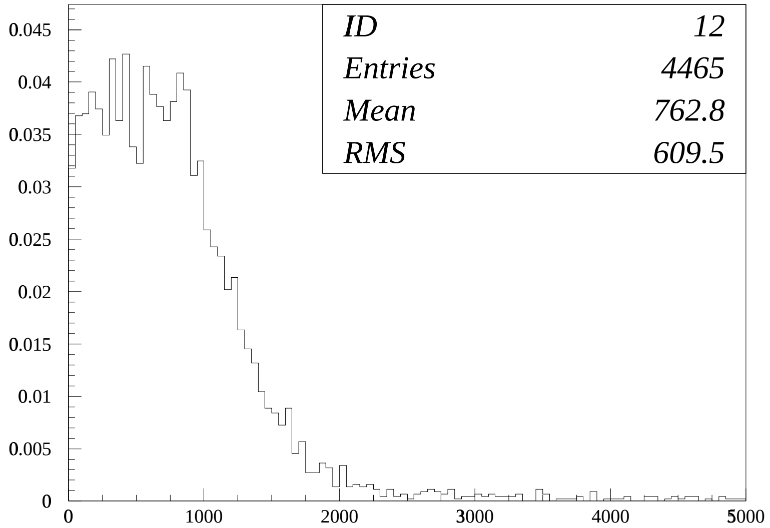

Corrected, cleaned TDCs, atmospheric neutrinos

Figure 4.7: Corrected TDC values for both Monte Carlo and data events (times are relative to the first time in the event; first time not shown).

Setting the derivatives

$$\frac{\partial \chi^2}{\partial \mathbf{x}_0} = \frac{\partial \chi^2}{\partial \mathbf{v}} = 0, \tag{4.3}$$

one obtains

$$\mathbf{v} = \frac{N \sum_i \mathbf{x}_i t_i - \sum_{ij} \mathbf{x}_i t_j}{N \sum_i t_i^2 - \sum_{ij} t_i t_j} \tag{4.4}$$

and

$$\mathbf{x}_0 = \frac{1}{N} \sum_i \mathbf{x}_i - \mathbf{v} t_i. \tag{4.5}$$

In the first stage of the fit, the above procedure was used. The second stage involved the elimination of hits before re-fitting. Information in each OM's chi-squared term to reject noisy or very scattered hits. Each hit's contribution to the chi-squared was examined; if the partial chi-squared χ_i^2 for that term was greater than 5000 m^2, the hit was rejected. In addition, hits coming more than 1500 nsec after the beginning of the event were rejected, and hits isolated from their nearest neighbors in time by more than 300 nsec were eliminated as well.

After all hits were examined, the fit was performed again. If the number of hits used for the fit N_{used} was less than 9, the event was rejected.

It should be noted that χ^2 is essentially an event-shape variable: events which lie purely along a linear, constant velocity trajectory will have zero χ^2; fatter events or events with odd time sequences will have large χ^2. The distributions for χ^2 are in Figure 4.8.

Events were kept only if χ^2/N_{used} was less than 2500 m^2. The results of the fit for these events can be seen in Figures 4.9 and 4.10. The z-velocity can clearly be seen to provide some discrimination between up- and down-going events. Interestingly, the total velocity peaks at less than c for each case. This is due to scattering: hits from scattered photons arrive late and increase the duration of the event, which decreases the velocity.

At this point, an visual examination of background events with upward velocity and reasonable χ^2 showed that some events still did not consist of well-formed lines of hits with time increasing from one end of the line to the other. In certain events, the direction of time flow was along a very different direction from the geometric alignment of the hits. Figure 4.11 illustrates this. In order to reject these events, a cut was placed on $|\hat{\mathbf{d}} \cdot \hat{\mathbf{t}}|$, where $\hat{\mathbf{d}}$ was the direction of the track fitted using purely geometric information (fitting x and y as linear functions of z), and $\hat{\mathbf{t}}$ was the direction of the time-based line fit. The requirement then imposed was $|\hat{\mathbf{d}} \cdot \hat{\mathbf{t}} > 0.9|$. Distributions of $|\hat{\mathbf{d}} \cdot \hat{\mathbf{t}}|$ can be see in Figure 4.12.

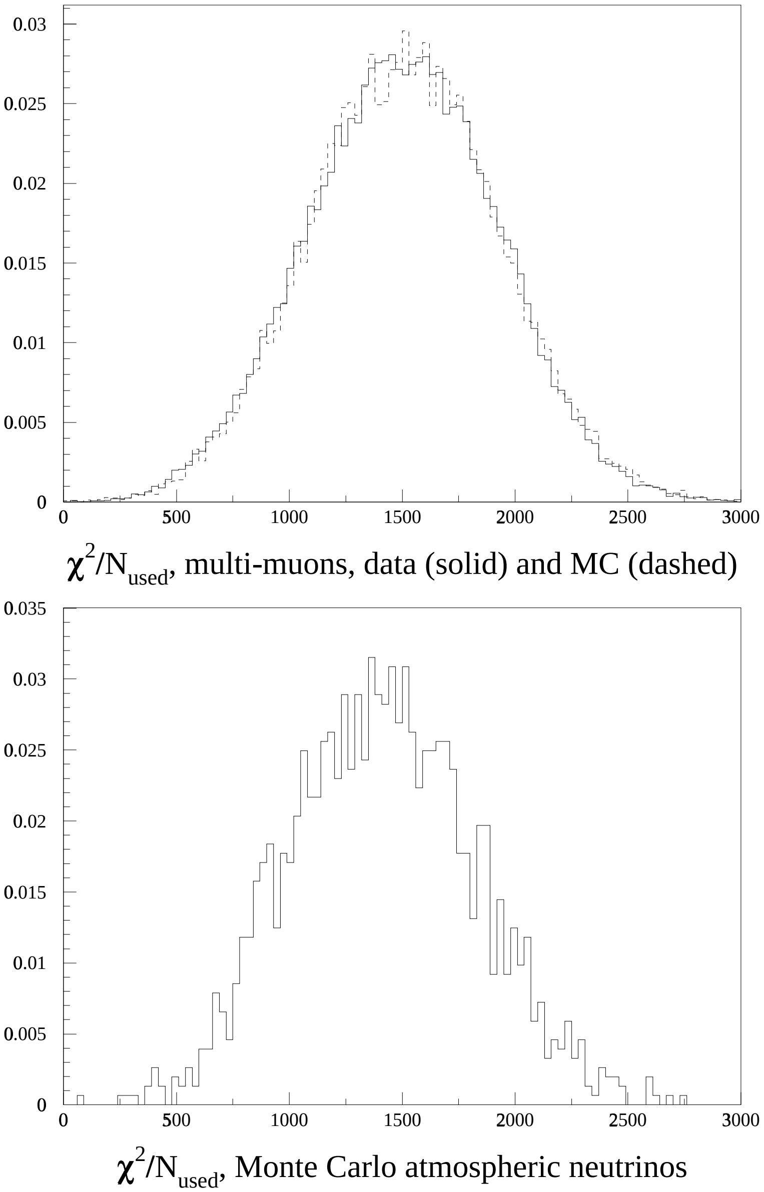

Figure 4.8: $\chi^2/N_{\mathbf{used}}$ (m^2) for data and Monte Carlo fitted events.

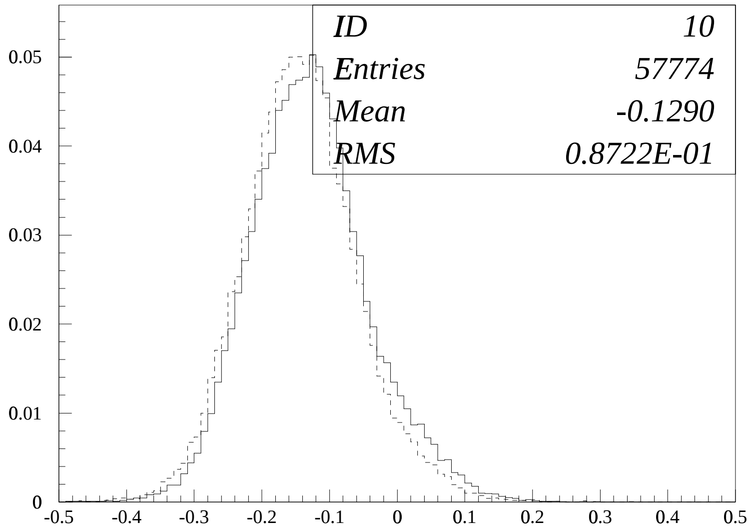

v_z (m/nsec), CR multi-muons, data (solid) and MC (dashed)

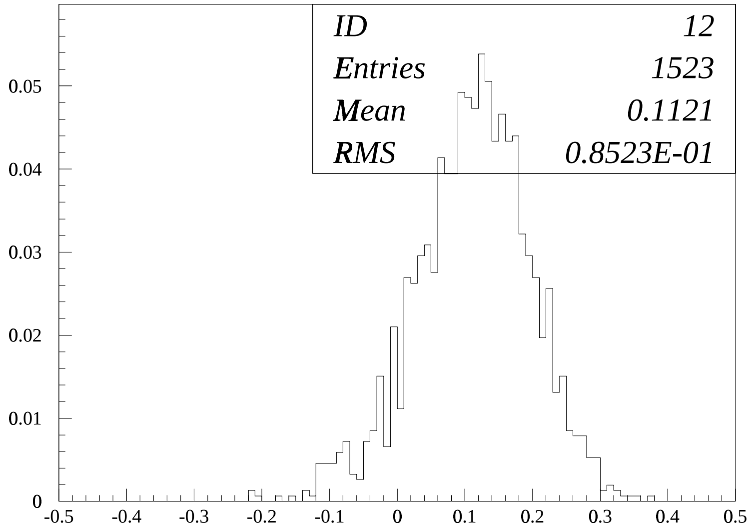

v_z (m/nsec), Monte Carlo atmospheric neutrinos

Figure 4.9: v_z (m/nsec) for data and Monte Carlo, after χ^2 cut.

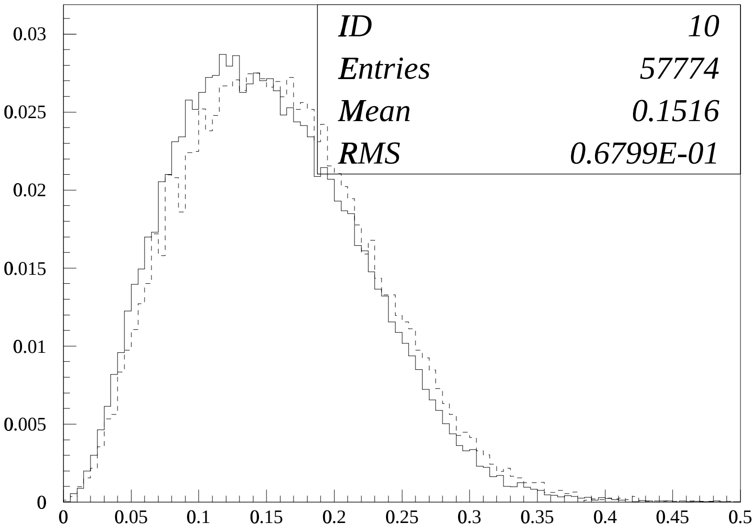

Velocity v (m/nsec), Data (solid) and MC multimus (dashed)

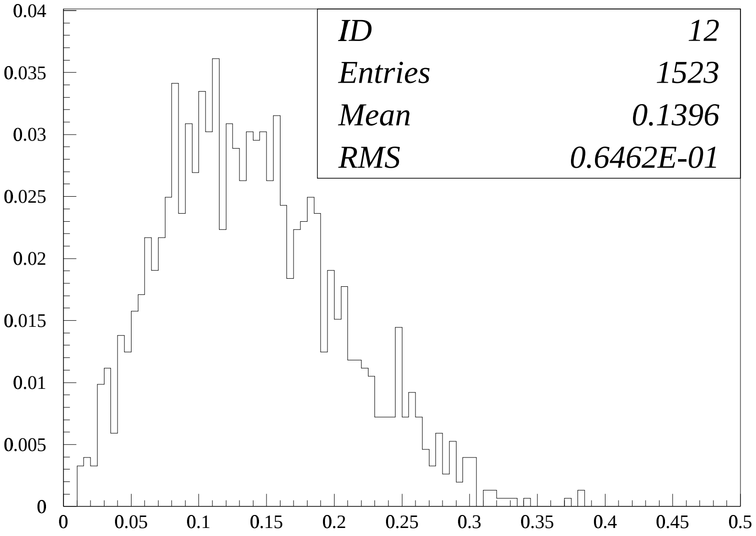

Velocity v (m/nsec), Monte Carlo atmospheric neutrinos

Figure 4.10: Total velocity $|\mathbf{v}|$ (m/nsec) for data and Monte Carlo, after χ^2 cut.

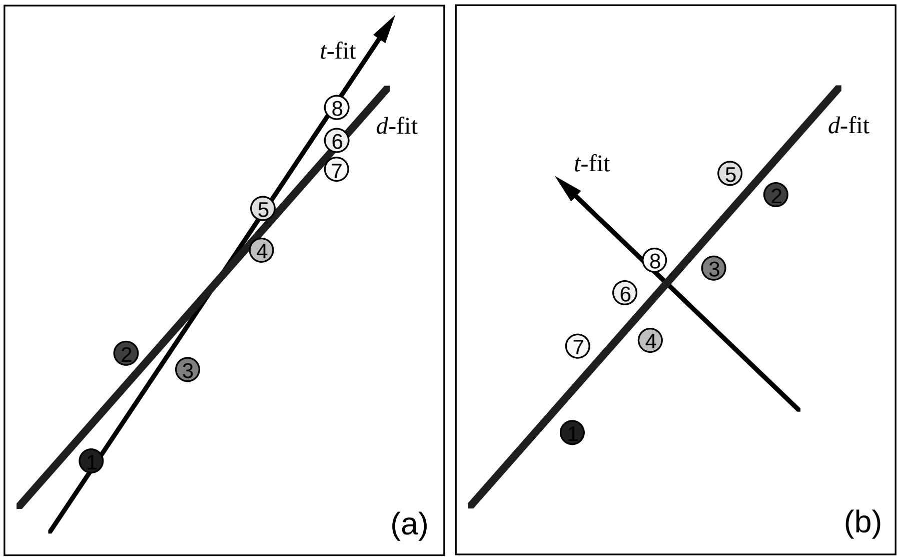

Figure 4.11: Well-fitted (a) and poorly-fitted (b) tracks. In (a), the dot product of the t-fit and d-fit directions is close to 1. In (b), time increases in a direction opposite the direction of the fit geometric track distance, and $\hat{\mathbf{d}} \cdot \hat{\mathbf{t}}$ is close to zero. The requirement in this analysis was $\hat{\mathbf{d}} \cdot \hat{\mathbf{t}} > 0.9$.

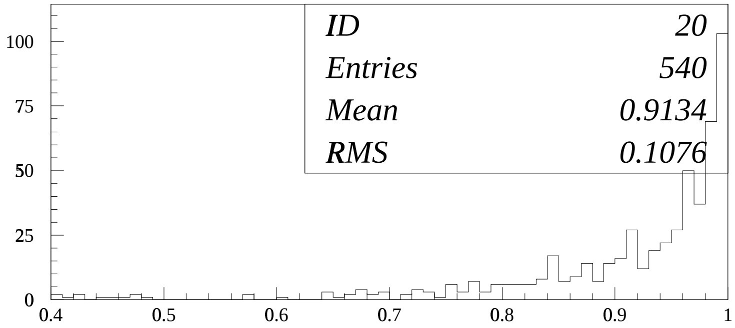

|d • t|, data

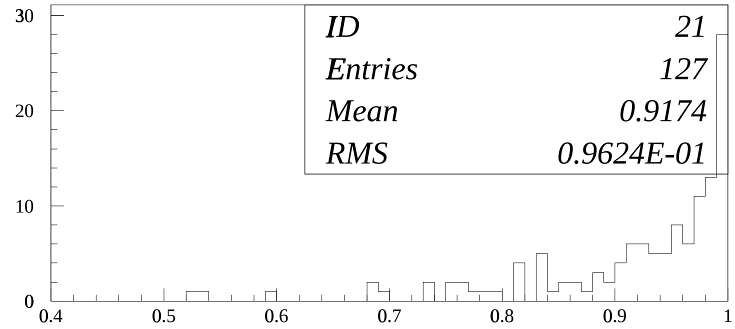

|d • t|, MC multimuons

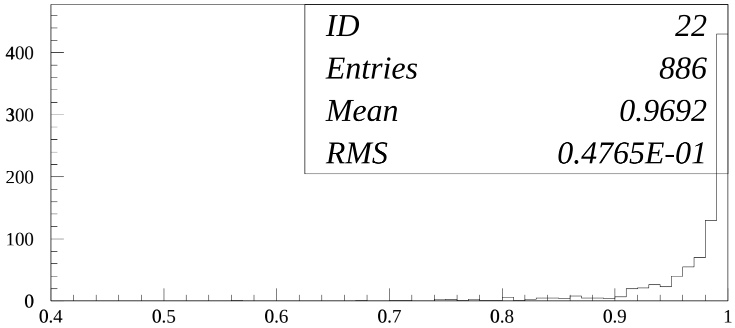

|d • t|, MC neutrinos

Figure 4.12: Distributions of $|\hat{\mathbf{d}} \cdot \hat{\mathbf{t}}|$ for data and Monte Carlo. Events with $|\hat{\mathbf{d}} \cdot \hat{\mathbf{t}}| < 0.9$ were rejected.

4.7 Other Event Variables

We also examined another variable, namely Z_{diff}, the average z-coordinate for the OM hits coming during the first half of the duration of the event minus the average z for the second half of the event. This also clearly discriminates between up- and down-going events. See Figure 4.13. Since Z_{diff} is highly correlated with z-velocity, requiring $Z_{\text{diff}} < 0$ doesn't significantly change signal or background rate when $v_z > 0.1$ m/nsec. However, Z_{diff} is calculable very quickly, so it is useful for real-time data filtering.

Yet another variable discussed in a previous analysis[23] was R_Q, the ratio of the sum of ADCs in the first half of the event to the total sum of ADCs. That quantity is shown in Figure 4.14. A cut was placed demanding $R_Q < 0.6$, providing a modest increase in signal/background.

4.8 Event Rate Calculation

Based on the 8-fold rates given in Section 4.4.2, one can calculate the event rate due to the progressive series of applied cuts. If N_{pass} is the number of events passing the cuts, then the rate for that sequence of cuts is given by

$$R_{\text{pass}} = R_8 \, \frac{N_{\text{pass}}}{N_8}.$$

The rates for the sequence of cuts proposed as an AMANDA-B filter are as follows (errors are statistical):

Cut	Data rate (Hz)	MC μ rate	MC ν rate
Raw 8-folds	25.	28.3	5.7910^{-5}
Overlapping 8-folds	22.	21.0	$(4.36 \pm 0.06)10^{-5}$
Usable fit 8-folds	19.	16.6	$(2.93 \pm 0.05)10^{-5}$
Successful fit	11.	8.41 ± 0.05	$(1.24 \pm 0.03)10^{-5}$
$Z_{\text{diff}} < 0$	1.2	0.743 ± 0.016	$(1.08 \pm 0.02)10^{-5}$
$R_Q < 0.6$	0.25 ± 0.01	0.194 ± 0.008	$(6.16 \pm 0.22)10^{-6}$
$\chi^2/N_{\text{used}} < 2500\text{m}^2$	0.25 ± 0.01	0.191 ± 0.008	$(6.11 \pm 0.22)10^{-6}$
$\hat{\mathbf{d}} \cdot \hat{\mathbf{t}} < 0.9$	$(7.1 \pm 0.3)\ 10^{-2}$	$(6.02 \pm 0.46)\ 10^{-2}$	$(4.65 \pm 0.19)10^{-6}$
$v_z > 0.1$ m/nsec	$(1.4 \pm 0.2)\ 10^{-2}$	$(6.57 \pm 1.51)\ 10^{-3}$	$(3.89 \pm 0.18)10^{-6}$
Final (events/day)	1200 ± 140	568 ± 130	0.33 ± 0.02

The signal efficiency starting with 8-fold events is about 1/15. The efficiency for muon data is 1/1800; for Monte Carlo, it is 1/4300. Events passing the cuts are shown in Figures 4.15-4.17.

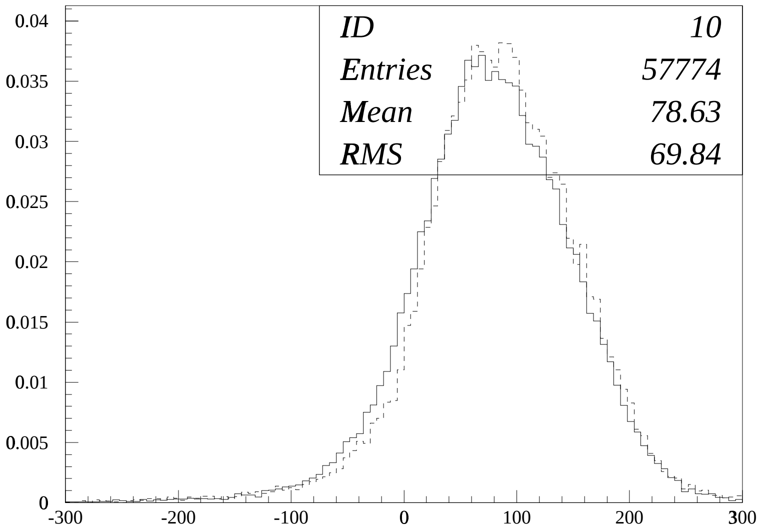

Z_{diff}, data (solid) and MC multimuons (dashed)

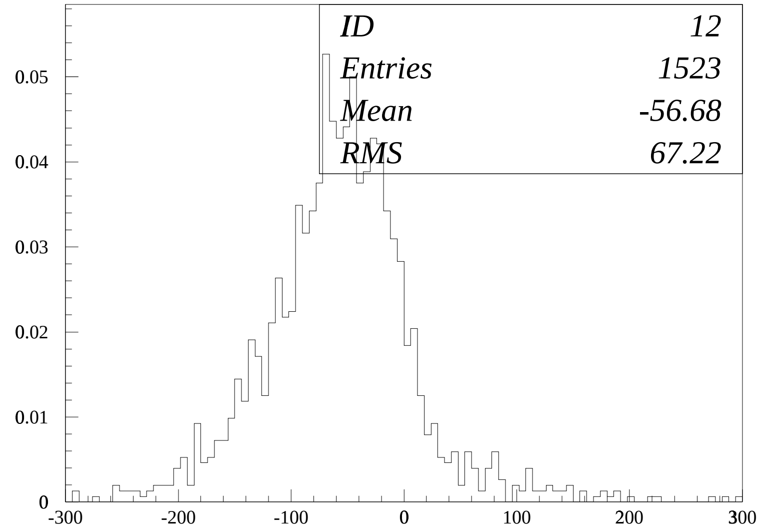

Z_{diff}, MC neutrinos

Figure 4.13: Z_{diff} for data and Monte Carlo, for fitted events.

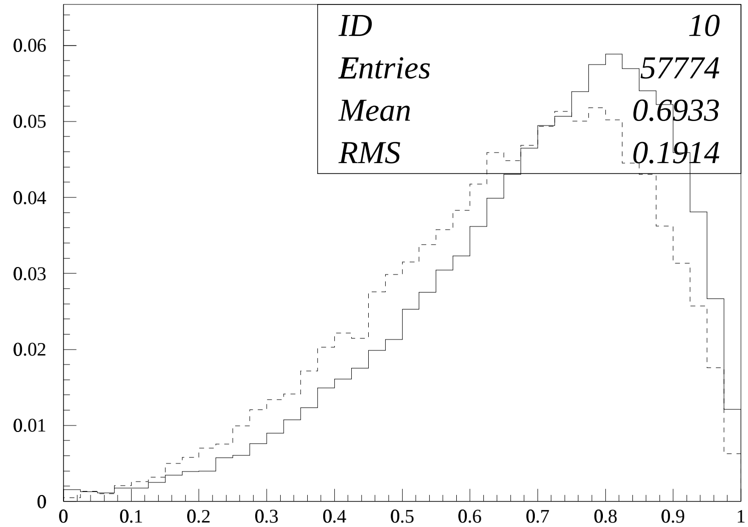

R_q distribution, data (solid) and MC multimus (dashed)

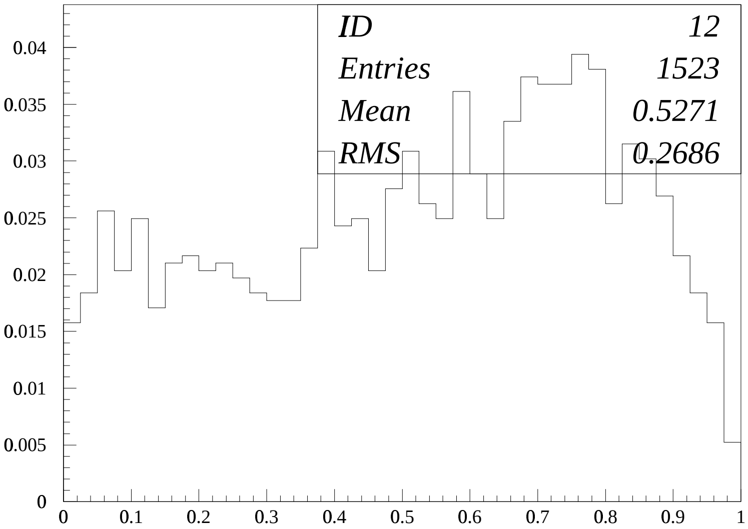

$\mathbf{R}_q$ distribution, Monte Carlo atmospheric neutrinos

Figure 4.14: The variable R_Q for fitted events.

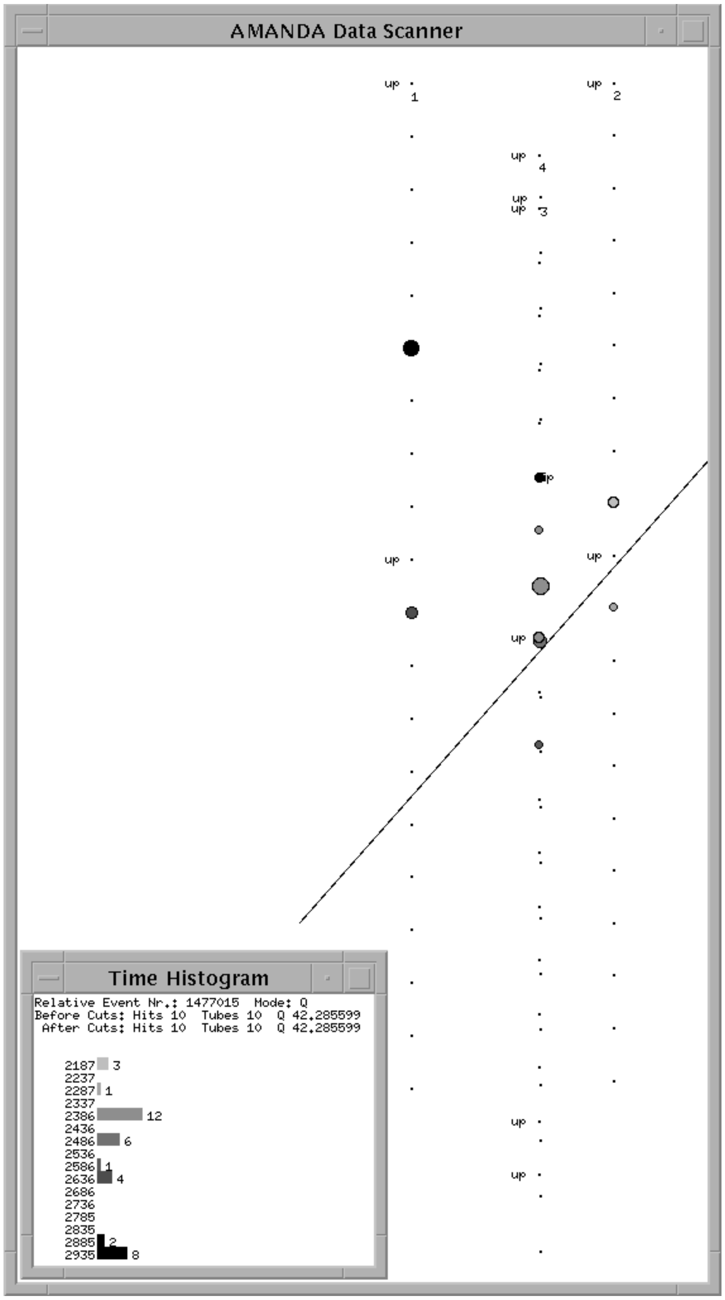

```
Relative Event Nr.: 1477015  Mode: Q
Before Cuts: Hits 10  Tubes 10  Q 42.285599
 After Cuts: Hits 10  Tubes 10  Q 42.285599
```

Figure 4.15: Simulated cosmic ray muon bundle which passes the filter.

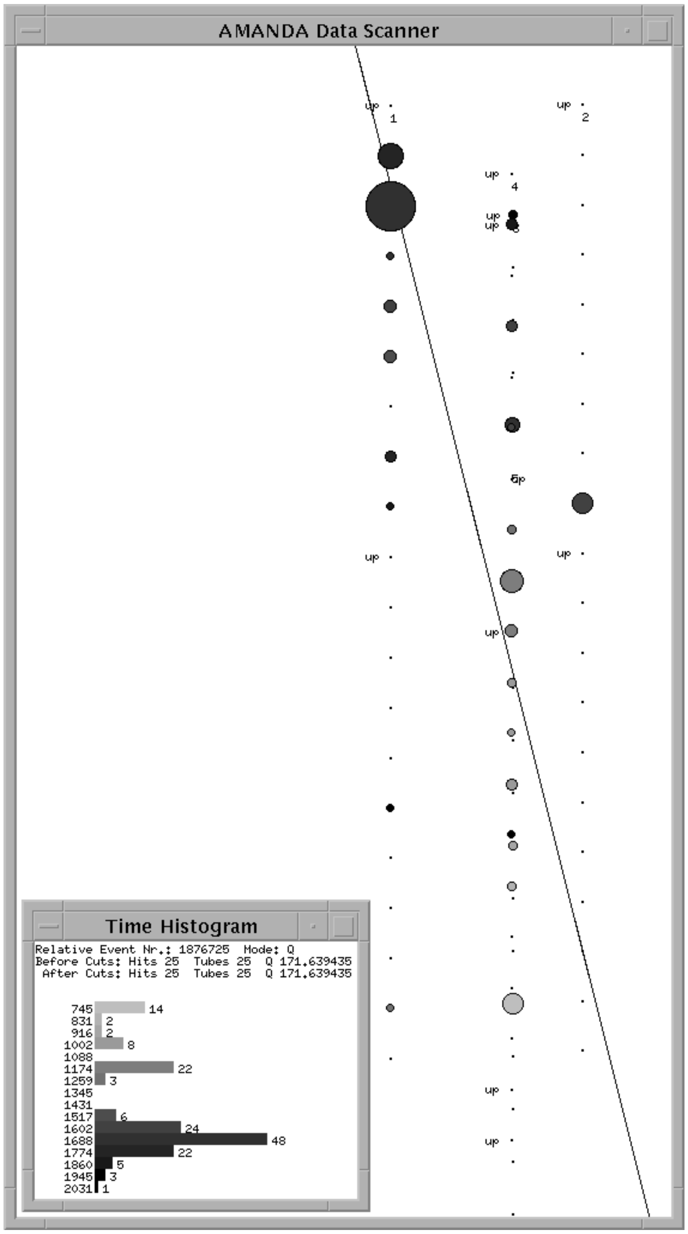

```
Relative Event Nr.: 1876725  Mode: Q
Before Cuts: Hits 25  Tubes 25  Q 171.639435
 After Cuts: Hits 25  Tubes 25  Q 171.639435
```

Figure 4.16: Simulated atmospheric neutrino-induced muon event which passes the filter.

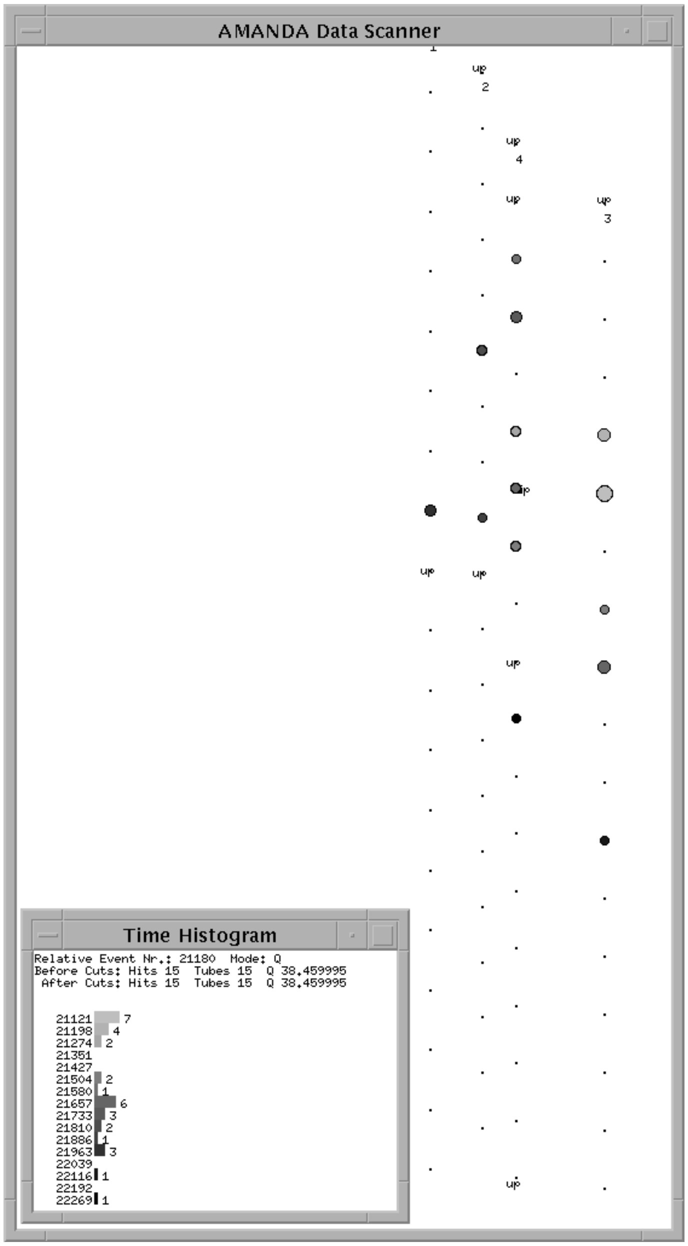

```
Relative Event Nr.: 21180  Mode: Q
Before Cuts: Hits 15  Tubes 15  Q 38.459995
 After Cuts: Hits 15  Tubes 15  Q 38.459995


   21121 7
   21198 4
   21274 2
   21351
   21427
   21504 2
   21580 1
   21657 6
   21733 3
   21810 2
   21886 1
   21963 3
   22039
   22116 1
   22192
   22269 1
```

Figure 4.17: An event from AMANDA-B data which passes the filter.

4.9 Conclusions

After a complete simulation of cosmic ray muon bundles, atmospheric neutrinos, and an analysis of AMANDA-B data, the following results are to be noted:

- `RAVEN` reproduces many features of the data. These include:
    1. The total 8-fold trigger rate;
    2. The timing distributions for 8-fold events, after TDC delay and amplitude corrections;
    3. Distributions derived from the line fit (χ^2/N_{used}, v_z, and $|\mathbf{v}|$);
- The filter provides a large increase in signal/noise for this detector. Data and Monte Carlo agree qualitatively on a cut-by-cut basis.

It should be mentioned at this point that, while `RAVEN` reproduces bulk properties of muon data fairly well, a study is underway[36] which indicates that the match is not perfect. In the study, a small set of vertically-incident muons which trigger both AMANDA-A and AMANDA-B in the 1996 data set is examined. Arrival times t of hits from muons is plotted versus OM depth z. The slope of z versus t is quite close to the expected value of the speed of light, with less time scatter in individual hits than is seen in events generated by `RAVEN`. This result may indicate that the ice properties chosen for the simulation are more pessimistic than they should be, in the blue region which is difficult to measure by direct laser calibration but is most relevant for the detection of Čerenkov light. This discrepancy should be borne in mind less one get overly excited about the agreement between simulation and data presented above.

This caveat notwithstanding, the study of the filter indicates that a similar filtering algorithm should be pursued for the expanded 11-string array running over the 1997 Austral Winter season, so that data with an enriched fraction of neutrino events can be retrieved in near real-time. A study of the expanded array, and a proposed neutrino filter, is the subject of the next chapter.

Chapter 5

Application: Simulating an Expanded AMANDA-B Array

> ... He could do this bacause the provident Baloyne, reaching deep into government coffers, had supplied the Project with a battery of high-resolution neutrino inverters. In addition, the radiation from the heavens was amplified several hundred million times–the physicists built the necessary equipment.
>
> –*His Master's Voice,* [1, p. 94]

5.1 Simulating an Expanded AMANDA Array

The AMANDA collaboration plans to expand the existing four string AMANDA-B detector during 1996-1997 Austral Summer season. The plan for the coming deployment is to add a second central string and six new strings placed concentrically to fill out the array. The new central string is to consist of 20 OMs spaced by 20 meters. The additional six will contain 36 OMs spaced by 10 meters.

Simulation can help answer the following questions:

- What rate is expected for a given multiplicity threshold in the array? The question will help determine in advance what threshold the array should be set at in order to stay below the given maximum rate of data collection.[1]
- What arrangement of strings will give an optimal sensitivity to upward-going neutrinos, and minimal sensitivity (after placing cuts on the data) to down-going muons?

---

[1] However, the difficulty of predicting high-multiplicity rates should be re-iterated: small errors in OM efficiencies can translate into large uncertainties in rates when large multiplicities are required. See Section 3.6.5.

- What cuts are optimal for filtering the data stream for neutrinos? Once the detector is in place, simulation should indicate exactly what procedure will be used to select events to be sent "off the ice," minimizing the contribution from cosmic ray background with respect to the neutrino signal.

To this end, three configurations were simulated. The radial distance of the six new outer strings was varied in each case. Figure 5.1 shows the geometries simulated.

The designs shown in Figure 5.1 reflect several constraints:[2]

- The existing four-string array was simulated according to positions surveyed in [26]. Dead, up-looking, and down-looking tubes were all accounted for in the `.geo` geometry files.
- Strings 5-10 contain 36 OMs separated by 10 meters.
- String 11 contains 20 OMs separated by 20 meters (as a companion to String 4).
- All new strings (5-11) contain down-looking OMs only.
- The new strings are placed at the same depth and positioned such that their centers (relative to top and bottom OM) were were at the average of the centers of the original four strings.

The first stage of the analysis was to run cosmic-ray multimuon events and atmospheric neutrinos, saving 8-fold triggers. The simulation proceeded as in Chapter 4, with the same ice and OM properties (`.pes` and `.pmt` files). A few points were immediately apparent:

- Rates and average multiplicities for an eleven-string array are much higher than for AMANDA-B. Raw 8-fold rates are shown in Table 5.1. The increase for atmospheric neutrinos is much higher than for cosmic ray background, because the optical modules are all pointed down and have a higher sensitivity to upward-going light. Figures 5.2 and 5.3 show the multiplicity distributions.
- A preliminary scan of the neutrino events at this stage showed that most of the muons triggering were short-lived tracks inside and just outside the array, which looked quite challenging to reconstruct. However,

---

[2] The admittedly cutesy name "Daisy" reflects the origin of the third design: AMANDA collaborators at DESY in Hamburg, Germany proposed the geometry.

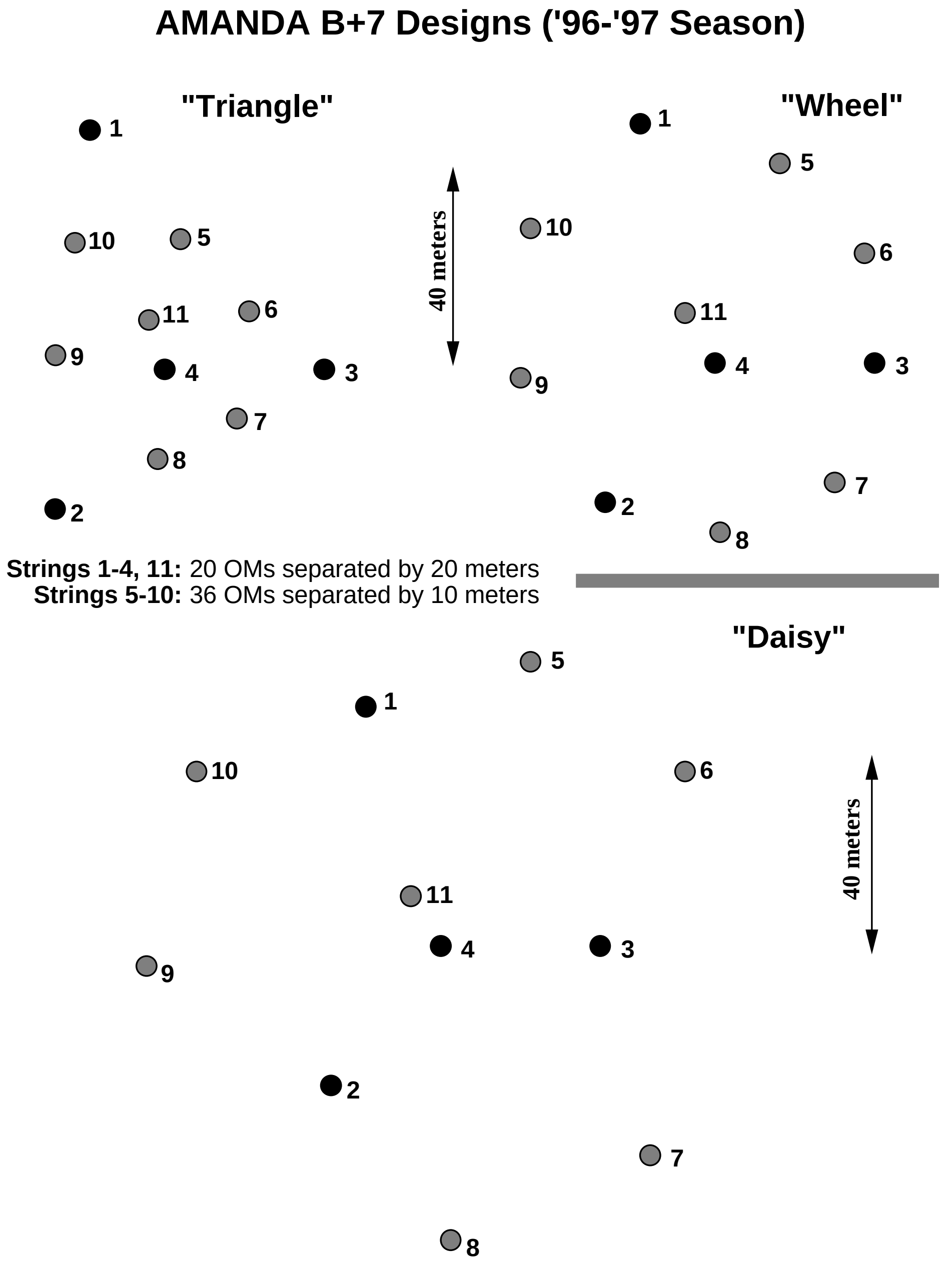

Figure 5.1: Three different designs of an expanded AMANDA-B array: "triangle," "wheel," and "daisy."

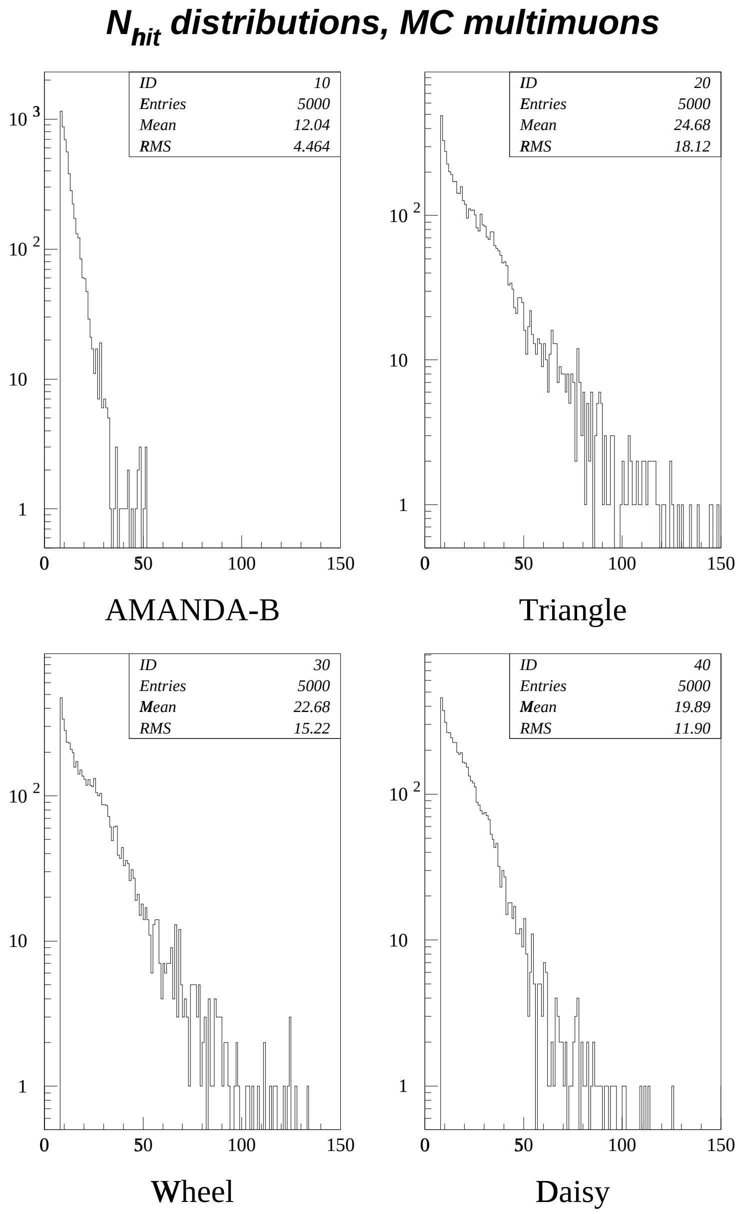

Figure 5.2: Cosmic ray multimuon hit multiplicities in the 4 string and 11 string arrays, before filtering.

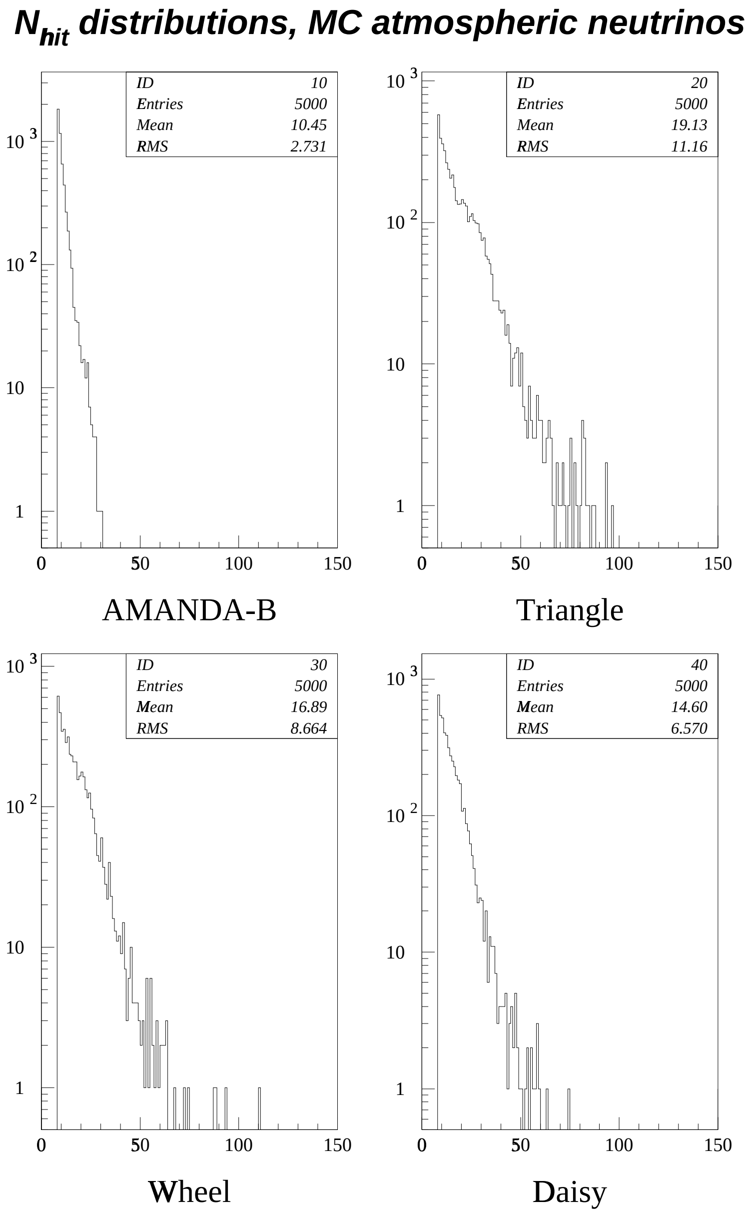

Figure 5.3: Hit multiplicities for events from neutrino-induced muon events in the 4 string and 11 string arrays, before filtering.

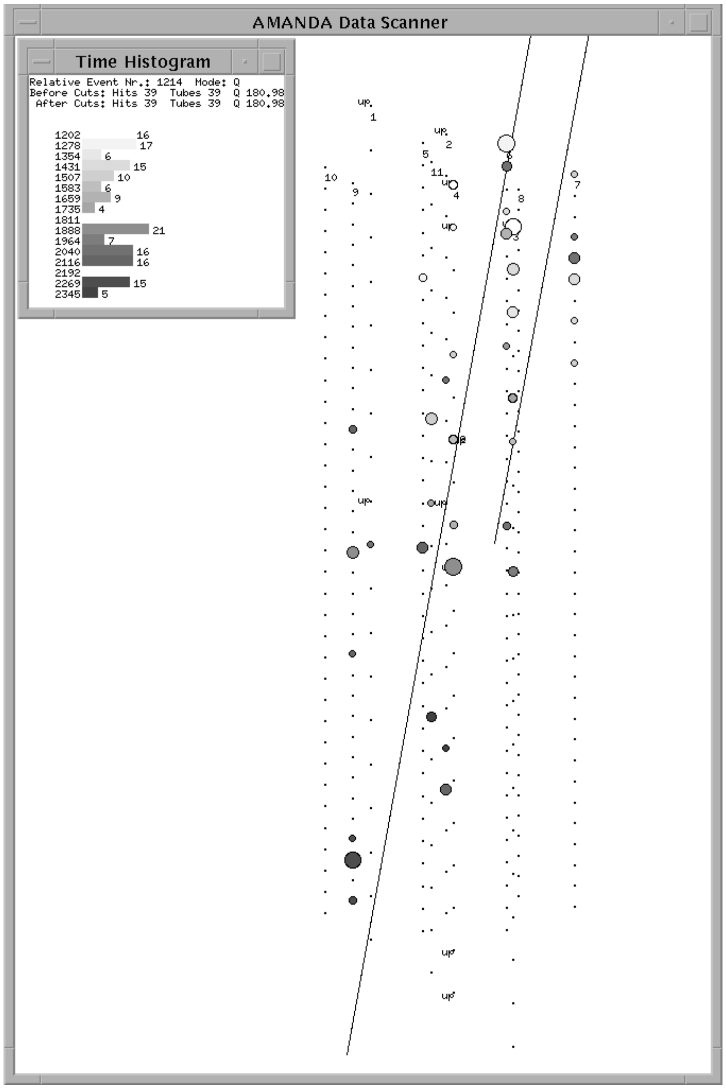

```
Relative Event Nr.: 1214  Mode: Q
Before Cuts: Hits 39  Tubes 39  Q 180.98
 After Cuts: Hits 39  Tubes 39  Q 180.98
```

Figure 5.4: A simulated multimuon event in the "Daisy" configuration.

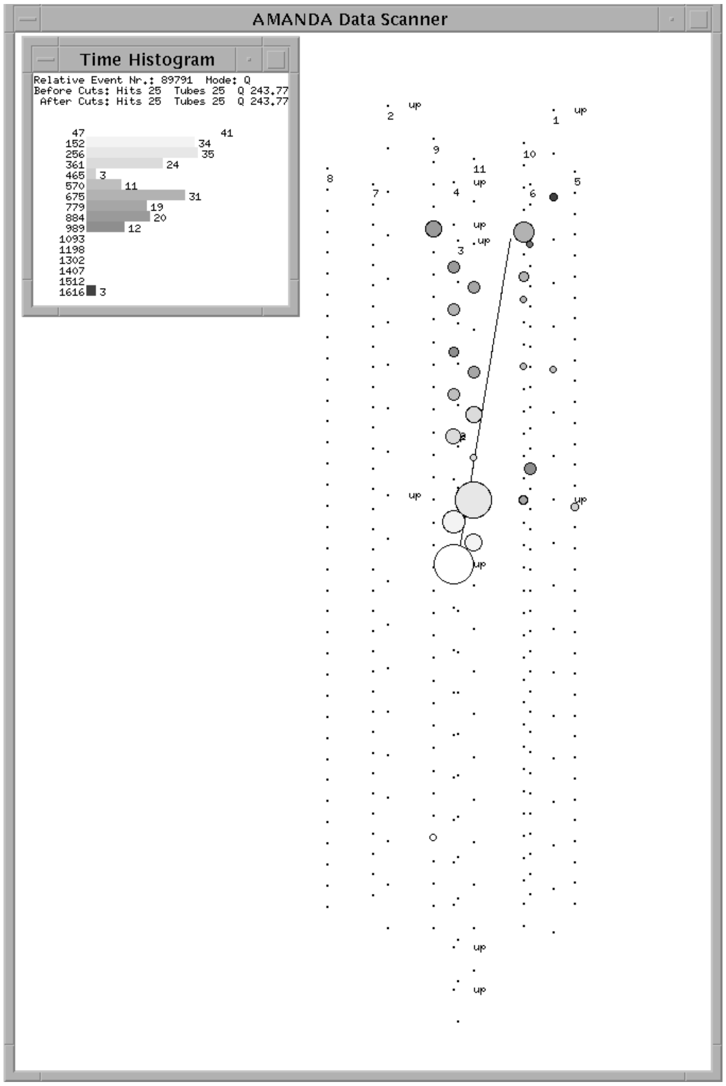

```
Relative Event Nr.: 89791  Mode: Q
Before Cuts: Hits 25  Tubes 25  Q 243.77
 After Cuts: Hits 25  Tubes 25  Q 243.77
```

Figure 5.5: A simulated atmospheric neutrino event in the “Daisy” configuration.

many high-multiplicity events also remained. At high multiplicities, the events tended to be easily discriminated by eye to be upward-going single muons. The events were much more clearly read on the scanner than events simulated (or real data taken) in AMANDA-B. This is mostly due to the large multiplicities of events in the expanded array designs.

Table 5.1: 8-fold event rates calculated for the different 11-string geometries simulated.

Detector	CR Background	Atmospheric Neutrinos
AMANDA-B	25. Hz (data)	0.86 /day
Triangle	121.0 ±0.4 Hz	58.4 ±0.6 /day
Wheel	131.8 ±1.6 Hz	63.9 ±0.8 /day
Daisy	153.2 ±0.2 Hz	71.2 ±0.9 /day

5.2 Filtering for Neutrinos in the Expanded Array

Each set of events generated in the new array was passed through `anaboth` to generate distributions of the same quantities used in the previous chapter to filter events in AMANDA-B. Since large multiplicities were available, a minimum of 17 hits after hit removal was demanded.

After performing the line fit, but before placing any cuts other than requiring sufficient multiplicity for the fit, the energy threshold of the array was examined. This is shown in Figure 5.6, with a minimum fitted hit multiplicity of 17 for the expanded arrays, compared to 9 for AMANDA-B. Some features are immediately apparent. The first is that the muon energy threshold is 10-30 GeV for atmospheric neutrino events, and roughly 150 GeV for cosmic ray muons. The reason for the difference in threshold is twofold: first, most of the tubes are pointing down, so the array is more sensitive to up-going muons. Second, the muon energies are taken at the physics plane, some 200 meters before the top of the array, requiring an energy difference of about 40 GeV for minimum-ionizing muons to reach the array. Another feature that is readily apparent in atmospheric neutrinos is the increase in threshold with the spacing between the strings. The reason is obvious—the farther apart the OMs, the

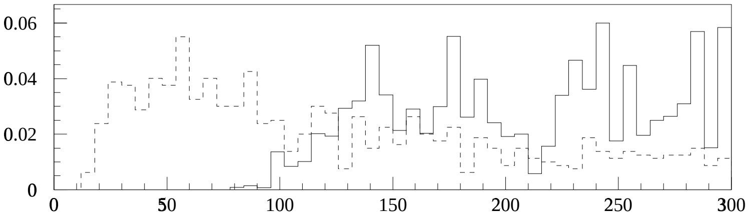

E_μ (GeV): AMANDA-B

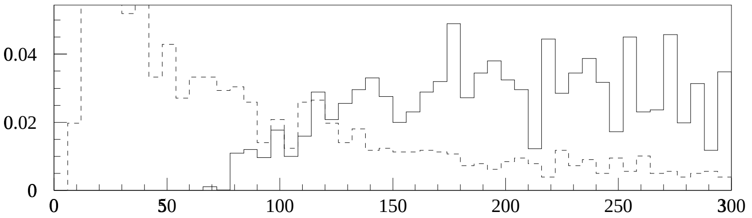

E_μ (GeV): Triangle

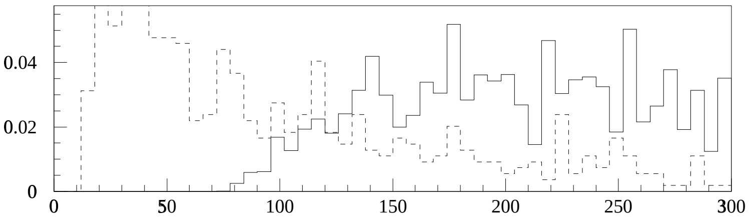

E_μ (GeV): Wheel

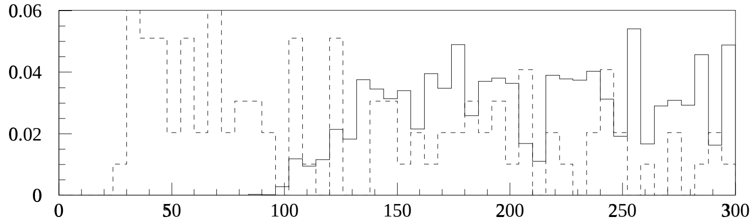

E_μ (GeV): Daisy

Figure 5.6: Muon energy E_μ for the different arrays simulated. The solid line is for cosmic ray muons; the dashed, for muons from atmospheric neutrinos.

more energy required for a muon to traverse a sufficient distance to trigger the minimum multiplicity of hits.

The variables used in Chapter 4 were examined for the 11 string arrays. Some remarks about each variable follow. (Fitted hit multiplicities for each distribution shown in the figures were 17 or more, unless otherwise indicated.)

z-velocity: Still a useful discriminator between up-going and down-going events. The 11-string distributions are narrower than for the four-string AMANDA-B array, and separation between the two distribution increases as the spacing increases; see Figure 5.7. The tails of the distribution for cosmic-ray muon are shown in Figure 5.8. The canonical cut for z-velocity was kept at 0.1 m/nsec.

Total velocity v: Shows the same feature as in the AMANDA-B analysis: atmospheric neutrino events have smaller velocities than cosmic ray muons. Interestingly, the discrepancy is lessened at large spacings. No cut was placed on this quantity.

χ^2/N_{used}: Signal and background are more separated in the expanded array than in AMANDA-B, at least for Triangle and Wheel (Figure 5.10). However, an examination of χ^2/N_{used} for upward going events shows no separation. χ^2/N_{used} was required to be less than 2500 m^2 was required, as for the AMANDA-B analysis; the cut has minimal effect on either signal or background.

R_Q: The fraction of total ADCs in the first half of the event relative to the total sum of ADCs, R_Q, is shown in Figure 5.11. The variable seems to have lost what little discriminatory power it had, and is therefore dropped from the filter.

$|\hat{\mathbf{d}} \cdot \hat{\mathbf{t}}|$: The dot product between the purely spatial and space-time line fit directions, $|\hat{\mathbf{d}} \cdot \hat{\mathbf{t}}|$, didn't look promising until that quantity for up-going events ($v_z > 0.1$) was examined (Figure 5.12). Although the statistics are marginal for the Daisy configuration (even after over a week of round-the-clock running on seven DEC Alphas!), the distributions are more populated in regions of lower $|\hat{\mathbf{d}} \cdot \hat{\mathbf{t}}|$, especially for the Daisy array. This strongly suggests retaining a cut on this variable. In order to minimize bias by tuning the cuts to get rid of a few existing events, the cut of 0.9 was kept.

A visual scan of events passing the cuts $N_{\text{used}} \geq 17$, z-velocity > 0.1, $\chi^2/N_{\text{used}} < 2500$ m^2, and $|\hat{\mathbf{d}} \cdot \hat{\mathbf{t}}| > 0.9$ showed that many of the surviving background events originated at the bottom of the array. These were muon events traveling at an angle and passing below the array, whose Čerenkov light travelled upwards and thus mimicked a ν_μ signal. Based on this, the z-coordinate z_{COM} of the center of mass of the hit OMs was examined (Figure 5.13). A requirement that z_{COM} be greater than -150 meters (essentially using the bottom of the array as a veto) was added to the list of cuts. (This cut doesn't seem to significantly improve signal/background in the four-string array).

The cuts chosen ("canonical cuts") were as follows:

$$\boxed{\begin{array}{c} N_{\mathrm{used}} \geq 17 \\ z\text{-velocity} > \ 0.1 \ \mathrm{m/nsec} \\ \chi^2/N_{\mathrm{used}} < 2500 \ \mathrm{m}^2 \\ |\hat{\mathbf{d}} \cdot \hat{\mathbf{t}}| > 0.9 \\ z_{\mathrm{COM}} > -150 \ \mathrm{m} \end{array}}$$

The results for this filter were:

Detector	CR Background	Atmospheric Neutrinos
Triangle	3433 ±858 /day	2.42 ±0.13 /day
Wheel	1496 ±225 /day	2.47 ±0.17 /day
Daisy	104 ±60 /day	1.84 ±0.15 /day

These are plotted in Figure 5.17. The background rate for Daisy is based on three events, shown in Figures 5.14, 5.15 and 5.16.

A few other sets of cuts were examined, none of which gave a signal to background ratio which rivaled that of Daisy's in the canonical cuts given above. However, the general trend of increasing signal/background as the string spacing increased was borne out in each case.

5.3 Summary and Conclusions

The expanded AMANDA-B array was investigated using `RAVEN`, which reproduces the 8-fold data rate, as well as distributions of quantities useful for filtering, in the existing four-string array.

Some results of the simulation were:

- A predicted data rate of 120-150 Hz for 8-fold events (Table 5.1).
- The array's energy threshold for cosmic ray muons is about 150 GeV, and about 25 GeV for muons from atmospheric neutrinos (Daisy configuration).

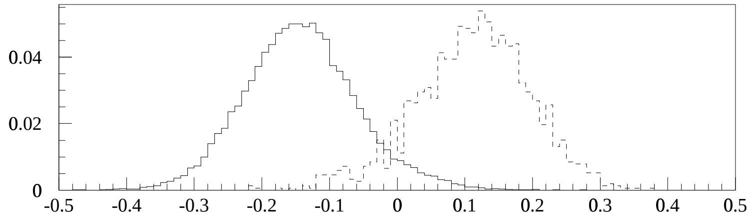

V_z for AMANDA-B

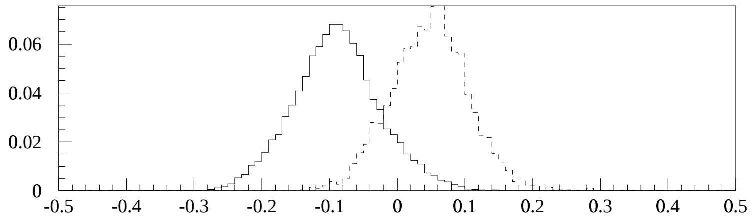

V_z for Triangle

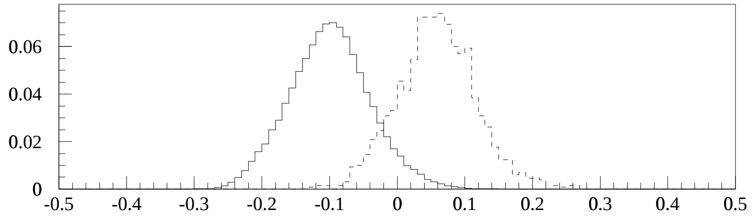

V_z for Wheel

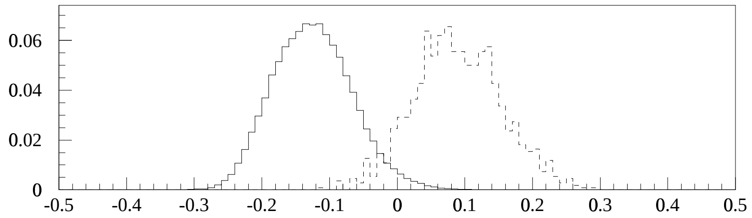

V_z for Daisy

Figure 5.7: z-velocity (m/nsec) separation for the different arrays simulated. The solid line is for cosmic ray muons; the dashed, for muons from atmospheric neutrinos.

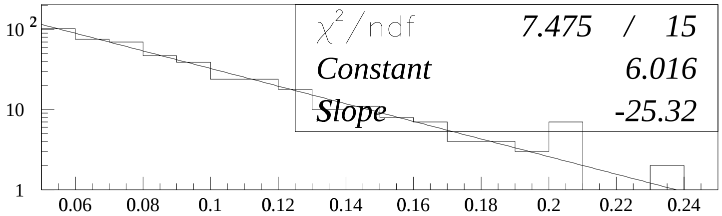

V_z for AMANDA-B

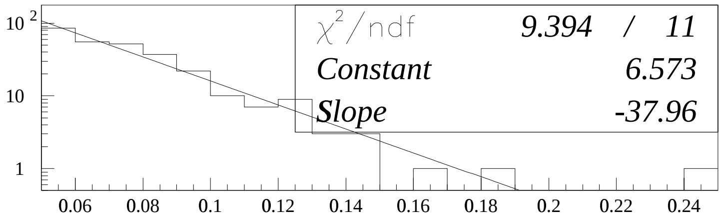

V_z for Triangle

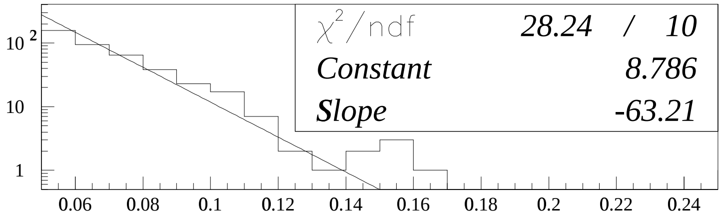

V_z for Wheel

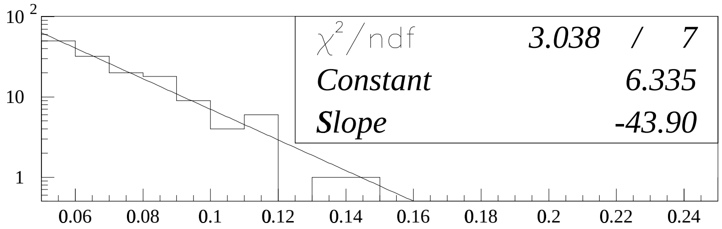

V_z for Daisy

Figure 5.8: Closeup of z-velocity (m/nsec) tail, with exponential fit, for the different arrays simulated.

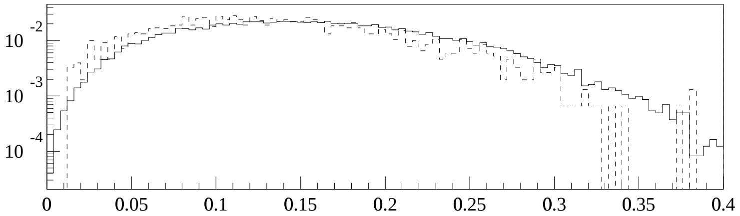

Total velocity for AMANDA-B

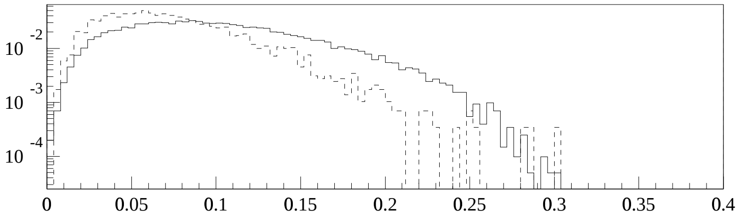

Total velocity for Triangle

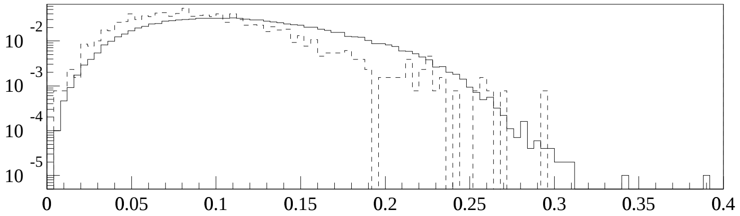

Total velocity for Wheel

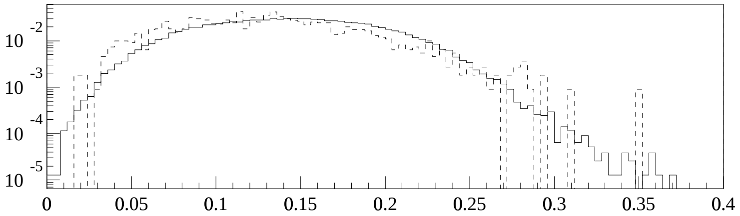

Total velocity for Daisy

Figure 5.9: Total fit velocity (m/nsec) for the different arrays simulated. The solid line is for cosmic ray muons; the dashed, for muons from atmospheric neutrinos.

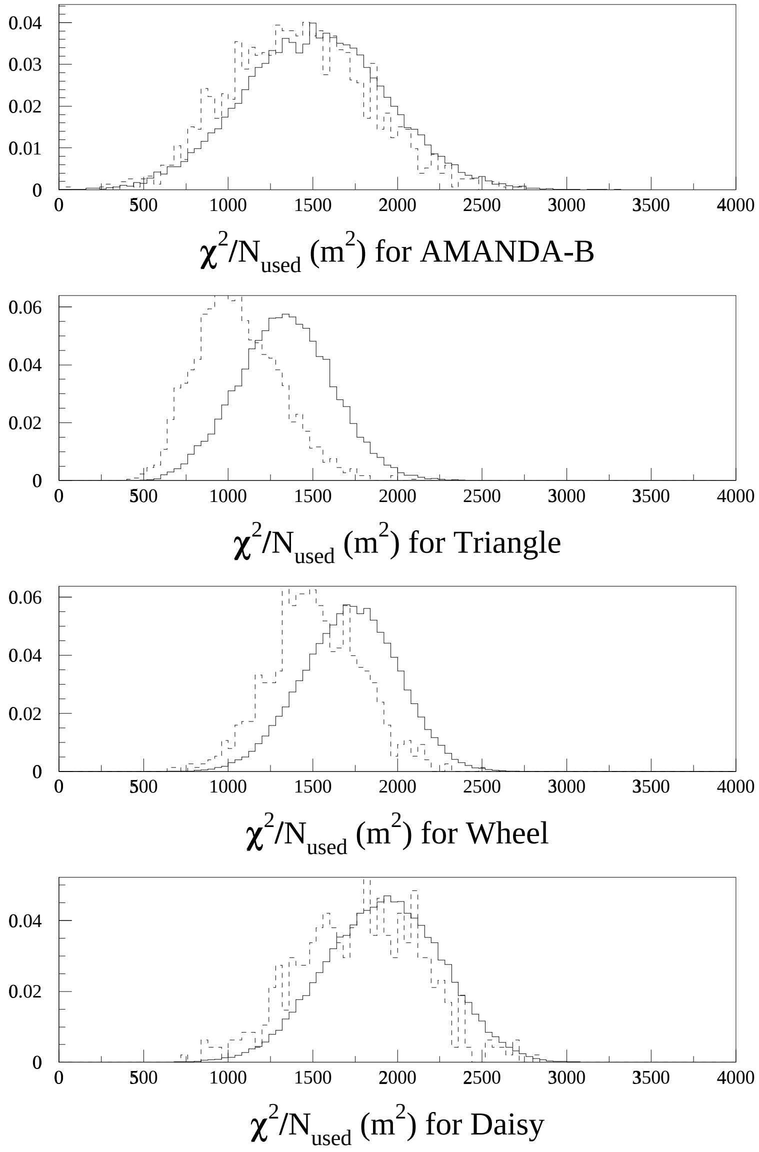

Figure 5.10: χ^2/N_{used} for the different arrays simulated. The solid line is for cosmic ray muons; the dashed, for muons from atmospheric neutrinos.

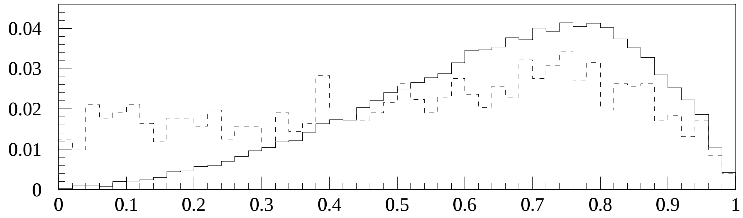

R_Q for AMANDA-B

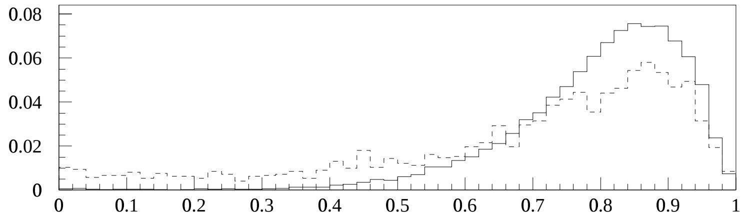

R_Q for Triangle

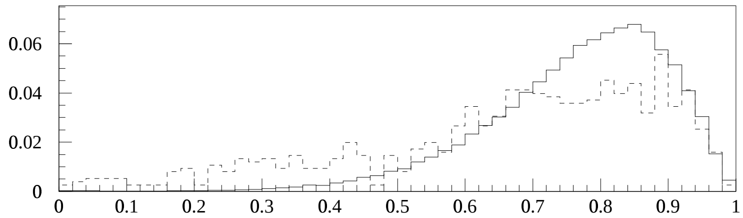

R_Q for Wheel

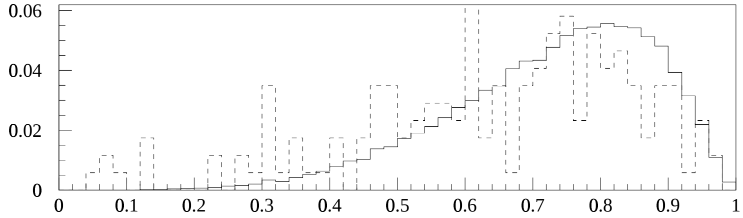

R_Q for Daisy

Figure 5.11: R_Q for the different arrays simulated. The solid line is for cosmic ray muons; the dashed, for muons from atmospheric neutrinos.

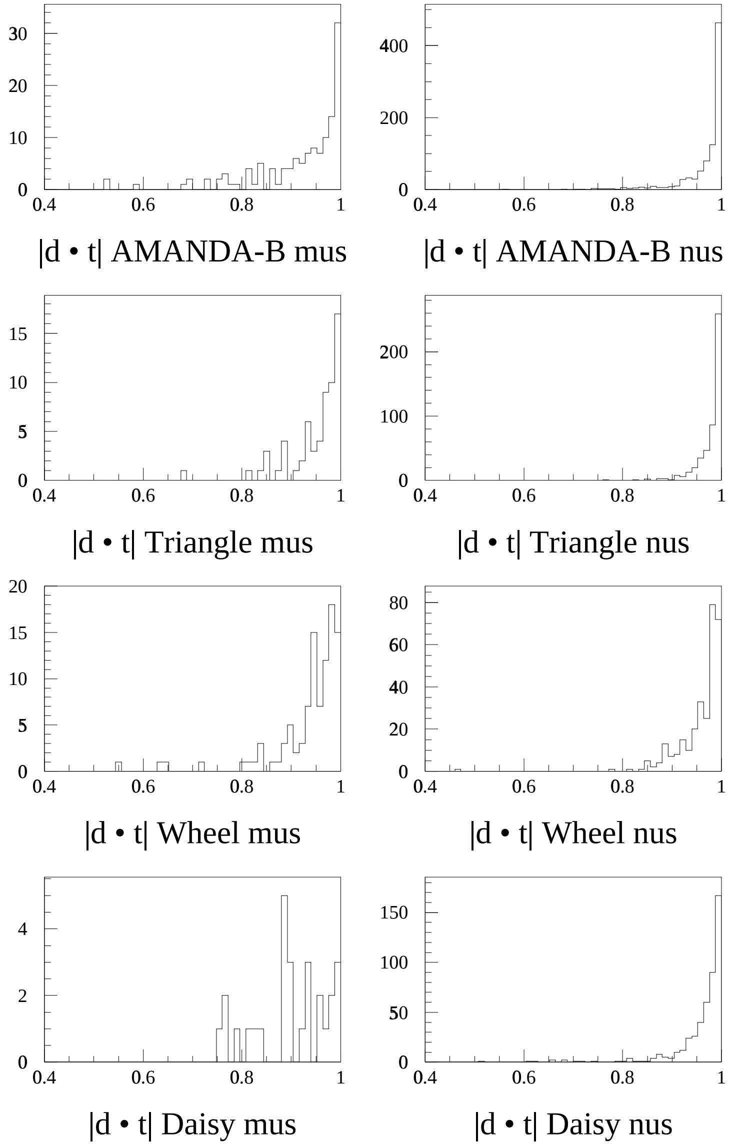

Figure 5.12: $|\hat{\mathbf{d}} \cdot \hat{\mathbf{t}}|$ for the different arrays simulated; only events with $v_z > 0.1$ are shown. The column on the left is for cosmic ray muons; on the right, for muons from atmospheric neutrinos.

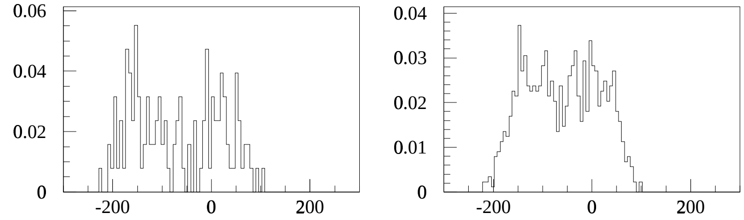

Z_{com} for AMANDA-B Z_{com} for AMANDA-B

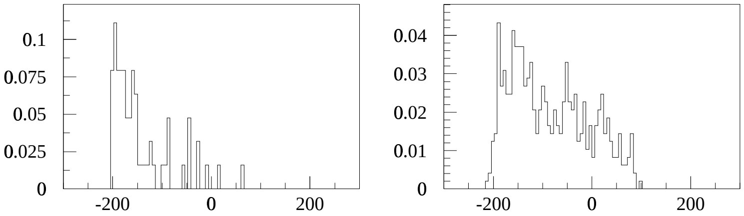

Z_{com} for Triangle Z_{com} for Triangle

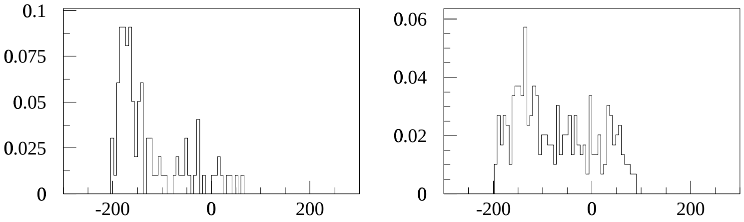

Z_{com} for Wheel Z_{com} for Wheel

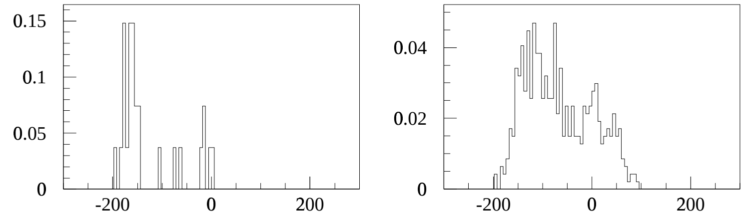

Z_{com} for Daisy Z_{com} for Daisy

Figure 5.13: z-coordinate of center of mass of hit tubes (z_{COM}), for the different arrays simulated; only events with $v_z > 0.1$ are shown. The column on the left is for cosmic ray muons; on the right, for muons from atmospheric neutrinos.

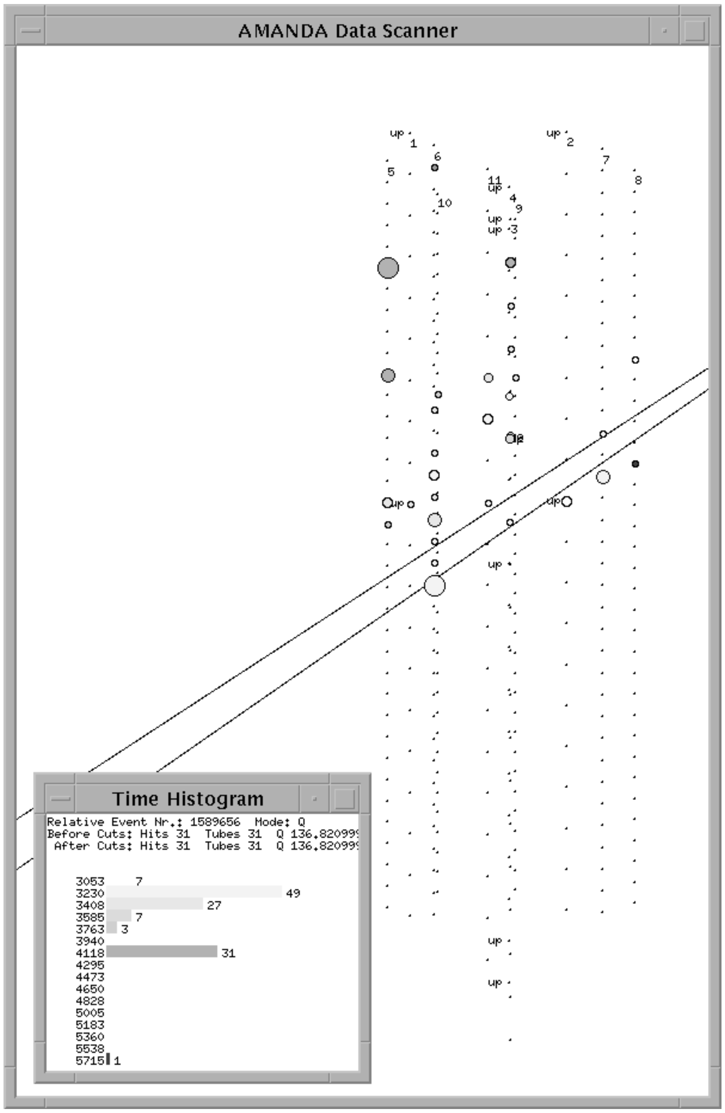

```
Relative Event Nr.: 1589656  Mode: Q
Before Cuts: Hits 31  Tubes 31  Q 136.82099
 After Cuts: Hits 31  Tubes 31  Q 136.82099


    3053    7
    3230             49
    3408        27
    3585  7
    3763 3
    3940
    4118         31
    4295
    4473
    4650
    4828
    5005
    5183
    5360
    5538
    5715 1
```

Figure 5.14: A simulated cosmic-ray muon event in the “Daisy” configuration, which passes the canonical filter (event 1589656).

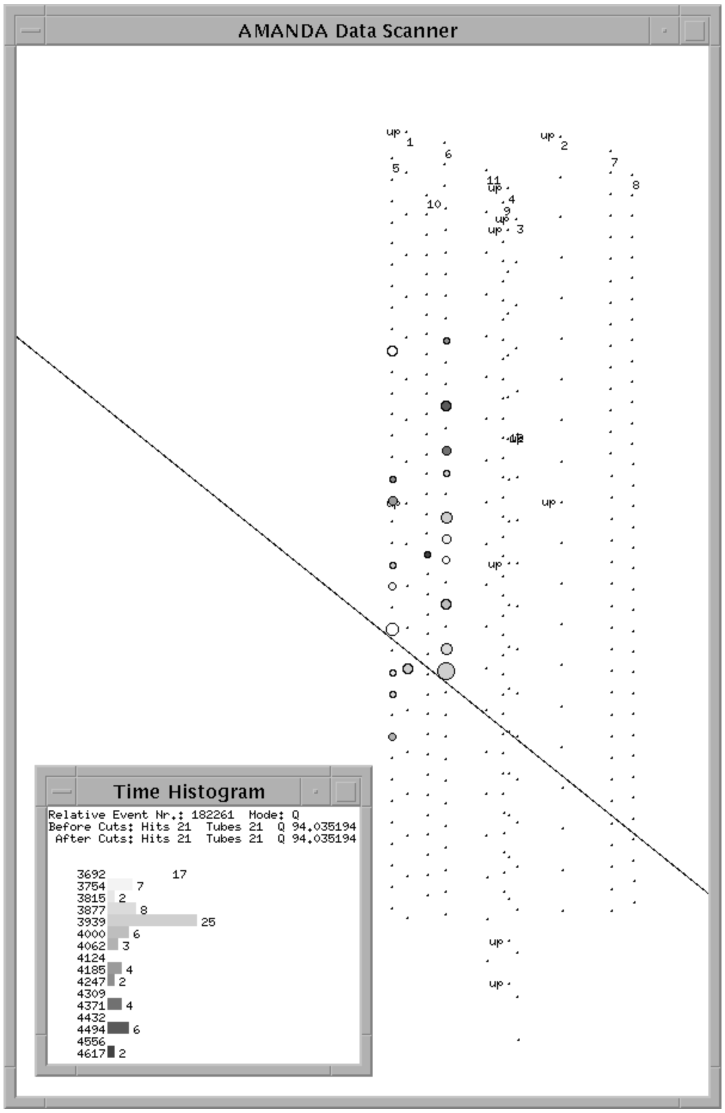

```
Relative Event Nr.: 182261  Mode: Q
Before Cuts: Hits 21  Tubes 21  Q 94.035194
 After Cuts: Hits 21  Tubes 21  Q 94.035194
```

Figure 5.15: A simulated cosmic-ray muon event in the “Daisy” configuration, which passes the canonical filter (event 182261).

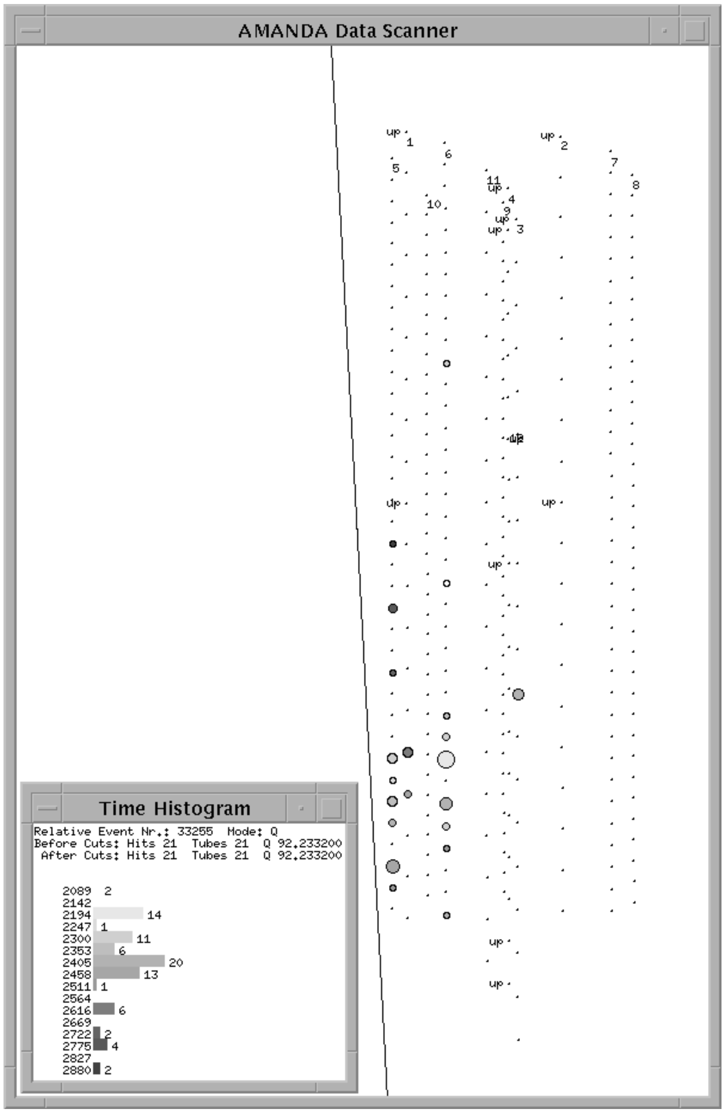

```
Relative Event Nr.: 33255  Mode: Q
Before Cuts: Hits 21  Tubes 21  Q 92.233200
 After Cuts: Hits 21  Tubes 21  Q 92.233200


    2089  2
    2142
    2194 14
    2247 1
    2300 11
    2353 6
    2405 20
    2458 13
    2511 1
    2564
    2616 6
    2669
    2722 2
    2775 4
    2827
    2880 2
```

Figure 5.16: A simulated cosmic-ray muon event in the "Daisy" configuration, which passes the canonical filter (event 33255).

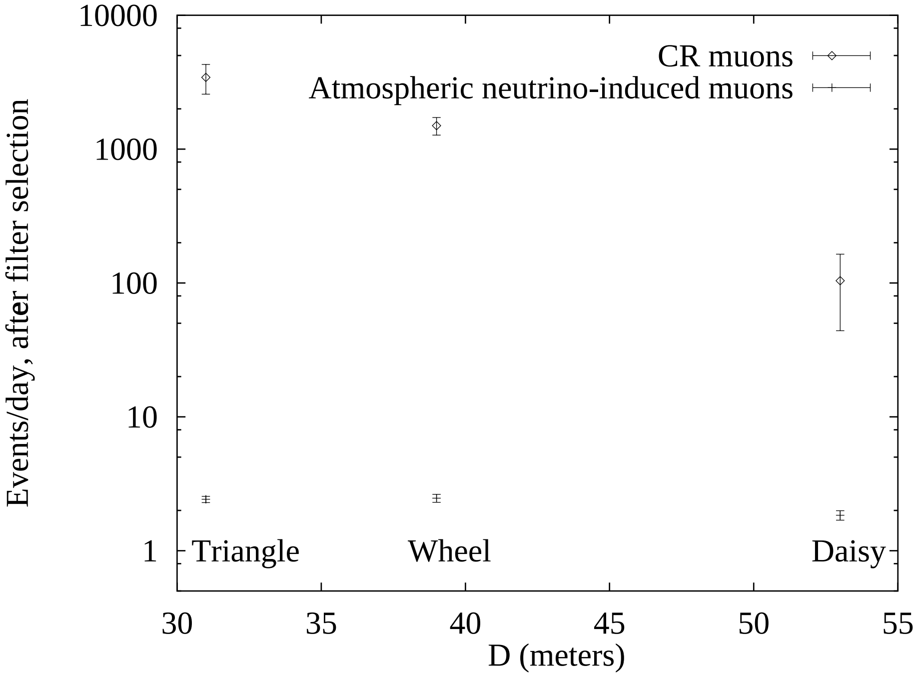

Figure 5.17: Daily rate of signal and background events passing the filter, versus the average distance D of strings from the center. (The two central strings are excluded from the average.)

A filter is available which brings the signal to background ratio to about 1/60, for the Daisy configuration.

It should be emphasized that we do *not* conclude that the atmospheric neutrino signal will be sixty times weaker than background in the expanded AMANDA-B array. The filter is one stage of a data selection procedure which begins with the raw data collection and ends in a complete, iterative track reconstruction procedure using a maximum-likelihood fit. The fit, developed by AMANDA collaborators at DESY[33], uses a distance-dependent parametrization for the distribution of photon arrival times relative to the expected (unscattered) times.

The full maximum-likelihood fit has proven much more effective than the line fit, and can reconstruct muon track directions to within a few degrees. However, its computation is more time-intensive. The utility of the filter is its ability to quickly reject background events, and save potential signal events for transmission from the South Pole for further processing. The filter will be implemented in the data extraction system when the author travels to the South Pole in January, 1997; the exact cuts placed on muon data will depend on available bandwidth, measured raw trigger rates, and the size of the event record. Further improvements to the filter may be possible and will be investigated.

Analysis at DESY with the full fitter indicates that large spacings are optimal for the expanded array. The filter analysis bears this out as well, with a signal/background ratio ten times larger for Daisy than for Wheel, for the canonical filter cuts.

Chapter 6

Application: Detection of Supernovae Showers in AMANDA-B

> I knew that such an effect was impossible, but I trusted Donald. If anyone in our hemisphere knew nuclear reactions, he did. I asked about the range of the effect. Yes, already, even before I was aware of it, came evil thoughts.
>
> –*His Master's Voice*, [1, p. 135]

6.1 Introduction

Although AMANDA was designed originally for the detection of muons with energies of several GeV or more, the instrument is also sensitive to low energy $\bar{\nu}_e$ events from supernovae[11,12]. Most of the energy in the explosion is expected to come after the deleptonization pulse, in a ten second burst of thermalized neutrinos. The dominant cross section in ice is for electron antineutrinos on protons, namely $\bar{\nu}_e + p \rightarrow e^+ + n$. The positrons are emitted with a random orientation with respect to the neutrino direction, and travel a short range ($\mathcal{O}$(10cm)), emitting a few thousand Čerenkov photons. The signature of a nearby supernova is a statistical excess in OM counting rate relative to the ~400 Hz thermal noise per tube, over a period of 10 seconds.

6.2 Effective Volume for Supernova Detection

The programs `photon_table` and `distmc` in the `RAVEN` distribution provide the capacity for calculating the supernova detection capabilities of the AMANDA-B detector.

The problem is simplified by the fact that the shower directions are oriented randomly in the detector, that the showers occur anywhere within the ice with equal probability, and that the detection probability of a single shower is small. This enables us to find the efficiency for a single photon, and calculate the effective volume for a positron shower by scaling by the number of photons in the shower.

Consider a single photon starting at the origin, and an OM at a point $(\rho, \cos\psi)$ with an orientation $(\cos\theta_p, \phi_p)$. One can generate a table of photon crossings as in Section 3.4.2, with $N_P = 1$, and then proceed to calculate $N_{\mathrm{pe}}(\rho, \cos\psi, \cos\theta_p, \phi_p)$. Since the direction of the photon is arbitrary, the table N is generated with an isotropic distribution of initial photon directions.

In the case of supernova positrons, the photons are generated with equal probability at any point in the ice. Evaluating the detection probability is equivalent to averaging N_{pe} over spatial coordinates $(\rho, \cos\psi)$ and directions $(\cos\theta_p, \psi_p)$ of the OM. Averaging over directions first,

$$N_1(\rho) = \frac{1}{4\pi} \sum_{\cos\theta_p} \sum_{\phi_p} N_{\mathrm{pe}}(\rho, \cos\psi, \cos\theta_p, \phi_p)\ \Delta\phi_p\ \Delta(\cos\theta_p). \tag{6.1}$$

Since the photons' inital directions are isotropic, there is no ψ dependence. One can either pick an arbitrary bin for $\cos\psi$, or one can average over all the bins for increased statistics. $N_1(\rho)$, then, is the probability for detection of a photon at a distance ρ, regardless of orientation of the OM.

To find the efficiency averaged over all space points, or, equivalently, the effective volume of the OM for a single photon, we average over space coordinates. Let R_{max} be radius of a test volume outside of which the probability for detection is small. The volume of this region $V_{\mathrm{test}} = (4/3)\pi R_{\mathrm{max}}^3$. The efficiency is then

$$\epsilon = \langle N_1 \rangle = \frac{4\pi \sum_\rho \rho^2 N_1(\rho) \Delta\rho}{V_{\mathrm{test}}}. \tag{6.2}$$

The effective volume for a single OM is therefore:

$$V_{\mathrm{eff}}^{\gamma} = \epsilon V_{\mathrm{test}} = 4\pi \sum_\rho \rho^2 N_1(\rho) \Delta\rho. \tag{6.3}$$

For a positron shower creating N_γ photons,

$$V_{\mathrm{eff}}^{e^+} = N_\gamma V_{\mathrm{eff}}^{\gamma}. \tag{6.4}$$

This approach ignores correlations between different photons in the same shower. Since the probability of one shower triggering one OM is small, the approximation is valid.

6.3 An Analytic Solution

One can obtain an analytic solution for $V_{\rm eff}^{e+}$ in ice with no scattering, if one considers only a single photon wavelength λ and thus a fixed absorption length $\tilde{\Lambda}$. In this case, the solution of Equation 3.10 obtains, with $N_P = 1$:

$$N_{\rm pe}(\rho, \theta_p) = A_{\rm eff}(\theta_p, \tilde{\lambda}) \frac{e^{-\rho/\tilde{\Lambda}}}{4\pi\rho^2}. \tag{6.5}$$

If $\langle A \rangle$ is the OM effective area averaged over all orientations of the OM, then Equation 6.1 becomes

$$N_1(\rho) = \langle A \rangle \frac{e^{-\rho/\tilde{\Lambda}}}{4\pi\rho^2}. \tag{6.6}$$

and the effective volume is

$$V_{\rm eff}^{\gamma} = \int_0^{\infty} \langle A \rangle \; e^{-\rho/\tilde{\Lambda}} d\rho = \langle A \rangle \; \tilde{\Lambda} \tag{6.7}$$

The rather simple result is that the effective volume of an OM scales linearly with the absorption length and the collection area of the OM. For a wavelength $\tilde{\lambda}$ of 390 nm, the value of $\langle A \rangle$ for an AMANDA-B OM is 9.16 cm^2; if $\tilde{\Lambda} = 310$ meters, then Equations 6.4 and 6.7 yield $V_{\rm eff}^{e+} = 852{\rm m}^3$.

6.4 Calculating the Effective Volume using RAVEN

With `photon_table` and `distmc`, RAVEN provides a more complete treatment, including the Čerenkov wavelength distribution, with or without scattering, and a wavelength-dependent absorption model. Four cases were simulated:

CLEAR-310: No scattering. Peak absorption length of 310 meters.

CLEAR-90: No scattering. Peak absorption length of 90 meters.

HG-310: Henyey Greenstein scattering, with 7 meter mean free path between scattering centers, $\langle \cos\theta_{\rm scatt} \rangle = 0.8$. Peak absorption length of 310 meters.

HG-90: Same scattering model, peak absorption length of 90 meters.

For example, the inputs to `photon_table` for HG-310 were:

```
1000        ! Number of photons to generate
400         ! Number of bins in rho
1           ! Number of bins in cos(psi)
10          ! Number of cos(theta_OM) bins
1           ! Number of phi_OM bins
200         ! Number of time bins
1.E7        ! Geometrical scattering length of component 1
700.        ! Geometrical scattering length of component 2 (cm)
hg
0.8         ! avg(cos(theta)), component 1
0.8         ! avg(cos(theta)), component 2
40000.      ! rho_max in (cm)
1.          ! Step size in CM (effectively a point source)
8000.       ! max time, nsec
1234561     ! Seed
isot_hg_sc7m_ab310m_1cm_double.photons
isot
```

The numbers of bins, `rho_max` and `t_max` were chosen such that the integrand $N_1(\rho)\rho^2$ was very small at the extremes and the error due to integration by a simple sum was small. Only one bin in $\cos\psi$ or ϕ is needed, since an isotropic source of photons is generated. Again, this is valid since the photons are generated with equal probability anywhere in space.

The photon files (e.g., `isot_hg_sc7m_ab310m_1cm_double.photons` were run through `distmc`:

```
photon_file  isot_hg_sc7m_ab310m_1cm_double.photons
pe_output    isot_hg_sc7m_ab310m_1cm_double.pes
pmt_file     up.pmt
lo_lambda    300.0000
hi_lambda    600.0000
atten_type   4               ! Specify 310 meter absorption curve
```

The output of `distmc` provided $N_1(\rho)$, $N_1(\rho)\rho^2$, and the integral of $N_1(\rho)\rho^2$ as a function of ρ. Figure 6.1 shows the resulting $N_1(\rho)$ for the four different ice models.

Table 6.1: Effective per OM for a single photon, and for a positron shower generating 3000 photons. Units are cubic meters.

Model	V_{eff}^{γ}	$V_{\text{eff}}^{e^+}$
CLEAR-310	0.325	975.
HG-310	0.324	972.
CLEAR-90	0.158	474.
HG-90	0.138	414.

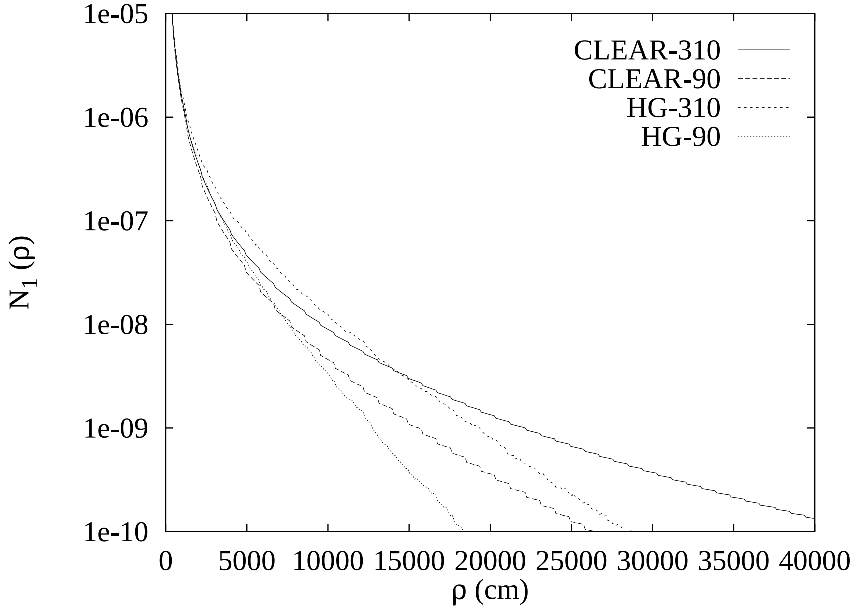

Figure 6.1: $N_1(\rho)$ versus ρ for the different models.

Table 6.1 shows the resulting effective volume for the four ice models simulated. Some features can be noted immediately. The most striking is that there is no strong dependence of effective volume on scattering length. This can be understood by the fact that a scattered photon and an unscattered photon have the same average track length. Integrating over distances from the emitter to the source, one sees an enhancement for scattered light at near distances and a deficit at large distances, which cancel out in the total effective volume (see Figure 6.1).

Equation 6.7 is roughly borne out in the ratios of effective volumes at different peak absorption lengths. The deviation from this relationship presumably comes from the fact that the photon wavelength varies, an fact that is not accounted for in the analytic calculation.

6.5 Dependence of Effective Volume on Supernova Temperature

The supernova detection efficiency of an OM can be reduced to a product of the average number of photons per shower and the effective volume per photon.

The production of photons by positron showers was studied[12] by generating a sample of positrons whose energies followed a Fermi-Dirac distribution weighted by the neutrino interaction cross-section for $\bar{\nu}_e + p \rightarrow e^+ + n$. Events following the resulting energy spectrum were generated with an electromagnetic shower Monte Carlo simulation[3] which took into account the scattering of positrons, energy loss, brehmsstrahlung and pair production. The showers produced optical Čerenkov photons in the wavelength region $[300, 600]$ nm. The resulting dependence of number of photons on supernova temperature is shown in Table 6.2. The choice of an ice properties model and a supernova temperature determines the effective volume of an AMANDA-B optical module.

Table 6.2: Average number of photons and standard deviation for different supernova temperatures.

S.N. Temp.	N_γ	σ_{N_γ}
2 MeV	1646	860
4 MeV	3469	1660
8 MeV	6884	3004

6.6 Can AMANDA-B See a Supernova at the Center of the Galaxy?

Although the main purpose of this chapter is to illustrate the calculation of the effective volume of an AMANDA OM for positrons from $\bar{\nu}_e$s, one can use the result to determine the sensitivity of the entire array of OMs to a supernova at a distance d from earth. The center of the galaxy is used as a reference, since it has the highest density of stars, and may provide a source of supernova events not easily detected with optical telescopes.

The calculation follows Reference [12]. Fortunately, the problem is greatly simplified by the recent detection of neutrino events from supernova 1987A. One can simply scale the results for the detection of 11 events from SN1987A in the Kamiokande detector. In other words, if the distance from the supernova to Earth is d,

$$N_{\text{events}} = 11 \left(\frac{N_{\text{OM}}\, V_{\text{eff}}^{e^+}}{V_{\text{kam}}} \right) \left(\frac{52 \text{ kpc}}{d} \right)^2 \tag{6.8}$$

assuming the energy yield in neutrinos from SN197A to be characteristic of future events.

The Kamiokande volume $V_{\mathrm{kam}} = (2.14\ \mathrm{kton})(0.8) = 1.71 \times 10^3\ \mathrm{m}^3$[32], where the factor 0.8 comes from the fact that the Kamiokande instrument has an energy threshold (whereas AMANDA, as a pure counting detector, collects photons from all positron showers).[1]

The AMANDA-B detector is slated to expand to 11 strings in the 1996-1997 Austral Summer season: 79 existing plus 245 new OMs, giving 299 modules (assuming a 90% survival rate for the new OMs). If one assumes the HG-90 ice model and an average of 3000 photons per positron (a supernova temperature of roughly 4 MeV), one obtains

$$N_{\mathrm{events}} = 795 \left(\frac{52\ \mathrm{kpc}}{d}\right)^2 . \tag{6.9}$$

In this case, the expanded AMANDA-B effective volume is $1.24 \times 10^5\ \mathrm{m}^3$, and a supernova at the center of the galaxy (8.5 kpc) will give 2.97×10^4 events.

To determine the statistical significance this signal, consider the background noise rate. The average noise rate per OM in AMANDA-B is $\nu_{1\mathrm{pe}} \sim 400$ Hz. In a ten-second interval with 299 OMs, this gives

$$\langle N_I \rangle = (10\ \mathrm{sec}\ N_{\mathrm{OM}}\ \nu_{1\mathrm{pe}}) = 1.20 \times 10^6\ \mathrm{events}$$

per interval on average.

Since the statistics are Poisson and the mean is large, one can approximate the distribution of N_I as a Gaussian with mean $\langle N_I \rangle$ and standard deviation $\sigma = \sqrt{\langle N_I \rangle}$. The excess in standard deviations N_S is

$$N_S = \frac{N_{\mathrm{events}}}{1.09 \times 10^3}.$$

Using the numbers given above (11 Kamiokande events, 52 kpc to SN1987-A, 400 Hz phototube noise rate), one gets $N_S = 27$ for an event in the center of the galaxy. The probability of noise fluctuating at such a level, even for a century's-worth of 10 second intervals, is vanishingly small.

A determination of the exact distance threshold for detection requires an error analysis of the quantities involved: the distance to SN1987A, and especially the expected event yield from Kamiokande, are not precisely determined. Also, the AMANDA-B OMs do not completely conform to Poisson

---

[1] Note that the effective volume is for the e^+, not the $\bar{\nu}_e$.

statistics[35]—their noise distributions are broader than expected in the Poisson case by a factor 1.5. Nonetheless, a supernova at the center of the galaxy, comparable in yield to 1987A, will clearly yield a dramatic signal excess.

Triggers to implement a supernova trigger by monitoring excesses in total counting rates in the AMANDA OMs are in place[34,35], and are also planned for the deployment of the additional seven strings this 1996-1997 Austral Summer season.

Appendix A

Using RAVEN

> ... There was a large shape beneath a white cover. At first I took this for some piece of gymnastics equipment or a a rocking horse (even that would not have surprised me), but it was a brand-new, very handsome IBM cryotronic calculator, which indeed proved useful to me. Wanting to join more closely to the machine, the engineers at IBM had him work it also with his feet. Every time I pressed the "clear" pedal I expected, by reflex, to drive into the wall—the pedal was so much like a car accelerator.
>
> –*His Master's Voice*, [1, p. 81]

A.1 How to Install RAVEN

Current and past versions of `RAVEN` are available at:

`http://alizarin.physics.wisc.edu/jacobsen/raven/source/`

Generally the latest version is the most complete and correct. As of this writing, that version is `V24`.

To run `RAVEN` "straight out of the box," you will need a compiler that understands DEC FORTRAN extensions (`STRUCTURE` definitions, `INCLUDE` files, etc.). The data extraction program `newamab`, which writes data in the `RAVEN` `.evt` format, requires a C compiler. The CERN libraries `genlib`, `packlib`, and `kernlib` are also required, for HBOOK routines and the random number generator.

The distribution comes with a UNIX-style `Makefile` which shows the interdependencies of the various source files. One must first edit the `Makefile` and put in the correct choice for the `COMPILE_EXECUTE` variable (see self-explanatory comments in `Makefile`). The CERN library path should also be changed by modifying the `ALPHACERN` variable.

On an Ultrix or Digital Unix platform, typing "`mkdir bin; mkdir obj; make`" should then be sufficient to get the latest version running once you have copied over all the source (`.f`) and include (`.inc`) files.

Early incarnations of `RAVEN` were written on VMS machines and the code should run with little or no modification on that operating system.

A list of source files and their functions can be found in Appendix B.

A.2 The Design Philosophy of `RAVEN`

For maximum flexibility and speed, `RAVEN` consists of several programs dedicated to different stages of the event simulation. Thus, a change in the location of one optical module does not necessitate the re-generation of several million muon bundles. Several different types of event selection and reconstruction can proceed for a single Monte Carlo run. Certain symmetries in the simulation problem are exploited to improve calculation speed. Examples of these symmetries will be discussed below.

`RAVEN` programs, most specifically `genevent`, are designed to operate in various "modes" of operation selected by the user. For example, `genevent` has modes for generating single cosmic ray muons, cosmic ray muon bundles, atmospheric neutrinos, or point sources of neutrinos. Independent of this choice, the user can choose which ice properties to simulate ("clear," "dusty" or "bubbly" ice). Each of these modes, as well as various other parameters such as number of muons to generate, are selected in the program input via a set of well-defined input commands.

In writing the `RAVEN` programs, we attempted as much as possible to adhere to the stylistic rules for programming in large projects. Changes are documented in the `History` file within each version directory. Most parameters which aren't specified by input commands (such as the speed of light or the index of refraction of ice) are given in `INCLUDE` files (the FORTRAN equivalent of C header files). Long variable or subroutine names such as `distmc_pmt_response_to_track` were favored over short names. And information was grouped together using the `STRUCTURE` construct of DEC FORTRAN (analogous to the `struct` construct in C), to favor organization and readability at some expense to portability. For example, rather than have separate variables for muon energy, direction, etc., we have:

```
INCLUDE 'newmc.inc'                ! Constants and structure defs.
RECORD /bundle_muon/ bun_mu        ! Muon bundle record

bun_mu.nmu = 2                     ! Two muons in this bundle
bun_mu.mus(1).energy  = 80.        ! First muon has 80 GeV
bun_mu.mus(1).thetamu = 180.       ! Muon is traveling straight down
bun_mu.mus(2).energy  = 120.       ! This muon is more energetic
bun_mu.mus(2).isource = iATMOS_NU  ! Muon from atmospheric neutrino
! ... and so on ...
```

A.3 `RAVEN` Simulation Programs: Input, Output and Control Flow

Figure A.1 describes the flow of information within the current `RAVEN` distribution. The program `airshow` is not packaged with the distribution proper, but is discussed in Ref. [14].

An example of a physics analysis which uses all the programs in Figure A.1 proceeds as follows. Let's say you wanted to calculate the number of events expected per unit time in AMANDA-B for a specified trigger condition, for both down-going, cosmic ray muons, and for muons from atmospheric ν_μ's. First, `photon_table` generates a file containing the flux of scattered Čerenkov photons due to a finite length of track. The resulting flux table is given as input to `distmc`, which creates a field of optical module responses due to the track segment.

`genevent` can now run, using the results of `distmc` to calculate the response of the detector to muon tracks. However, since you want to simulate down-going muon bundles from extensive air showers, you will want to first run `airshow` to create a file of multi-muon events (or use a pre-existing file multi-muon file). `genevent` will then take these muons, and write out a file containing OM hit times. A separate `genevent` run can simulate muons from atmospheric neutrinos.

`genevent` generates muon track information and then finds the times of photoelectrons in each hit OM; after all the times have been found, other properties such as OM pulse generation (since each OM can be hit multiple times, but the OMs have limited power to resolve separate hits) TDC/TOT values for each pulse, and ADC values for each channel. Resulting N-fold coincidence events are then written to an output file in the `RAVEN .evt` format.

The resulting events are finally passed on to an analysis program, of which `anaboth` is an example. The number of events passing the trigger for both the CR μ and ν_μ case are then compared with the number generated for each in `genevent` and the flux for each, giving the event rate (see Sec. 2.2).

More detailed instructions for running each program, including input file specifications, can be found below, in Sec. A.5.

A.4 The `RAVEN` Event Format

The events written by `genevent`, `newamab` and `anaboth` share a common format, described in the file `FORMAT` in the distribution. An example event follows:

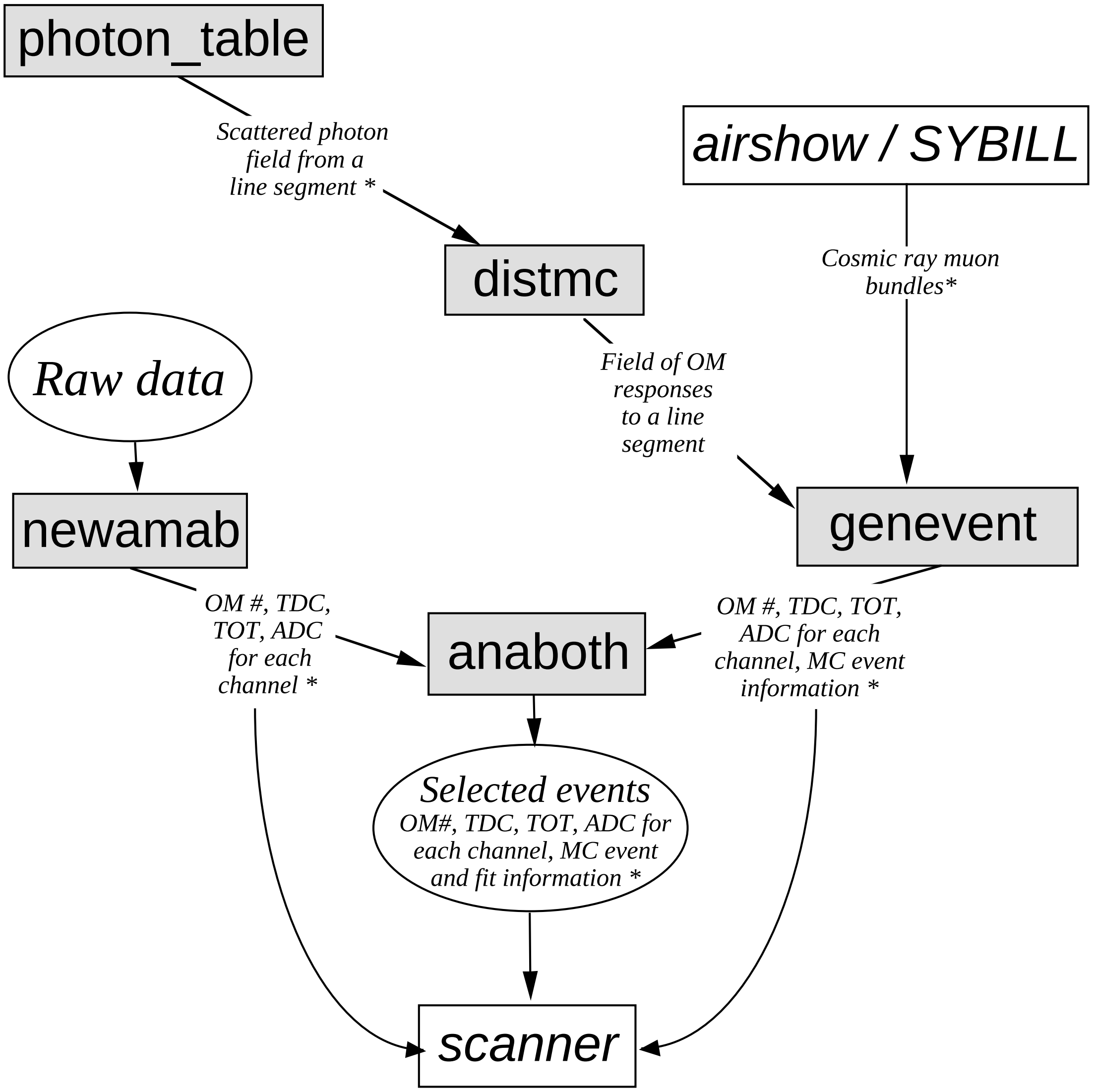

Figure A.1: Flow of control within the `RAVEN` suite of programs. Italicised text indicates files on disk passed from one program to the next. Presence of a (*) indicates that the files are ASCII files. (`scanner` and `airshow` are not distributed with the `RAVEN` package at this time)
.

```
EH      1214   3  43   12.230 166.360 190.310  1
MU 1  30.6 2 166.34  190.06 12357. -4130. 40000. 9013. -4723.   26026.    6447.
MU 2 164.7 1 66.37  190.45  9164. 787. 40000. -7535.   -2293.  -30029.    1034.
MU 3 102.8 2 166.32  190.40 12307. 854. 40000. 1615.   -1108.   -4659.    2814.
SH    1   2 3    0.67     0.64E+05    11635.   -4258.   36983.
SH    3   2 1    0.70     0.67E+05     6486.    -214.   15687.
HT    1   1   1   457.14    1441    562
HT    7   1   1   257.14    4124    555
HT   10   1   1    57.14    1827    512
HT   15   1   1   171.43    2295    547
HT   22   1   1   257.14    2317    555
HT   27   1   1    85.71    2078    525
HT   29   1   1   171.43    1701    547
HT   30   2   1  1334.21    1866    574
HT   33   1   1   200.00    1971    550
HT   41   4   1   814.28    1203    747
HT   43   1   1    85.71    1403    525
HT   44   2   1   628.57    1447    564
HT   45   2   1   371.43    1462    659
HT   46   4   1   424.97    1564    766
HT   65   1   1   257.14    1412    555
HT   66   1   1   371.43    1455    560
HT   68   3   1    35.16    1671    520
HT   73   1   1   257.14    2146    555
HT  108   1   1    85.71    3310    525
HT  118   1   1   400.00    2551    560
HT  120   1   1    57.14    1959    512
HT  121   1   1    85.71    1525    525
HT  122   2   1   456.13    1537    563
HT  127   1   1   228.57    1958    553
HT  131   1   1   142.86    1902    542
HT  154   1   1   457.14    1300    562
HT  155   1   1   142.86    1425    542
HT  162   3   2   140.81    1589    555    2369    365
HT  163   1   1   200.00    1934    550
HT  214   1   1    28.57    2135    470
HT  247   1   1    28.57    1996    470
HT  250   1   1    28.57    2133    470
HT  252   1   1    57.14    2135    512
HT  255   1   1   171.43    3058    547
HT  258   1   1   285.71    2333    556
HT  262   1   1   400.00    2419    560
HT  278   1   1   342.86    2254    559
HT  286   1   1   457.14    2257    562
HT  290   1   1   114.29    6044    535
HT  302   1   1   200.00    1794    550
HT  304   1   1    85.71    1629    525
HT  310   1   1     4.00    2222    365
HT  314   1   1   200.00    2448    550
EN
```

The file format is inspired by the DUMAND event format. In this example, Monte Carlo event number 1214 consists of a bundle of three muons causing 43 OMs to be hit. One of the hit OMs (number 162) had a secondary pulse. Muons 1 and 3 also generated relatively small (0.67 and 0.70 GeV) electromagnetic showers.

The format[1] is currently defined as follows:

MC Event Header (`EH`, Monte Carlo events only):

1. Event number
2. Number of muons
3. Number of OMs hit
4. Primary energy (TeV)
5. Zenith angle (degrees) of primary
6. Azimuth (degrees) of primary
7. Mass (AMU) of primary

Data Event Header (`DH`, data events only):

1. Event number
2. Number of OMs hit
3. GPS time (seconds)
4. Data register

Muon information (`MU`, Monte Carlo only):

1. Muon energy (GeV)
2. Number of showers from this muon
3. Zenith angle (degrees)
4. Azimuth (degrees)
5. Start X,Y,Z (cm)
6. End X,Y,Z (cm)
7. Distmu (distance of closest approach to the origin)

Shower information (`SH`, Monte Carlo only):

---

[1] Only **`RAVEN`** format number two is presented here.

1. Muon responsible for this shower
2. Shower number (≥ 2)
3. Vertex type (1=Brehm, 2=e^+e^- pair, 3=Hadronic photoproduction)
4. EM energy radiated (GeV)
5. Light output from Čerenkov particles in shower
6. Position X,Y,Z (cm) of shower

Hit information (`HT`, data and Monte Carlo):

1. Optical module number
2. Number of PEs generated (0 for data)
3. Number of output pulses generated
4. ADC value for this channel
5. TDC, TOT .... for each pulse in this channel (up to 5)

In addition, event files begin with a one-line file header. For example:
`FH 2 MC 24` (Monte Carlo version 24, format number 2), or
`FH 2 DATA 190 0` (Real data, format 2, day 190, run 0).

A.5 Running `RAVEN`

In order to simulate the response of an ice detector to a flux of muons, several things must be done. These include a full specification of the detector to be simulated (optical module properties and array geometry); properties of the ice (scattering and absorption); and various options for `genevent`.

A.5.1 Detector Array Geometry

The event generator `genevent`, the analysis program `anaboth`, and the event display program `scanner` all require the array geometry to be specified in an input file (`.geo` file).

The format is simple and is easily illustrated by an example `.geo` file:

```
1700    ! Depth of center of detector ("detector plane"), meters
2       ! Number of strings

0. 0.   ! String 1 x,y in meters
2       ! Number of OMs for string 1

0.      ! z coordinate (meters), 1st OM
up.pmt
10.     ! z coordinate of 2nd OM
dead.pmt

0. 20.  ! String 2 x,y in meters
3       ! Number of OMs for string 2

15.     ! z coordinate
up.pmt
5.      ! z coordinate
dead.pmt
-5.     ! z coordinate
down.pmt
```

The lines ending in `.pmt` indicate the file name used to define the optical module parameters for each OM, described below.

It should be noticed that there is an implicit assumption that the strings are all oriented vertically. Future versions of `RAVEN` should allow for arbitrary OM positions in order to deal with small-angle deviations from vertical in the strings, and for km^3-scale detectors where triggering subunits may be clusters of modules rather than strings. (Of course, as it stands, one could kludge the existing format for an arbitrary string orientation, by treating each PMT as its own "string.")

A.5.2 Optical Module Parameters

The OM parameters are required by `genevent`, `anaboth` and `distmc`. The parameters for each type of OM are specified in a file (whose extension is, by convention, `.pmt`).

An example `.pmt` file follows:

```
11.5       ! Radius of tube in CM
0.         ! Delay, ns
0.         ! Sigma(delay), ns
1.8        ! Dark current, kHz (CURRENTLY HARD-CODED AT 560 Hz)
0.5        ! ADC noise, p.e.s
1          ! Orientation: 1=looking up. 2=looking down.
2          ! Type: 1=flat 2=spherical 5=dead (OBSOLETE)
10.0       ! Average pulse amplitude mV
0.15       ! Amplitude sigma
200.0      ! Amplifier gain
5.0        ! Double pulse resolution (ns)
-100.0     ! Discriminator forward threshold mV in update mode
-35.0      ! Discriminator backward threshold mV in update mode
 50.0      ! Discriminator width (ns) in update mode
```

```
-30.0     ! Discriminator forward threshold mV in BG mode
-30.0     ! Discriminator backward threshold mV in BG mode
365.0     ! Discriminator width (ns) in BG mode
3         ! Max. No of AP. to generate
0.25      ! Probability that each PE will generate 1st AP
2000.0    ! Ave. time (ns) of the 1st AP wrt time of real hit
1000.0    ! Sigma (ns) of the 1st AP
0.25      ! Probability that each PE will generate 2nd AP
3000.0    ! Ave. time (ns) of the 2nd AP wrt time of real hit
1000.0    ! Sigma (ns) of the 2nd AP
0.25      ! Probability that each PE will generate 3rd AP
4000.0    ! Ave. time (ns) of the 3rd AP wrt time of real hit
1000.0    ! Sigma (ns) of the 3rd AP
1         ! Obsolete
1.        ! Obsolete
1.        ! Obsolete

4 ! Hard threshold efficiency values (don't change)
0.0 0.5 0.5 1.0
0.0 0.0 1.0 1.0

0.01 0.22 0.265 0.29 0.295 0.3 0.3 0.3 0.295 0.29 0.285 0.275 0.27 0.26 0.25
0.24 0.225 0.215 0.20 0.18 0.16 0.14 0.12 0.095 0.08 0.065 0.05 0.035 0.03 0.02
0.015   ! QE as a function of wavelength; 300-600 nm in 10 nm bins.

  9.9214539E-04 2.9742057E-03 8.8781239E-03 2.6170608E-02
  7.4423663E-02 0.1926782 0.4090070 0.6530852 0.8149738 0.8882678
  0.9156799 0.9251837 0.9283913 0.9294639 0.9298214 0.9299406
  0.9299803 0.9299935 0.9299978 0.9299992 0.9299998 0.9299999
  0.9300000 0.9300000 0.9300000 0.9300000 0.9300000 0.9300000
  0.9300000 0.9300000
  0.9300000 ! Billings glass transmission as a function of wavelength

0.90 ! 1st dynode efficiency:
0.989 ! Obscuration factor (obscuration area/total area)

1.066977  1.066787  1.065932  1.064613  1.063175  1.061827
1.060708  1.059870  1.059312  1.059026  1.058989  1.059178
1.059593  1.060223  1.061065  1.062131  1.063454  1.065055
1.066977  1.069284  1.072060  1.075414  1.079446  1.084369
1.090427  1.097910  1.107120  1.118780  1.133619  1.152245
1.176380  1.207939  1.248960  1.301423  1.370929  1.461763
0.0 ! Angle-dependent Fresnel transmission coefficients for hemis. PMTS
```

The most relevant quantities are outlined in Section 3.6; the remaining quantities refer to the specific details of the phototube electronics, a description of which can be found in Reference [18].[2]

---

[2] It should be noted that the physical radius of the phototubes used to date in AMANDA is 9.271 cm, not 11.5; however, optical effects due to the glass pressure housing increase the effective area somewhat.

A.5.3 Ice Properties: `photon_table`, `distmc`

Unless one wishes to generate muons traveling through clear ice with no scattering (a case which apparently doesn't obtain in the two ice depths studied to date), one must first run `photon_table` to calculate a table of scattered photons for a range of positions, photon directions and time. `photon_table` has options for different scattering models (Henyey-Greenstein or spherical geometrical optics); monochromatic light (laser calibration) or Čerenkov light; and angular distribution (isotropic or Čerenkov cone).

The use of `photon_table` is easily illustrated by example:

```
3000     ! Number of photons to generate
100      ! Number of rho bins to use
8        ! Number of cos(psi) bins
8        ! Number of cos(theta) bins
3        ! Number of phi bins
300      ! Number of time bins
1.E7     ! Component 1 scattering length (turn off)
700.     ! Component 2 scat. length (7 meters)
hg
0.8      ! avg(cos(theta_scatt)), component 1
0.8      ! avg(cos(theta_scatt)), component 2
20000.   ! rho_max in (cm)
200.     ! Size of the track segment to be generated
4000.    ! max time
1234561  ! Random number seed
cer_hg_sc7m_ab100m.photons
cer
```

In this case, a single Henyey-Greenstein scattering component is specified with the `hg` input. To specify geometrical optics, one enters `geo` instead of `hg`, followed by the ratios of the indices of refraction of each component compared to ice (N_{ice}/N_1, N_{ice}/N_2), which governs the angular distribution of scattering. The last two lines specify the file name for the table, and the choice of initial photon direction (`cer` indicates that the photons are emitted at the Čerenkov angle θ_c; `isot` would indicate that a randomly-oriented photon should be generated).

The example input file would be appropriate for muon generation.

To simulate a laser pulse, one could use:

```
3000     ! Number of photons to generate
.
.
.
20000.   ! rho_max in (cm)
1.       ! Size of the track segment (point source)
4000.    ! max time
1234561  ! Random number seed
isot_hg_sc7m_ab100m.photons
isot
```

In this case, a point-like (1 cm long) emitter of photons is specified, with an isotropic angular distribution.

The table created by `photon_table` is then read in by `distmc`, which also reads in an optical module (`.pmt`) file (see below). The switches which specify the photon table file name, the `.pmt` file name, and other options are:

`photon_file <photon_table.dat>` : File name of photon field, from `photon_table`.

`pmt_file <std_8in_up.pmt>` : File name of OM specification file to use.

`pe_output <distmc.pes>` : File name for output field of OM responses.

`seed <666>` : Random number seed.

`lo_lambda <300 nm>` : Lower bound on wavelength (should be kept to 300 nm).

`lo_lambda <600 nm>` : Upper bound on wavelength (should be kept to 600 nm).

`atten_type <4>` : Number of absorption curve to use when calculating OM response. 4=310 meter peak absorption length. 17=90 meter peak absorption length. See `genphoton.f` for the entire list of possible absorption lengths.

`atten_mul <1>` : Scaling factor to multiply absorption curve.

`monochrome` : Consider only fixed wavelength light. Default: use $1/\lambda^2$ Čerenkov spectrum.

`lambda_mono <375 nm>` : The fixed wavelength, in nanometers, to use with the `monochrome` option.

Here is an example `distmc` input file, which runs the `photon_table` output file `cer_hg_sc7m_ab100m.photons` with absorption length curve number 15 (100 meters at peak), and the optical module described by `up.pmt`:

```
photon_file  cer_hg_sc7m_ab100m.photons
pe_output    cer_hg_sc7m_ab100m.pes
pmt_file     up.pmt
seed         666         ! Random number seed
lo_lambda    300.0000    ! Lower wavelength bound
hi_lambda    600.0000    ! High wavelength bound
atten_type   15          ! Attenuation curve # to use
```

A.5.4 Generating Events: Running `genevent`

`genevent` is run by specifying a list of commands on the standard input stream (typing at the terminal or re-directing from a file). The list of commands and their descriptions follows. Each command is followed by its default value and units, in parentheses, then by a description.

`num_muons (500)` : Number of muons to generate.

`r0max (100 meters)` : Radial size of test area or volume.

`cr_z_dist (10000 cm)` : Height of physics plane above detector plane (cosmic-ray multimus start here).

`fast_crs (false)` : Do single cosmic ray muons, taking muon energies and angles from a file created during a previous run.

`param_crs (false)` : Do single cosmic ray muons, energies and angles at the ice surface taken from a parametrization by Matsuno *et. al.*, [9]; muons propagated to physics plane before generation of Čerenkov light.

`save_cr_ecosth (false)` : If running `param_crs`, save energy E_μ (GeV) and cosine of zenith angle $\cos\theta_\mu$ of muons surviving to the physics plane. Write E_μ, $\cos\theta_\mu$ pairs to an output file.

`ecosth_file (tmp.muons)` : File name to store E_μ and $\cos\theta_\mu$ if `save_cr_ecosth` is specified.

`atmospheric_nus (false)` : Generate atmospheric neutrinos throughout the test volume.

`atnu_threshold (10 GeV)` : Lowest muon energy for atmospheric neutrinos.

`agn_nus (false)` : Generate a flux of muons from a point source (fixed direction in space).

`agn_nadir_ang (0 degrees)` : Nadir direction (0=below) of the point source.

`agn_flux` (1×10^{-10} `Hz/cm`^{2}) : Flux of muon-induced neutrinos from this point (obsolete).

`agn_thresh (1 GeV)` : Lower energy bound for muons from point source.

`agn_spect (2)` : Index for muon energy spectrum (default: $E^{-2}GeV$). If -1, use fixed energy of agn_thresh.

`agn_area (false)` : Do effective area (through-going flux) rather than effective volume (volumetric flux).

`agn_area_dist (10000 cm)` : Distance from origin of the test area.

`agn_area_len (10000 cm)` : Size of side of square test area.

`agn_azimuth (0 redians)` : Azimuth of vector from origin to center of test area.

`multimus (false)` : Simulate muons from pre-generated muon bundles (from SYBILL/airshow).

`multimu_file (muons.list)` : Source file of pre-generated muon bundles.

`atten_type (4=310 meter peak)` : Absorption curve to use.

`ice_clarity (1)` : Scaling factor for absorption curve.

`precut_safety_factor (3.5)` : See Section 2.4.

`do_distmc (false)` : Use OM response field generated by `distmc`.

`pefile (distmc.pes)` : File name for `distmc` OM response file.

`fast_bubbles (false)` : Do fast bubble simulation. See Section 3.5.2.

`electro_ala_igor (false)` : Do the most complete and realistic simulation of the OMs and digital electronics (TDCs, ADCs, discriminators).[3]

`data_write (false)` : Write events to output file in the `RAVEN .evt` format.

`dwrite_file (fort.30)` : File name for event output.

`geo_file (amanda.geo)` : Geometry file name.

`hist_file (<none>)` : HBOOK output file for histograms and ntuples.

`seed (1234567)` : Random number seed.

`output_hits (1)` : Number of OM hits required before before writing the file to `dwrite_file`.

`physics_code (0)` : Code which specifies method for muon propagation (stochastic or deterministic energy loss). See Section 2.4.

`dark_noise (false)` : Simulate dark noise at a rate of 560 Hz/channel.

An example `genevent` input file follows:

---

[3] This command should always be given to circumvent older code which needs to be cleaned out.

```
! This file runs atmospheric neutrinos...
atmospheric_nus
num_muons    4000000      ! Number of muons to generate
r0max        1500.        ! Basically, the radius in meters of test volume
geo_file     amab.geo     ! OM geometry file
hist_file    gennu_4.his  ! Histogram file for PAW output
seed         123432       ! Random seed
output_hits  4            ! Required number of hits for writing to event file
physics_code 2            ! Don't do shower production within the detector
dark_noise                ! Simulate dark noise
data_write                ! Write out events to gennu_4.evt
dwrite_file  gennu_4.evt  ! Event output file
electro_ala_igor          ! Simulate full electronics
do_distmc                 ! Take dusty ice inputs from the following files
pefile       /d10/mclib/inplib/amab/mu.4.220.pes
```

Another sample file for simulating point sources:

```
agn_nus                 ! Turn on point source of neutrinos
agn_nadir_ang   42.     ! Direction in degrees of Markarian 421
agn_spect       2.      ! Generate (energy)**(-2) power law spectrum
agn_thresh      1000.   ! Generate muons of energy 1 TeV and greater
```

This list of commands generates a through-going muon flux starting at random points within the test volume, with an E^{-2} power-law spectrum and a lowest energy bound of 1 TeV.

Alternatively,

```
agn_nus                 ! Turn on point source of neutrinos
agn_nadir_ang   42.     ! Direction in degrees of Markarian 421
agn_spect       -1.     ! Fix energy at threshold
agn_thresh      500.    ! 500 GeV muons only
agn_area                ! Do effective area rather than effective volume
agn_area_dist  20000.   ! Test area starts 200m from origin
agn_area_len   30000.   ! And is 300m x 300m in size
```

generates muons starting in a 300 m $\times$ 300 m square, 200 m from the origin, whose normal is 42^o from the vertical. The muons all propagate in a direction perpendicular to the plane of the square. Energy is fixed to 500 GeV.

A.5.5 Interpreting a `genevent` Run

`genevent` produces copious output in a variety of forms. Of greatest interest is the `.evt` event file, described above. `genevent` also writes a great deal of debugging and status information to the standard output stream. This includes:

- A summary of the inputs for the run,
- A summary of the array geometry,

- Output from various initializations (muon propagation, `distmc` routines, etc.),
- Various warning messages,
- At the end of the run, an event summary, which includes the number of muons and number of events generated, number of times the array triggered, number of events written to the `.evt` file, and more.

An HBOOK file is created by `genevent` if the `hist_file` command is given. This file, readable by the PAW analysis package available with the CERN library[30], is useful for debugging the software and checking the events. Specifically, NTUPLEs 992 (event ntuple) and 995 (event ntuple, without events caused purely by dark noise) are of interest.

A.6 Event Selection and Reconstruction

Events written in `.evt` form by `genevent` can be processed in a variety of ways. An event display program `scanner` (borrowed from the IMB and DUMAND experiments) is available which reads both the `RAVEN` `.evt` and `.geo` file formats. `scanner` allows one to visually check the integrity of the events and the array geometry.

Further data analysis can be done with analysis packages which may be written by individuals at a later date. One program, `anaboth`, is included in the `RAVEN` distribution. `anaboth` reads in Monte Carlo `.evt` files from `genevent` and `.evt` files created from the raw AMANDA data by `newamab`. `anaboth` and `newamab` are used for the analyses presented in Chapters 4 and 5.

Appendix B

A List of Source Files in the `RAVEN` Software Distribution

`anaboth.f`	Analysis and filter program for `RAVEN` event files
`anaboth.inc`	Constants for `anaboth.f`
`bubbles.f`	Subroutines for simulating muons passing through ice with bubbles
`constants.inc`	Physical and mathematical constants for `photon_table`
`distmc.f`	Support subroutines for `distmc` and `genevent` (scattered light)
`distmc.inc`	Constants for routines in `distmc.f` and `distmc_main.f`
`distmc_main.f`	Main subroutines for use in `distmc`
`dwrite.f`	Output subroutines for `genevent`
`electronics.f`	Subroutines for treatment of AMANDA electronics in `genevent`
`genevent.f`	Main event generation code
`genmuon.f`	Subroutines for the generation of muon tracks
`genphoton.f`	Subroutines for the generation of Čerenkov light from muons
`input.f`	Subroutines for the routines to process input commands in `genevent` and `distmc`
`input.inc`	Constants and data structures for `input.f` routines
`newamab.c`	Program which extracts raw AMANDA-B data and writes `RAVEN` event (`.evt` files
`newmc.f`	Many miscellaneous routines, primarily for `genevent`
`newmc.inc`	Constant and structure definitions for `RAVEN`
`nuflux.f`	Atmospheric neutrino flux generation routines
`photon_table.f`	Program which generates table of scattered photons
`pmtphyz.f`	Detailed treatment of photons hitting OMs. Currently not used
`prop.f`	Lipari/Stanev[13] subroutines for muon propagation and electromagnetic shower vertex generation
`reader.c`	R. Porrata's raw event reader subroutines for AMANDA-B
`reader.h`	Header file for `reader, newamab`
`sn.f`	Older Supernova treatment, superceded by `distmc`
`vel3.f`	Line fit subroutines for `anaboth`

Appendix C

Glossary

ADC Analog-to-digital converter. Measures either a peak voltage in an input channel, or the total charge under an analog pulse. In the context of AMANDA, corresponds roughly to number of photons detected by an OM.

Detector Plane The plane specified by $z = 0$; generally, the plane passing through the center of the detector.

Data Acquisition System (DAQ) In an experiment, the system which gets data measured by the instrumentation into one or several computers, to be stored or processed.

Extensive Air Shower (EAS) A shower of particles which occurs in the atmosphere, generated by a high-energy cosmic ray incident on the top of the atmosphere.

Monte Carlo Most generally, a statistical method for evaluating complex integrals. For this document, a computer simulation of an inherently statistical process. The basic idea is to generate large number of events with certain statistical properties or following certain rules, and then observe the properties of all or subsets of the events.

Nadir Angle Angle of incidence relative to the nadir (directly below the observer), i.e., a nadir angle of zero means the particle is moving directly upwards.

Ntuple A data structure consisting of a list of vectors, commonly with each vector representing an event, and each element of the vector corresponding to a quantity for that event. In this document, a data structure usable by the PAW data analysis package. For example, if the Ntuple represented AMANDA events, the event vector could consist of the muon energy, time, number of hits, etc.

Optical Module (OM) Generic term in the Monte Carlo for a light-sensing device. Consists of a photomultiplier tube in its pressure housing. Specified in input file by an entry in the geometry (`.geo`) file referring to a (`.pmt`) file.

Photoelectron An electron emitted from the photocathode of a photomultiplier tube which initiates a cascade in the dynode chain, causing a signal to be emitted from the tube.

Photomultiplier Tube A device which emits a measurable electronic pulse when struck by one or more photons. "A lightbulb in reverse." –Francis Halzen.

Physics Plane In `RAVEN`, a horizontal plane spaced a few absorption lengths above the detector. Point of generation of cosmic-ray muons.

Precut Cut applied to muon tracks which rejects the track if the distance of closest approach to the origin d_μ is less than some large distance (`rcutoff`, in `genevent`).

Standard Input Stream Unix parlance for data typed in at the terminal, or from a file if input is re-directed. Also known as `stdin`.

Standard Model A theory which describes elementary particles and their interactions, currently very well-established but incomplete. It postulates three families of particles each consisting of two quarks, a charged lepton, and a neutrino. The known interactions (electroweak and strong—gravitation is excluded) are derived from symmetry principles and are mediated by massive (W, Z) or massless (photon) particles.

Standard Output Stream Also known as `stdout`. Just like `stdin`, but in reverse.

TDC Time-to-digital converter. In AMANDA, converts the pulse from an OM into a digital value corresponding to the time for that pulse.

Zenith Angle Angle of incidence relative to the zenith (directly above the observer). A zenith angle of zero means the particle is traveling straight down.

References

1. Stanislaw Lem, *His Master's Voice.* Translated by Michael Kandel. Harcourt Brace Jovanovich Publishers, Orlando, Florida (1968). A sophisticated novel describing the detection and decoding of an extraterrestrial neutrino "letter," as well as the dark underbelly of scientific culture.

2. P. C. Mock (with AMANDA Collaboration), "Status and Capabilities of AMANDA-94." *Proceedings of the XXIVth International Cosmic Ray Conference*, Rome, Italy (1995), Vol. 1, p. 758.

3. E. Zas, F. Halzen and T. Stanev, "Electromagnetic Pulses from High-Energy Showers: Implications for Neutrino Detection." Phys. Ref. D **45**, 362 (1992).

4. C. Costa, private communication.

5. T. K. Gaisser, F. Halzen and T. Stanev, "Particle Astrophysics with High Energy Neutrinos." Phys. Rep. **258**, 173 (1995).

6. S. Barwick *et. al.*, "Neutrino Astronomy on the 1 km^2 Scale." J. Phys. G: Nucl. Part. Phys. **18** 225 (1992).

7. F. Halzen, "The Case for a Kilometer-Scale High Energy Neutrino Detector: 1996." University of Wisconsin–Madison preprint MADPH-96-937 (1996).

8. Edgar Allen Poe, "The Raven." (Excerpt) (1845)

9. S. Matsuno et. al., "Cosmic-ray Muon Spectrum up to 20 TeV at 89° Zenith Angle." Phys. Rev. D **29**, 1 (1984).

10. L. Volkova, "Energy Spectra and Angular Distributions of Atmospheric Neutrinos." Sov. J. Nucl. Phys. **31**(6), 784 (1980).

11. F. Halzen, J.E. Jacobsen, and E. Zas, "Possibility the High Energy Neutrino Telescopes Could Detect Supernovae." Phys. Rev. D **49**, 1758 (1994).

12. F. Halzen, J.E. Jacobsen, and E. Zas, "Ultratransparent Antarctic Ice as a Supernova Detector." Phys. Rev. D **53**, 7359 (1996).

13. P. Lipari and T. Stanev, "Propagation of Multi-TeV Muons." Phys. Rev. D **44**, 3543 (1991).

14. Serap Z. Tilav, Ph. D. thesis, University of Delaware, Newark, Delaware, (1991).

15. C. H. V. Wiebusch, "Preliminary Results on the Angular Response of the AMANDA Optical Module." AMANDA Internal Memo, April 9, 1996.

16. T. K. Gaisser, *Cosmic Rays and Particle Physics.* Cambridge University Press, Cambridge, UK (1990).

17. C. H. V. Wiebusch, *The Detection of Faint Light in Deep Underwater Neutrino Telescopes.* Ph. D. thesis, Physikalische Institute RWTH Aachen, 52056 Aachen, Germany, 1995.

18. I. Liubarsky, Ph. D. thesis, University of Wisconsin, Madison. In preparation.

19. R. Porrata, Ph. D. thesis, University of California, Irvine. In preparation.

20. Vijaya Kandhadai, Ph. D. thesis, University of Wisconsin, Madison (1996).

21. Albrecht Karle, private communication.

22. M. Moorehead and D. Lowder, private communication.

23. J. E. Jacobsen, "A First Look for ν_μ Candidates in AMANDA-B." Internal AMANDA memo.

24. J. E. Jacobsen, "Filtering AMANDA-B Muon Data for Neutrino Events: Monte Carlo and Data Studies." Internal AMANDA memo. Draft available at
`http://alizarin.physics.wisc.edu/jacobsen/amanda/candmc.ps`

25. University of Wisconsin - Madison AMANDA Group, `RAVEN` simulation programs.
`http://alizarin.physics.wisc.edu/jacobsen/raven`

26. A. Bouchta, "A Preliminary Position Calibration of the AMANDA-B Detector." AMANDA Internal Memo.

27. S. Tilav, private communication.

28. F. Halzen and R. Vázquez, private communication.

29. The AMANDA Collaboration, P. Askebjer *et. al.*, "Optical Properties of the South Pole Ice at Depths Between 0.8 and 1 Kilometer." Science, **267**, 1147 (1995)

30. René Brun, Olivier Couet, Carlo Vandoni, Pietro Zanarini, "PAW – Physics Analysis Workstation, The Complete Reference," Version 1.07 (Oct. 1989). CERN Program Library entry **Q121**, CERN, Geneva, Switzerland.

31. The AMANDA Collaboration, D. Lowder *et. al.*, "Hardware Design and Prototype Tests of the AMANDA Neutrino Detector." *Proceedings of the XXIIIrd International Cosmic Ray Conference*, Calgary, Canada (1993), Vol. 4, p. 569.

32. K. Hirata *et. al.*, Phys. Rev. Lett. **58**, 1490 (1987); "Observation in the Kamiokande-II Detector of the Neutrino Burst from Supernova SN1987A." Phys. Rev. D **38**, 448 (1988).

33. C. Spiering, C. Wiebusch, O. Streicher, D. Pandel, private communication. See the SiEGMuND Web Page, `http://sgi.ifh.de/ wiebusch/siegmund/siegmund.html`

34. The AMANDA Collaboration, R. Wischnewski *et. al.*, "A System to Search for Supernova Bursts with the AMANDA Detector." *Proceedings of the XXIVth International Cosmic Ray Conference*, Rome, Italy (1995), Vol. 1, p. 658.

35. S. Hundertmark *et. al.*, "Letter of Intent, AMANDA Upgrade and Feasibility Study for KM3." Submitted to the DESY Physics Research Committee, June 1996.

36. F. Halzen and S. Tilav, private communication.